CHEMICAL REACTIONS OF SIMULATED PRODUCER GAS WITH MOLTEN TIN-BISMUTH ALLOY

by

Keith J. Bourne

A thesis submitted in partial fulfillment of the requirements of the degree of

Masters of Science

(Mechanical Engineering)

at the

UNIVERSITY OF WISCONSIN-MADISON

2012

Approved

Advisor:_____ Date:_____

Abstract

A pyrolysis and gasification system utilizing molten metal as an energy carrier has been proposed and the initial stages of its design have been completed. However, there are several fundamental questions that need to be answered before the design of this system can be completed. These questions include: How will the molten metal interact with the products of biomass pyrolysis and gasification? Under what conditions is the metal oxidized significantly? Will any metal oxides produced inhibit or accelerate reactions important to gasification and pyrolysis?

In short, the purpose of this study is to better understand the pyrolysis and gasification of wood in the presence of a molten metal. The metal chosen for use in this study is the eutectic alloy composed of 42% tin and 58% bismuth which melts at 138°C.

A system has been designed to allow for various gas reactions to take place in a bubble rising through a column of molten tin-bismuth which can be heated up to 1000°C. To understand the kinetics of the reactions a method was developed that uses two microphones to measure the velocity of the bubble so that the residence time of the gas can be determined. The average bubble diameter over experimental conditions was found to be 6.7 mm with an average velocity of 0.21 m/s which agrees well with literature data.

The primary reactions of interest are the oxidation of tin-bismuth by water or air, reduction of tin-bismuth by hydrogen and carbon monoxide and decomposition of methane

in the presence of tin-bismuth. These reactions were carried out in both a reactor containing tin-bismuth as well as in an empty reactor that provided a control for comparison.

The measured decomposition rate of methane in a reactor without liquid tin-bismuth was similar to literature data. The rate of methane decomposition in tin-bismuth appears to be accelerated in the temperature range of 600-900° C. Furthermore, the products of this decomposition are uncertain, but appear to be both hydrogen and hydrocarbon chains between 2 and at least 4 carbons long. This increased decomposition of methane did not appear when the mixture of 1% of each CO, CO_2, CH_4, H_2, O_2 and 95% argon was heated in the presence of tin-bismuth up to 1000°C.

Tin was found to be oxidized rapidly by oxygen gas at temperatures between 200 and 1000°C. Near complete conversion of oxygen in the above described 6 gas mixture was observed at 400°C with a residence time of approximately 3.2 seconds in tin-bismuth, with almost all of the oxygen being used to form tin dioxide. Water was found to readily form tin dioxide and hydrogen at temperatures between 200 and 400°C.

Reduction of tin dioxide in this reactor was less successful. Carbon monoxide did not appear to be effective at reducing tin dioxide at temperatures between 200 and 800°C, while hydrogen may have reduced a detectable, but insignificant amount of tin-dioxide at 200 and 400°C. However, the apparent reduction of tin dioxide by hydrogen may have been due to an erroneous measurement.

Suggestions for future work include repeating the methane and tin-bismuth experiments to confirm the effect that tin-bismuth appears to have on methane decomposition with additional gas analysis equipment to better determine the composition of the produced gas. This study may be further extended to larger hydrocarbons or solids such as cellulose or wood. Further study into the reduction of tin dioxide is also needed. Literature suggests that CO and H_2 are more successful at reducing tin dioxide at higher temperatures, up to 1500°C, and with longer residence times.

The inability to reduce metal oxides effectively may require a re-design of the proposed pyrolysis and gasification system. The system may need to be either modified so that the liquid metal does not come into contact with any oxidizing agents, or a different molten material should found that will not oxidize so readily.

Acknowledgements

I would like to thank my research advisors for their support of this work. At the University of Wisconsin-Madison I was advised by Dr. Michael Corradini and Dr. Mark Anderson. At the USDA Forest Products Laboratory I was advised by Dr. Mark Dietenberger and in an unofficial capacity by Dr. Carl Houtman.

The vast majority of this study was completed at the USDA Forest Products Laboratory. I am indebted to all of my co-workers at FPL who provided support, supplies and advice throughout my course of study. In particular I would like to thank Chester Filipowicz, Dave Eustice and Geoffrey Severin for their help building the experimental facility.

Table of contents

1. Introduction

In recent years there has been a renewed interest in obtaining energy from renewable sources of biomass to reduce dependence on foreign oil and net carbon emissions to the atmosphere. According to a study by the US Department of Energy, the United States has enough biomass resources to replace approximately 30% of the nation's petroleum use with biofuels [1].

The idea of using biomass as an energy source is not a new one, and it has been used in a variety of ways from a simple campfire to fermentation of plant matter into alcohols to gasification of wood into synthetic gas. Modern efforts focus on improving the efficiency of these technologies to maximize the amount of usable energy obtained from the biomass source.

The purpose of this study is to better understand the pyrolysis and gasification of wood in the presence of a molten metal. Pyrolysis is the thermal breakdown of an organic material in the absence of oxygen forming some volatile gases such as hydrogen and methane, as well as higher order hydrocarbons known as pyrolysis oils and tars, in addition to a solid comprised primarily of carbon and inorganic substances [2]. Gasification is the thermochemical breakdown of carbonaceous material into hydrogen and carbon monoxide gas at elevated temperatures with a minimal amount of oxygen present, which prevents combustion [3]. Pyrolysis and gasification of wood are closely linked because wood must

first undergo pyrolysis before it can be gasified, and the conditions under which pyrolysis occurs greatly affects the pyrolysis products and thusly the gasification process.

1.1 Overview of Pyrolysis and Gasification

To understand how pyrolysis and gasification will be affected by a molten metal, one first needs to understand the basics of these thermochemical processes. The following is an overview of pyrolysis and gasification focusing on the conversion of biomass to gaseous fuels.

1.1.1 Pyrolysis

Pyrolysis is the thermal decomposition of an organic material in the absence of oxygen [2]. The lack of oxygen and the process temperature differentiates pyrolysis from combustion and gasification. Pyrolysis of biomass can be regarded in terms of cellulose, hemicelluloses and lignin, which are polymers that make up the majority of wood and other forms of biomass [4]. Cellulose decomposes between 240 and 350°C, hemicelluloses decomposes from 200 to 260°C while lignin decomposes from 280 to 500°C, so wood pyrolysis generally begins between 200 and 300°C [4]. However, lignin decomposes at a much slower rate than cellulose and hemicelluloses so lignin is generally considered to be thermally stable during pyrolysis [2]. The products of pyrolysis depend greatly upon the specific biomass and the conditions under which it is heated including the temperature, heating rate, residence time and moisture content of the biomass. Pyrolysis products

include hydrocarbon vapors (tars), aerosols, chars (charcoal), and permanent gases like hydrogen and carbon monoxide [2].

Pyrolysis is generally separated into two types: fast and slow, with the border between the two being somewhat ill defined. Typically, fast pyrolysis is considered to take place in less than two seconds, but may take as long as five seconds, while slow pyrolysis is anything longer than about 3 to 5 seconds [2]. Additional variables other than time help to differentiate between fast and slow pyrolysis.

Slow pyrolysis is sometimes called conventional pyrolysis and is the process used for centuries to make charcoal from wood. Slow pyrolysis is generally carried out at approximately 500°C with slow heating rates and long vapor residence times [4].

Fast pyrolysis is typically of more interest for fuel production as it can directly produce liquid fuels with about one-half the heating value of typical fuel oils [4]. These pyrolysis oils can be burned directly in combustion systems [4]. Fast pyrolysis differs from slow or conventional pyrolysis by four main characteristics: high heating rate, up to 1000°C/second in some cases; carefully controlled temperature generally in the range of 425 to 500°C; short vapor residence times; and rapidly cooled and condensed vapors and aerosols [4]. These characteristics all serve to maximize the production of bio-oil and minimize the residual char. The high heating rate allows the decomposition reactions to take place quickly and helps to keep the molecules in longer chains, while the short vapor residence times help to prevent the vapors from reacting with each other and decomposing

further into smaller molecules. Rapidly cooling and condensing the vapor and aerosol products also help to prevent decomposition to smaller less desirable and possibly gaseous products.

Dry wood which undergoes fast pyrolysis can yield 60-80% by weight bio-oil with the remaining components being permanent gases and char [2] [4]. The bio-oil is typically composed of 70 to 80% by weight polar organic compounds with 20 to 25% water content [2]. Oxygen may be up to 50% of the weight of bio-oil, which helps to make it unstable [4]. Reactions in un-treated bio-oil continue to proceed after production and result in the undesirable increase in viscosity and decrease in energy value [4]. The instability of bio-oil makes it difficult to transport over long distances or store, which is a major hurdle to overcome before it can become widely used. Currently there is a lot of interest in upgrading bio-oil to reduce its instability which will make pyrolysis a more attractive form of converting biomass to liquid fuels.

1.1.2 Gasification

Gasification is the endothermic partial thermal oxidation of a carbonaceous material which results in primarily the gases H_2, CO and CH_4 as well as solid char and some condensable liquids [3]. Solid chars and condensable hydrocarbons are the result of incomplete gasification. Gasification is usually performed at higher temperatures than pyrolysis, between 600 and 1000°C [5] [6]. The major difference between gasification and combustion is that in gasification, the amount of oxygen is limited to favor the production

of CO and H_2 rather than CO_2 and H_2O. The source of oxygen depends on the specific process but can be, among other sources, air, O_2, or steam [5]. A general form of the gasification reaction can be seen in equation 1.1.

$$C_xH_y + xO \rightarrow xCO + \frac{y}{2}H_2$$

Equation 1.1- Gasification reaction

The exact conditions under which gasification take place have a large effect on the end products. For example, increasing the temperature increases the amount of gas produced from gasification, but the specific temperature controls the composition of the gas [5]. Four major reactions that take place are shown below in equations 1.2 to 1.5. Each has its own kinetic and equilibrium characteristics. The water gas shift reaction favors the production of CO_2 and H_2 at temperatures below about 800°C, while CO and H_2O are favored at higher temperatures. Thermodynamically, methane steam reforming favors the production of H_2 and CO above 600°C, but due to kinetic considerations steam reforming only becomes dominant above 850°C [5]. Similarly, the water gas reaction produces CO and H_2 above 750°C and the Boudourd reaction dominates the CO-CO_2 reactions to form CO above 850°C [5].

(1.2) $CO + H_2O \leftrightarrow CO_2 + H_2$ Water Gas Shift (WGS)

(1.3) $CH_4 + H_2O \leftrightarrow CO + 3H_2$ Methane Steam Reforming

(1.4) $C + H_2O \leftrightarrow CO + H_2$ Water Gas Reaction

(1.5) $C + CO_2 \leftrightarrow 2CO$ Boudourd Reaction

Equation 1.2 to 1.5- Important reactions taking place during gasification [5]

Because the conditions under which gasification takes place affects the composition of the gas so significantly, it is important to look at several common types of gasifiers to investigate how they work and their relative advantages and disadvantages. Gasifiers can be grouped by several features including the format of the flow, the structure of the bed, and the method of heating. A gasifier can either be heated directly or indirectly. In a directly heated gasifier, a portion of the feedstock is combusted with air or another oxygen source in the same space that gasification is taking place. This method has the advantage of having a minimal resistance to heat transfer between the heating source and the endothermic gasification reactions. However, direct heating requires careful control of the oxidizer used in combustion and, if air is used as an oxidizer, dilutes the produced gas with nitrogen, lowering the heating value. Indirect heating involves combustion taking place outside of the gasifier space, with the energy then needing to be transferred to the feedstock being gasified. This method has the advantage of the combustion products being in a separate stream from the gasification products, which allows cheap oxidizers like air to be used, but has increased resistance to energy transfer resulting in possible efficiency

losses. The flow and bed types of a few common gasifier types are described below along with some of their other features and advantages and disadvantages.

Updraft Gasifiers

As the name implies the flow of gas in an updraft gasifier is from the bottom to the top. These are also known as counter current gasifiers because the feed comes in the top and moves in the opposite direction of the gas [6]. These are a type of fixed bed gasifier, which means that the feedstock forms a bed which moves very little, it only moves down to replace consumed feedstock below. As can be seen in the schematic of an updraft gasifier, figure 1.1, feedstock enters the top and slowly moves down as the feedstock below is consumed. Air or another oxidizing agent such as steam enters at the bottom and moves up through the bed reacting along the way.

The bed may be separated into four zones from the bottom up: the hearth or oxidizing zone, the reduction zone, the distillation or pyrolysis zone, and the drying zone [6]. In the hearth zone the oxidizing agent, often air, oxidizes the remains of the feedstock at the bottom of the bed providing the energy for the rest of the reactions though heat transfer through the bed and through the hot gases moving towards the gas outlet at the top. Above the oxidizing zone is the reduction zone, where the oxygen content is limited and remaining oxygen is reduced to CO by the carbon in the feedstock while also producing H_2 as shown above in equation 1.1. Above the reduction zone, the feedstock undergoes pyrolysis releasing CO, H_2, CH_4 and larger hydrocarbons. The hot gases moving up through

the bed are cooled to below pyrolysis temperatures near the top, but are still hot enough to dry the incoming feedstock.

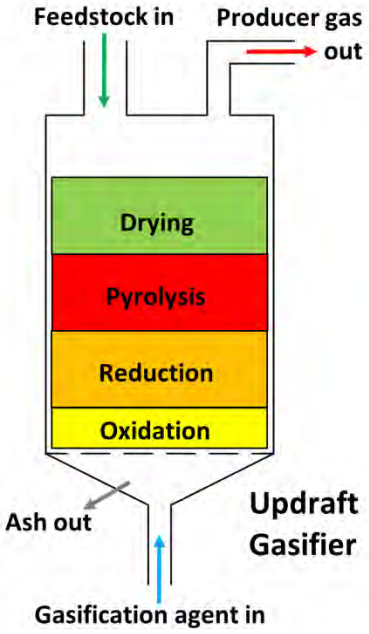

Figure 1.1- Schematic of updraft gasifier

The major advantages of this type of gasifier are the simplicity of the design making it easier and less expensive to build and operate as well as being able to use a variety of feedstocks [6]. The disadvantages of updraft gasifiers include the high occurrence of tunneling in the bed [6], as well as the poor quality of producer gas due to the large amount of tars present [5]. Tunneling is when the bed does react evenly and a vertical tunnel forms allowing oxygen to reach the top, potentially causing an explosion. This may be alleviated by a moving grate which shakes the bed to collapse voids before they form tunnels. The large amount of tar present in the produced gas is a result of the pyrolysis products not passing through a higher temperature region to reform the larger hydrocarbons into CO and

H_2. The producer gas may be reformed after it exits the gasifier to remove tars, or combusted before the tars condense.

Downdraft Gasifiers

Like updraft gasifiers, downdraft gasifiers are considered fixed bed. They are also known as concurrent gasifiers because the gas flow moves in the same direction as the feed. As can be seen in the schematic of a downdraft gasifier in figure 1.2, the feedstock and secondary air enter the top of the gasifier, while primary air enters the gasifier in the oxidation zone. The secondary air helps to dry the fresh feedstock, before moving through the rest of the bed [7]. The reactions that take place in the various zones are similar to those taking place in updraft gasifiers but they do not have the benefit of the hot gases which move up in an updraft gasifier. The primary air enters in the oxidation zone, oxidizing the feedstock to produce heat which drives all of the other reactions. The biggest difference between updraft and downdraft gasifiers is that in a downdraft gasifier all of the gases produced in earlier stages, flow through the hot oxidizing and reduction zones reforming the majority of the tars [5]. This lack of tars in the producer gas is one of the major advantages of downdraft gasifiers, while some disadvantages include the requirement of having a more processed feedstock, and the need to recover energy from the high temperature producer gas exiting the gasifier [5]. An example of a downdraft gasifier is the CPC BioMax gasifier which is described in section 1.2.4.

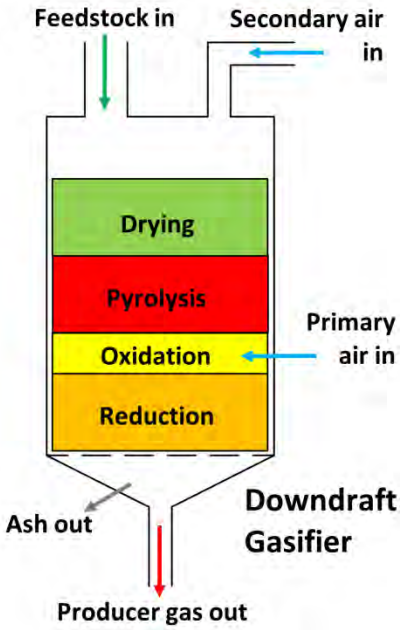

Figure 1.2- Schematic of downdraft gasifier

Fluidized Bed Gasifiers

In order to improve heat transfer so that the throughput may be increased, some gasifiers, known as fluidized bed gasifiers, force a fluidizing agent through the bed, mixing it. The bed is made up of the feedstock as well as a bed medium such as silica or alumina. The fluidizing agent is usually air, steam or oxygen, sometimes mixed with an inert gas. If the fluidizing agent is put in at a lower velocity, so that the bed bubbles gently, it is known as a bubbling fluidized bed. If the velocity of the fluidizing agent is higher and throws the bed and bed medium, if used, violently around the gasifier it is known as a circulating fluidized bed [5]. Circulating fluidized bed gasifiers have a cyclone separator at the exit which separates the gases from the unreacted chars and bed medium and re-circulates these

solids back into the bed. Fluidized bed gasifiers can be heated either directly or indirectly as described earlier. The advantages of fluidized bed gasifiers over fixed bed gasifiers are the increased heat transfer rates, which lead to higher throughput, and greater flexibility of feedstocks [6]. The major disadvantages include high tar content in the producer gas and the high level of particulates in the producer gas, as well as the large amounts of energy needed to fluidize the bed [6].

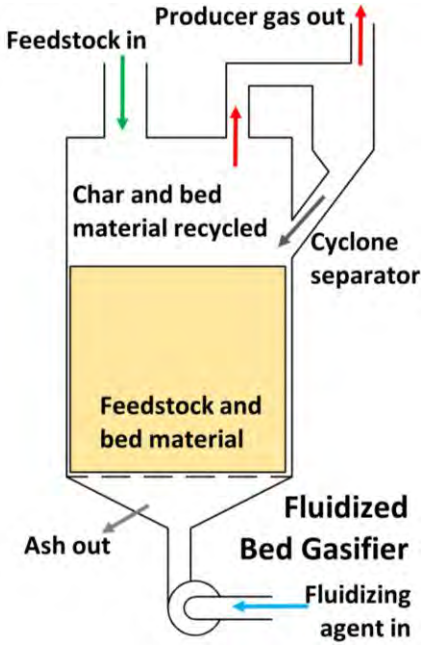

Figure 1.3- Schematic of fluidized bed gasifier

Molten Metal Gasifiers

Molten metal gasifiers are uncommon and few have made it to the commercial stage, however, they will be described as they are the focus of this study. A molten bath gasifier may be thought of as a fluidized bed gasifier with the solid alumina or silica bed

medium replaced by a molten metal. Since the molten metal is a fluid, it does not require a fluidizing agent to be blown through it. The possible advantages of a molten metal gasifier include high heat transfer from the metal to the feedstock due to the high thermal conductivity of molten metal. Another possible advantage is the use of the molten metal as a catalyst as in the HydroMax gasifier described below [8]. Disadvantages include the high cost of some molten metal alloys, the high temperatures required to keep the metals molten, and material compatibility issues between the metals and their containers.

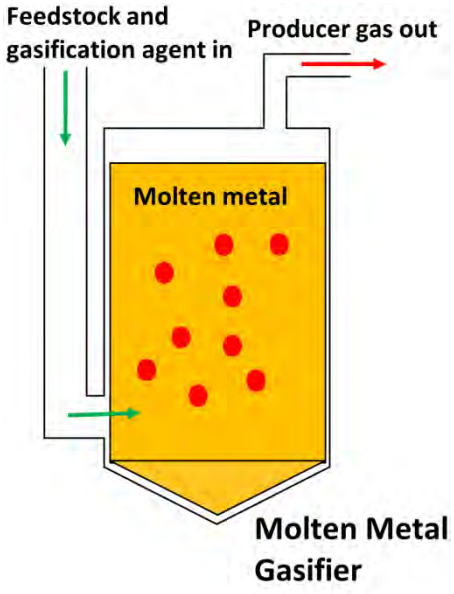

Figure 1.4- Schematic of molten metal gasifier

1.2 Current Technology

The following is a review of four thermochemical methods of converting biomass energy into a more usable form. The first is a lead bath pyrolysis unit designed in the 1970s to pyrolyze municipal solid waste that has since been abandoned. The second is a molten

iron gasifier that is currently being tested at the laboratory scale. The third is a solid oxide fuel cell that uses molten tin as the anode which is undergoing pilot scale testing. The third is a downdraft gasifier which is in commercial production.

1.2.1 Barber Coleman Lead Bath Pyrolysis Unit

In 1975 the Resource Recovery Systems division of Barber Coleman Company built and tested a pyrolysis system that utilized molten lead as a heat transfer medium. This pilot scale unit consisted of a moving lead bath held at 760°C that was used to convert simulated municipal solid waste (MSW) into gaseous fuels. The waste was fed into the lead pool by a screw feeder. The material then floated on the pool while being heated from above by radiant heaters and from below by the molten lead. At the end of the pool the remaining solids were removed and stored for sorting and disposal while the gases were collected, analyzed and flared. This system has a reported efficiency of 60% with 25% moisture content in the feed. [9]

The Barber Coleman lead bath pyrolysis system reportedly produced about 65% by volume H_2, CO, and CO_2, 20% CH_4 and 15% larger order hydrocarbons [9]. This reactor appears to be primarily limited by heat transfer to the feedstock floating on the lead bath. While the material is in the reactor it is floating on top of the lead bath and is heated from below by it, while also being heated from above by radiant heaters. So, at higher feed rates the thickness of the feedstock is greater and the center is heated much more slowly than the top and bottom. This limiting factor prevented large amounts of char from being

converted on the first pass, slowing the overall throughput and probably making the system uneconomical.

1.2.2 HydroMax Molten Iron Gasifier

Diversified Energy of Gilbert, Arizona is developing a gasifier that has its origins in iron ore smelting which they are calling HydroMax [8]. This technology utilizes an iron-tin alloy as an energy carrier and catalyst. According to Eatwell-Hall the tin does not take place in any reactions and is only present to reduce the melting point of the alloy [10]. The reactor is a refractory lined vessel containing the iron-tin alloy at a temperature of 1300°C and pressures from 1 to 3 atmospheres [8]. The reactor is cycled between an oxidation reaction and a reduction reaction to produce hydrogen gas, carbon monoxide and carbon dioxide. During the oxidation stage, superheated steam is injected into the molten metal forming primarily hydrogen gas and FeO. Then, carbon or a carbon containing feedstock like coal or biomass is injected into the reactor. The carbon then reduces the FeO to pure iron and forms carbon monoxide and carbon dioxide gas as well as some hydrogen if the feedstock was biomass or another hydrocarbon.

(1.6) Oxidation: $H_20 + Fe \Leftrightarrow H_2 + FeO$ ΔH=-21.3 [kJ/mol] ΔG=-14.1 [kJ/mol]

(1.7) Reduction: $FeO + C \Leftrightarrow Fe + CO$ ΔH=157.2 [kJ/mol] ΔG=2.6 [kJ/mol]

(1.8) Overall: $H_20 + C \Leftrightarrow H \Leftrightarrow H_2+CO$ ΔH=135.9 [kJ/mol] ΔG=-202.7 [kJ/mol]

Equations 1.6 to 1.8- Reaction system of HydroMax gasifier taking place at 1300°C and 1 atm [11]

The high operating temperature can cause material selection problems, heat loss problems and issues with introducing the carbon feedstock into the reactor. However, the high temperature also helps assure rapid carbon conversion as well as tar cracking with low residence times. And while oxidizing the melt with steam is exothermic, the oxidation of the carbon by FeO is endothermic and results in the overall process being endothermic requiring 135.9 kJ/mol of carbon [11].

1.2.3 Liquid Tin Anode-Solid Oxide Fuel Cell (LTA-SOFC)

Another promising biomass reforming technology is the liquid tin anode-solid oxide fuel cell (LTA-SOFC) invented by Dr. Thomas Tao and being developed by CellTech Power LLC of Westborough Massachusetts. A schematic of a LTA-SOFC can be seen in figure 1.5. This cell uses cathode and electrolyte materials that are common for high temperature fuel cells, namely strontium doped lanthanum magnate (LSM) for the cathode, and yttria stabilized zirconia (YSZ) for the electrolyte [12]. The novel part of this cell is the use of liquid tin for the anode and the use of a porous ceramic separator to contain the anode and separate it from the fuel source [12].

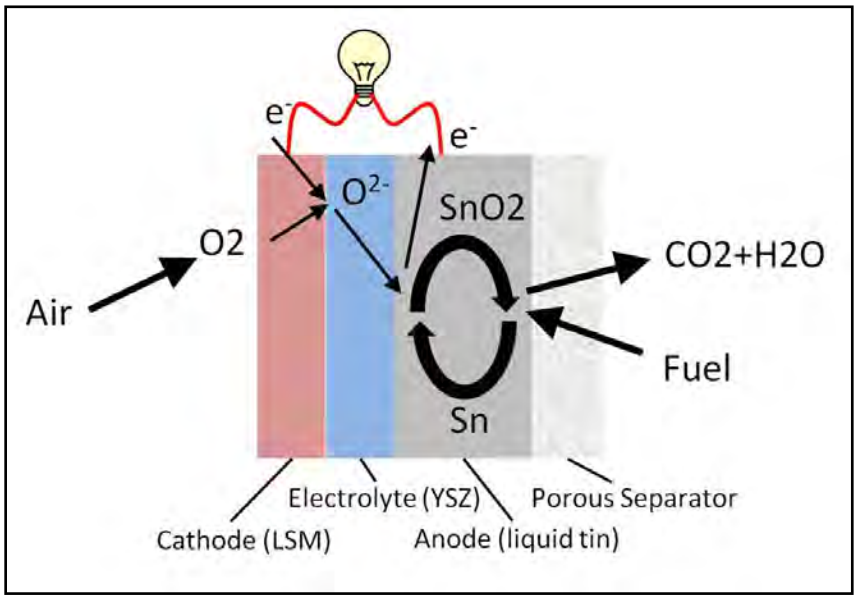

Figure 1.5- Schematic of Liquid Tin Anode-Solid Oxide Fuel Cell [13]

The entire cell is contained in a porous ceramic separator that contains the liquid tin, but allows gaseous fuels and exhaust products to pass through the 100-200µm pores [13]. Air enters the cell on the cathode side where O_2 molecules split into two O molecules and each pick up two electrons to form two O^{2-} ions [14]. The oxygen ions then travel across the YSZ electrolyte and react with tin to form SnO_2 and free electrons in the anode. This creates an electrical potential which can be used to drive a current to output electrical energy. The cell can also be operated in battery mode, where the electrical potential is allowed to build up and store energy in the cell until the circuit is closed and the energy released [15]. The oxidized tin then diffuses through the anode to the interface with the porous separator where it reacts with carbonaceous fuel or hydrogen gas to form a combination of CO_2 and H_2O exhaust gas. These exhaust gases diffuse away from the cell through the porous separator where they are eventually vented.

The system can be adequately described by three reactions; the cathode half reaction, the anode half reaction and the fuel oxidation reaction as described in equations 1.9 to 1.11.

(1.9) $O_2 + 4e^- \rightarrow O^{2-}$ Cathode Half Reaction

(1.10) $Sn + O^{2-} \rightarrow SnO_2 + 4e^-$ Anode Half Reaction

(1.11) $SnO_2 + C_xH_y \rightarrow Sn + (y/2)\ H_2O + xCO_2$ Fuel Oxidation Reactio

Equations 1.9 to 1.11- LTA-SOFC system reactions [12]

Natural gas, hydrogen, JP-8 and coal have all been reportedly tested in LTA-SOFC systems [13]. The cell operates at 1000°C, so solid and liquid fuels will volatize outside the porous separator and decompose into simpler, gaseous hydrocarbons through pyrolysis and gasification processes [13]. It is these gaseous hydrocarbons that then diffuse through the porous separator and react with tin dioxide at the anode. The process and thermodynamics are different for each fuel, but using methane as a generic fuel source for a simple thermodynamic analysis is appropriate.

(1.12) 2 Sn + 2 O2 ⇔ 2 SnO2 ΔG = -608 [kJ/mol], ΔH = -1138 [kJ/mol]

(1.13) CH4 + 2 SnO2 ⇔ Sn + CO2 + 2 H2O ΔG = -192.3 [kJ/mol], ΔH = 335.9 [kJ/mol]

Equations 1.12 and 1.13- Thermodynamics of LTA-SOFC cell reactions at 1000°C using methane as fuel [11] [16]

Because both Gibbs free energy changes are negative it is apparent that the process is product favored at 1000°C. The net enthalpy change for the two reactions, based on one mole of methane, is -1138 + 335.9 = -802.1 [kJ/mol], so the system does not require additional heat input, and in fact releases a significant amount of energy.

A benefit of this system over combustion and gasification systems is that it directly produces usable heat and electricity without the need for steam boilers and turbines or other generation equipment. Because of this, and the ability of the LTA-SOFC to use multiple fuel sources, it has the potential to be a compact and portable electrical and heat generation unit.

1.2.4 Community Power Corporation BioMax Gasifier

A common problem when dealing with biofuels is that the high transportation costs from the harvest site to the energy conversion plant prevent the fuel from being economical if it is shipped more than about 50 miles [17]. This estimate can vary widely depending on the material, fuel costs and local infrastructure available (roads, rail or barges). This limited shipping area suggests that in some cases a distribution of many smaller energy conversion plants may be more economical than large regional plants.

One company that is developing small biofuel plants that can be deployed locally is the Community Power Corporation (CPC). They make 25, 50 and 75 kWe (kilowatts of electricity equivalent) units and have in the past make 5, 10 and 15 kWe units. The units consist of a feed drying and delivery system, gasifier, gas cooling, gas cleaning and energy

conversion units. The gasifier is a an air blown downdraft gasifier and the energy conversion unit is either an internal combustion engine and electrical generator, a gas burner, a catalytic system to produce liquid fuels, or a combination.

CPC calls their gasifier technology BioMax. The unit can accept a feedstock of woodchips or pellets which can be dried in the feed system by heat recovered from the gas exiting the gasifier. The feedstock is augured into the top of the gasifier automatically. Also entering the top of the gasifier is the secondary air which is being drawn in by a downstream blower. The feedstock is then further dried by heat released from the reactions occurring below, and releases water vapor which travels with the secondary air down through the gasifier. Further down the feedstock is heated to around 600°C and pyrolysis occurs releasing volatiles and tars and leaving solid char. Below this, the primary air is introduced which oxidizes some of the char, tar and volatiles which produces carbon dioxide and heat which increases the temperature to around 800°C. Below the oxidation region is the reduction region. In the reduction region the char is gasified by the remaining oxygen (reducing the oxygen) from the secondary and primary air, as well as from the steam produced from the water vapor released in the drying region above. These reactions produce primarily hydrogen, carbon monoxide and methane gas along with smaller amounts of carbon dioxide and leave behind some char and ash which fall through a grate into a collection bin below. [7]

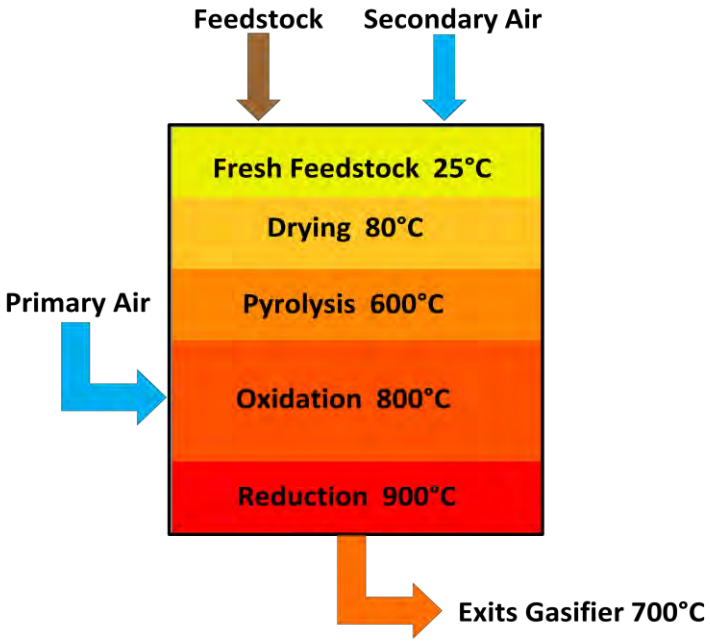

Figure 1.6- CPC BioMax Gasifier Schematic showing zones of gasifier and approximate temperatures [7]

The mixture of gas, called producer gas, leaves the bottom of the gasifier at approximately 700°C with small amounts of char and ash entrained. After exiting the gasifier the gas travels through a separator which removes most of the char and ash, through a heat exchanger that reduces the temperature to about 100°C and then through a filter. The filtered gas is then sent to an internal combustion engine, a burner or a set of reactors to convert it into liquid hydrocarbon fuels. The heat removed from the gas in the heat exchanger can be used to dry the raw feedstock or for space heating. [7]

The process is automated and controlled by a computer which monitors the process temperatures and adjusts the feed and airflows accordingly. The system is designed to require minimal input from an operator.

1.3 Literature Data

This study builds upon many others cited in the literature. The three main areas of literature data researched are the properties of molten metals, the dynamics of bubbles in molten metals and the chemical reactions expected to take place during pyrolysis and gasification of biomass in molten metals.

1.3.1 Molten Metal Properties

Many of the properties of molten tin-bismuth, which has been chosen for use in this study, are not well known and had to be found in literature. Two properties important to bubble formation and velocity relationships are surface tension and density. A 2001 paper by Moser, Gasior and Pstrus gives surface tension and density models for various alloys of tin and bismuth which were calculated from experimental data. Moser et al. compare their own experimental data with previous data cited to Zadumkin, Drath, Iida and Lang. The data is generally in good agreement, except for the data from Lang which varies from the others at higher temperatures [18]. The equations for a composition of 40% Sn and 60% Bi shown below in equation 1.14 and 1.15 were used to represent the 42% Sn, 58% Bi alloy used experimentally in this study.

$$\sigma = A - B\,(T)$$

Equation 1.14- Surface tension of tin-bismuth given by Moser with units of [mN/m], with A=450±9 [mN/m], B=0.0674±0.011 [mN/K-m], T=temperature [K] [18]

$$\rho = A + B(T)$$

Equation 1.15- Density of tin-bismuth given by Moser with units of [g/cm^2], with A=10.024±0.334 [g/cm^3], B=-0.00133±8.51e-4 [g/cm^3-K], and T=temperature [K] [18]

To calculate the thermodynamic equilibrium of many of the chemical reactions investigated in this research, it was necessary to obtain fundamental thermodynamic data including the Gibbs energy of formation and the standard enthalpy change. Most of the data was taken from the NIST-JANAF Thermochemical Tables [11]. The NIST-JANAF tables were lacking information on two key components: SnO_2 and Bi_2O_3. Kurchania and Kale give a linear relationship describing the Gibbs energy of formation of SnO_2 shown in table 1.1. The standard enthalpy change is reported by Kurchania and Kale to be independent of temperature between 860K and 1250K and equal to -569±1 [kJ/mol] [16]. As can be seen in the NIST-JANAF tables, the standard enthalpy change of metal oxides is generally nearly independent of temperature over a much larger range, so the enthalpy reported by Kurchania and Kale was extrapolated to remain unchanged from 298 K to 1500 K. Similarly, the Gibbs energy of formation of Bi_2O_3 was given by Kisimoto et al. and the standard enthalpy change of Bi_2O_3 was given by Ganesan et al., which can be found in table 1.1.

Molecule	Gibbs energy of formation	cited range [K]	Standard enthalpy change	cited range [K]	source
SnO2	-573.9+0.212(T) ±5 [kJ/mol]	860-1253	-569 ±1 [kJ/mol]	860-1250	Kurchania and Kale (2000)
Bi2O3			-568.4 ±0.5 [kJ/mol]	550-1150	Ganesan (2003)
Bi2O3	-576.5+0.2863(T) [kJ/mol]	771-1012			Kishimoto (2006)
Bi2O3	-543.4+0.2537(T) [kJ/mol]	1012-1067			Kishimoto (2006)

Table 1.1- Thermodynamic Data for tin dioxide and bismuth trioxide [16] [19] [20]

1.3.2 Bubble Measurements

In order to understand chemical reactions that are taking place inside of and at the surface of a gas bubble traveling through a molten metal it is necessary to first understand how a bubble forms and moves through a molten metal. A review of current literature data on bubble dynamics and methods for detecting bubbles in molten metal follows.

Bubble Formation Diameter

Geary and Rice describe a method of determining the size of a gas bubble when it forms in a liquid at an orifice involving a force balance on the bubble. The force balance, which can be seen in equation 1.16, involves buoyancy, gas momentum, surface tension, drag and inertial forces. On the left hand side of equation 1.16, the first term represents the buoyancy force, the second term is the gas momentum force, the third term is the surface tension force between the bubble and the orifice, and the fourth term is the drag force which depends on the bubble Reynolds number. The term on the right represents the inertial forces. When the equation becomes unbalanced, the bubble lifts off of the orifice and the equation is no longer valid [21]. With all other terms known or estimated, equation 1.16 can be solved for the bubble radius, r_H. Vafaei et al. describe a similar equation, but

with some terms ignored or offered with approximations depending on the conditions of bubble formation [22].

$$V\ \rho_L\ g + \frac{G^2 \rho_g}{\pi r_H^2} - 2\ \pi\sigma\ r_H\ \cos\theta - \ F_D = \frac{d}{dt}(\alpha\ \rho_L\ V\ U_b)$$

$$\text{With } F_D = \begin{cases} 6\ \pi\ r\ U_b & if\ Re < 1 \\ 5\ \pi \sqrt{\frac{\rho_L\ \mu}{2}}\ (r\ U_b)^{3/2} & if\ 1 \leq Re \leq 500 \end{cases}$$

Equation 1.16- Force balance on gas bubble in liquid at formation assuming $\rho_g << \rho_L$ [21] Variable definitions can be found in table 1.2.

Variable	Description	Variable	Description
V	Bubble volume	μ	Liquid viscosity
ρ_L	Density of liquid	r	Radius of bubble
ρ_g	Density of gas	U_b	Velocity of bubble
g	Acceleration of gravity	α	Virtual mass coef.
G	Gas volumetric flow rate	t	Time
r_H	Radius of orifice	F_D	Drag force
σ	Surface tension	Re	Bubble Reynolds number
θ	Gas-liquid contact angle		

Table 1.2- Description of variables in equations 1.16 and 1.17

Inspection of equation 1.16 under the conditions of very low gas flow rate leads to some simplifications. If the volumetric gas flow rate is very small, the gas momentum term

will become unimportant and can be ignored. A very low gas flow rate will also cause the velocity of the bubble (U_b) to become very small because, until the bubble lifts off, U_b can be calculated from equation 1.17 which depends on the gas flow rate. With a very small bubble velocity the drag force terms may be ignored, and the rate of change with time of the bubble volume and bubble velocity will be small so the inertial term may also be ignored.

$$U_b = \frac{G}{4\,\pi\,r^2}$$

Equation 1.17- Calculation of bubble velocity during formation of bubble [21]

Therefore, under the conditions of low gas flow rate, equation 1.16 will take the form of equation 1.18, which is described by Hernandez-Aguilar et al. as a simple model for predicting the size of a gas bubble forming in a liquid, under the additional assumption that the contact angle is also very small so that cos θ is approximately equal to one [23]. Hernandez-Aguilar et al found that the diameter of bubbles approached the value predicted by equation 1.18, but did not obtain it citing the probable significance of inertial forces [23].

$$V\,\rho_L\,g = 2\,\pi\,\sigma\,r_H\,\cos\theta$$

Equation 1.18- Simplified model for bubble size prediction equating only the buoyancy and surface tension terms [24] [23]

Equations 1.16 and 1.18 describe three different regimes of bubble formation. The first regime can be described adequately by equation 1.18 and will produce bubbles

unaffected by changes in the flow rate, with the bubble size determined by geometry and fluid properties. In the second regime, the size of the bubble can only adequately be described by all terms in equation 1.16, and will result in the bubble size being dependent upon the gas flow rate as well as the geometry. The third regime occurs when the gas flow rate becomes so large that the momentum and inertial terms of equation 1.16 are dominant and the geometry of the orifice has little effect on the bubble diameter, at this point equation 1.16 no longer holds [21].

Bubble Velocity

The flow of a gas bubble in a liquid can be described as falling into 4 different regimes as can be seen in figure 1.7. The smallest bubbles fall into the first regime in which the bubbles act like solid spheres and follow Stokes flow with very low Reynolds numbers. Slightly larger bubbles still have low Reynolds numbers but circulation inside the bubble causes the terminal velocity to be higher than predicted by Stokes flow. At a point determined by the specific system components, inertial forces on the bubble start to become significant and the flow transitions to a third regime where the bubbles are spheroids. In this regime the terminal velocity drops slightly with increasing diameter. In the fourth regime, the bubble takes on a spherical cap shape and the velocity begins to increase with diameter. [25]

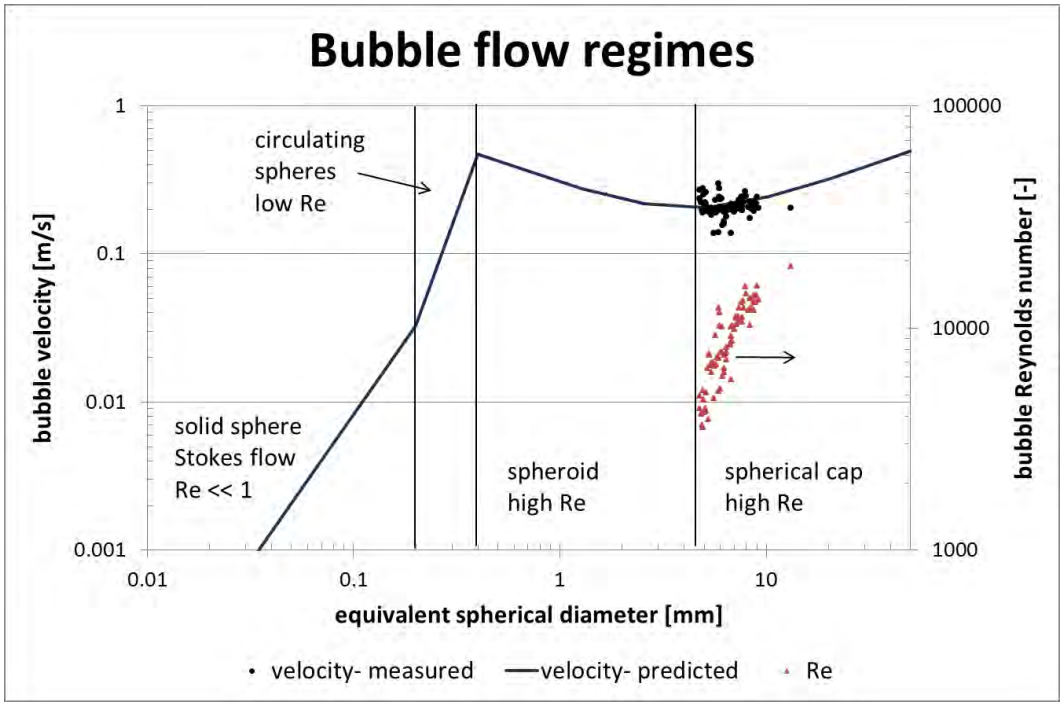

Figure 1.7- Bubble flow regimes based on shape of bubble and Reynolds number [25]

As can be seen in figure 1.7, the system in the current study has high Reynolds numbers and falls in to the spherical cap regime and is near the spheroid regime. A literature search has found a relatively simple model for the terminal velocity of a gas bubble in a low viscosity liquid that is valid in both of these regimes. This model was developed by Mendelson and can be seen in equation 1.19. Schwerdtferger presented data of 2.5 to 15 mm diameter argon bubbles rising through mercury that agrees well with Mendelson's model [26]. And, Zhang et al. present data of bubbles from 1 to 8 mm in diameter flowing through both a gallium-indium-tin alloy, as well as through mercury that agree well with Mendelson's model [27]. Although there is little data available regarding

metals at high temperature, it appears as though the model given in equation 1.19 is appropriate for use with 1-15 mm diameter bubbles rising through molten metals.

$$U_T = \sqrt{\frac{\sigma}{\rho\, r} + r\, g}$$

Equation 1.19- Model suggested by Mendelson for terminal velocity of bubble in molten metal calculated from the metal surface tension (σ), metal density (ρ), bubble radius (r), and gravitational constant (g) [25]

Bubble measurements in liquid metal

The noted absence of data regarding the velocity of bubbles rising through high temperature molten metals suggests that these measurements may not be easy to make. However, there are a few noted techniques that appear to be successful.

Schwerdtferger was able to successfully measure the rise velocity of an argon bubble in mercury using an ultrasonic pulse echo instrument that tracked the bubble's progress between two points separated by a known distance [26]. However, this was done at room temperature, and the pulse echo instrument was in contact with the mercury. The instrument would need to be adapted for use with metals at high temperature. Zhang et al. also used an ultrasonic transducer, also at low temperature [27].

Fu and Evans developed a capacitance probe to detect bubble motion based on the difference in capacitance between a molten metal and a gas bubble [28]. The probe consists of a partially exposed wire encased in a ceramic sheath that is placed in a molten

metal. The capacitance between the wire and the metal is measured; when a bubble touches the probe, the capacitance drops [28]. While this probe works at high temperatures, it is susceptible to errors if the bubble is not aligned co-axially with the probe, and the probe interferes with the motion of the bubble [28].

Schneider and Evans developed a probe that measures the pressure fluctuation caused as a bubble flows through a liquid metal [29]. The probe is simply a tube through which gas at a very low flow rate is passed. The purpose of the flowing gas is to keep the tube clear of metal. A simple microphone is installed in the line supplying the low gas flow. The bubbles resulting from the supplied gas flow cause a predictable time varying pressure fluctuation that is detectable by the microphone. As a larger bubble, the bubble being measured, passes the probe, it disturbs the steady pressure fluctuation and creates a larger signal detectable by the microphone [29]. Two of these probes could be put in a melt, separated by a known vertical distance and the time could be measured between large pressure fluctuations to determine the time the bubble takes to transit the known distance.

Along a similar line, Fu, Xu and Evans reported using a two microphone system to determine the bubble transit time through a molten aluminum column [30]. One microphone was held over the surface of the metal while the other microphone was in the line which supplied the gas to the bottom of the melt where the bubbles were formed. The microphone in the supply line detected a pulse that corresponded to the bubble leaving the orifice, while the bubble above the melt detected a pulse when the bubble arrived at the

surface. To determine the bubble transit time, gas flowing through the system was abruptly shut off by a solenoid valve. The two microphone signals could then be analyzed and the time measured between when the last bubble left the orifice, as detected with the supply line microphone, and when the last bubble arrived at the top surface, as detected by the top microphone [30]. A similar system that only employed one microphone located above the melt was employed by Andreini et al. in tin, lead and copper melts. Instead of measuring the time between the ends of two microphone signals, Andreini et al. measured the time between the solenoid valve being shut and the arrival of the last bubble at the top of the melt [24]. These microphone methods are robust, inexpensive, easy to implement and do not interfere with the motion of the bubble.

1.3.3 Chemical Reactions

In the literature there are several examples of chemical reactions similar to those expected to take place between the gases of interest and molten tin-bismuth. The three areas of greatest interest are methane reforming, oxidation of the molten metal and reduction of the oxidized molten metal. The following is an overview of some of the available literature data regarding these reactions.

Methane Reforming

In this study methane is being used as a simple model hydrocarbon representing the products of wood pyrolysis. As such it is important to understand how methane behaves in

reactions without catalysts to use as a baseline for comparison with its behavior in a molten metal system.

A 1968 paper by Palmer, Lahaye and Hou describes the kinetics and mechanism of the thermal decomposition of methane, un-catalyzed in a flow system. They study the temperature range 1050 to 1250°C with residence times up to 1 second. They concluded that methane decomposition under these conditions may best be expressed as a first order rate law with the rate constant given in equation 1.20, and the equation for the concentration of CH_4 at time t given in equation 1.21 [31]. They also suggest a mechanism as shown in equations 1.22 to 1.24.

$$k = \exp\left[14.6 - \frac{22.5 \times 10^8}{T}\right]$$

Equation 1.20- Rate constant of thermal methane decomposition proposed by Palmer with k having units 1/sec and T being temperature in Kelvin [31]

$$[CH_4] = -kt + \ln([CH4]_0)$$

Equation 1.21- First order rate law giving concentration of CH4 with [CH4]o being the initial concentration of methane, k being the rate constant described in equation 1.20, and t being the time of the reaction in seconds

(1.22) $CH_4 \rightarrow CH_3 + H$

(1.23) $CH_3 \rightarrow C(s) + \frac{3}{2} H_2$

(1.24) $(CH_3, CH_4) \rightarrow (C_2H_6,\ C_2H_4,\ C_2H_2)$

Equations 1.22 to 1.24- Mechanism of methane thermal decomposition suggested by Palmer, Lahaye and Hou [31]

Metal Oxidation

There are many examples of metal oxides being used as catalysts in hydrocarbon, hydrogen and carbon monoxide combustion and reforming [13] [10] [32] [33]. Before studying the reduction of metal oxides, first it must be determined what oxides can be formed and at what conditions.

A paper by Yuan, Yan and Simkovich studied the oxidation of tin and tin alloys with oxygen at temperatures from 600 to 800°C. They found that only tin dioxide (SnO_2) was formed but noted that tin monoxide (SnO) was probably an intermediary in the overall oxidation, equation 1.25, but decomposed according to equation 1.26 [34].

$$Sn + O_2 \rightarrow SnO_2$$

Equation 1.25- Overall oxidation reaction of tin [34]

$$2\,SnO \rightarrow SnO_2 + Sn$$

Equation 1.26- Decomposition of metastable SnO to SnO_2 [34]

In a study of the bismuth-oxygen phase equilibrium system, Risold et al. found that bismuth trioxide (Bi_2O_3) is the only stable bismuth oxide in the presence of liquid bismuth

[35]. Furthermore, Kishimoto et al. and Kurchania et al. determined the standard Gibbs free energy of formation of Bi_2O_3 and SnO_2 respectively, so that it may be predicted which oxide will form preferentially [19] [16]. As seen in figure 1.8, the free energy of formation of tin dioxide is lower than that of bismuth trioxide over the range of temperatures of interest, suggesting that tin dioxide will form preferentially over bismuth trioxide.

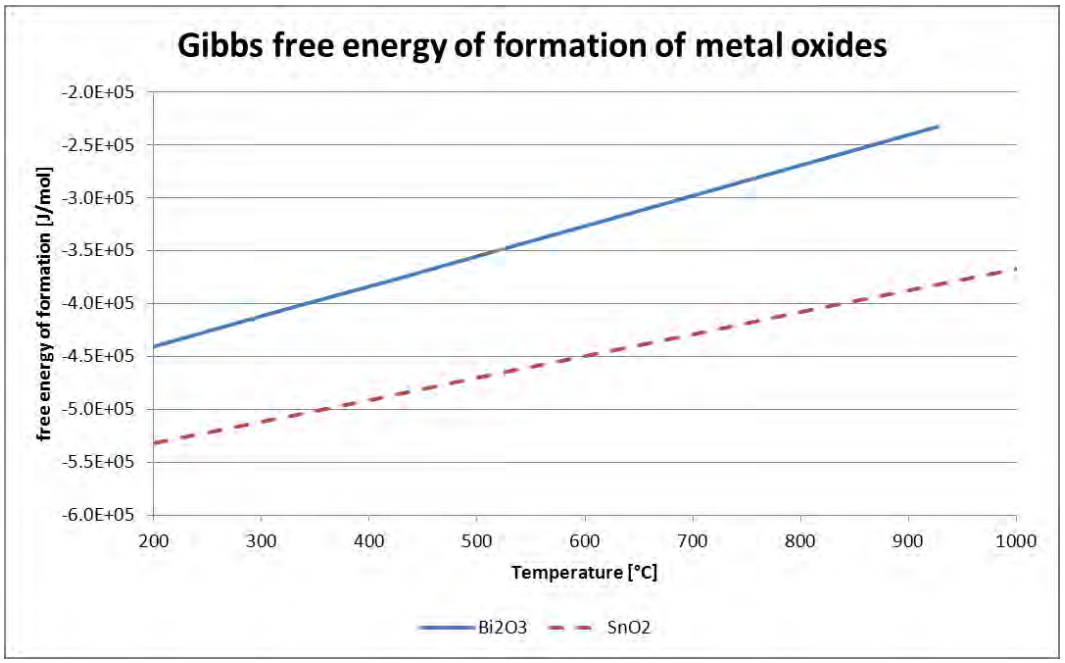

Figure 1.8- Free energy of formation of tin dioxide and bismuth trioxide, calculated from data by Kurchania and Kishimoto respectively [16] [19]

Tin Reduction

Considering the previous discussion, the focus of the discussion of metal oxide reactions now shifts to the reduction of tin dioxide. Two reducing agents will be discussed: carbon monoxide and hydrogen.

According to Van Deventer, the smelting of tin from its primary ore (Cassiterite) is generally done by reducing the ore, which is primarily SnO_2, with carbon as described in equation 1.27 and 1.28 [36]. The overall process uses carbon monoxide as an intermediary, so it stands to reason that the second part of the process, equation 1.28, should proceed alone if it had a source of carbon monoxide. Van Deventer measured only about 80% conversion of tin dioxide at 967°C with a 120 minute reaction time, and the same 80% conversion being obtained in under 10 minutes at approximately 1160 °C [36].

(1.27) $$C + CO_2 \rightarrow 2\ CO$$

(1.28) $$SnO_2 + 2\ CO\ \rightarrow Sn + 2\ CO_2$$

Equations 1.27 and 1.28- Tin dioxide reforming process [36]

Wierzchowski and Zatorski found that tin dioxide supported on alumina is an effective catalyst for the oxidation of carbon monoxide and methane at temperatures between 350 and 600°C [37]. They measured a rate of CO oxidation with SnO_2 and O_2 of $2x10^{-6}$ mol/min at 350°C and 0.08 atm of CO, with the rate decreasing with carbon monoxide partial pressure [37]. They found the rate to be independent of oxygen partial pressure.

Kim, Lee, Yoon and Kim investigated the reduction of tin dioxide by hydrogen gas in the temperature range 500-750°C. The reaction, shown in equation 1.29, was found to be thermodynamically favored to reduce tin dioxide above 550°C [32]. It was found that nearly 100% of the tin dioxide powder was reduced to tin in 10 minutes at a temperature of 750°C and hydrogen partial pressure of 1 atm [32]. Kim et al. found that the reaction was approximately first order with respect to hydrogen partial pressure using the apparent rate constant found in equation 1.30.

$$SnO_2 + 2\,H_2 = Sn + 2\,H_2O$$

Equation 1.29- Reduction of tin dioxide by hydrogen gas [32]

$$k_{apparent} = 1.76\ \times 10^{-1} exp(-7517.1/T)\ p_{H2}$$

Equation 1.30- Apparent first order rate constant ($k_{apparent}$) for reduction of tin dioxide with hydrogen gas as a function of temperature in Kelvin (T) and partial pressure of hydrogen (p_{H2}) [32]

2. Proposed molten metal gasifier

A patent was awarded to Dietenberger and Anderson in 2011 for an apparatus to produce synthesis gas via pyrolysis and gasification within a molten metal or liquid salt [38]. A general description of the apparatus follows. Wet biomass is inserted into a molten medium bath which is held at a temperature above 100°C, but below the degradation temperature of the biomass. This low temperature melt is used to remove the water from the biomass to prepare it for fast pyrolysis and gasification in a second melt held at a much higher temperature, approximately 600-1000°C. When the biomass is transferred into this high temperature melt it will undergo fast pyrolysis resulting in volatiles being released forming a char. The gases and char then move to a third section where gasification of the char and further cracking of the pyrolysis products occur resulting in primarily carbon monoxide and hydrogen exiting the reactor with little or no solid char remaining. The steam resulting from the drying of the biomass is to be collected and inserted, potentially along with other gases, into the melt at various places to aid in gasification.

2.1 Description of Proposed System

The choice of molten medium is an important one. Most importantly, the material must be liquid and have a low vapor pressure between 200°C and 1000°C to be useful in this design. Additionally, the material must not be prohibitively expensive, so alloys containing large amounts of gold, silver, gallium, thallium and indium were ruled out. Lithium and lead containing alloys were also ruled out for safety and toxicity concerns. Finally, the eutectic

alloy of 42% tin and 58% bismuth (by molecular composition) was chosen which melts at 138C.

The chosen tin-bismuth alloy is not without its problems. The foremost problem with the alloy is that nickel and other common components of 300 series stainless steels go into solution in tin. Previous experience has shown that there can be a significant reduction in the wall thickness of 316 stainless steel vessels containing tin-bismuth mixtures at temperatures at or above 800°C. However, an experiment at 350°C where various stainless steel alloys were left in molten tin-bismuth for 67 hours showed no measurable change in the samples.

A schematic of the proposed system is shown in figure 2.1. The reactor is required to maintain a temperature of 1000°C and pressure of 690 kPa. These parameters will allow for a wide range of tests to be performed.

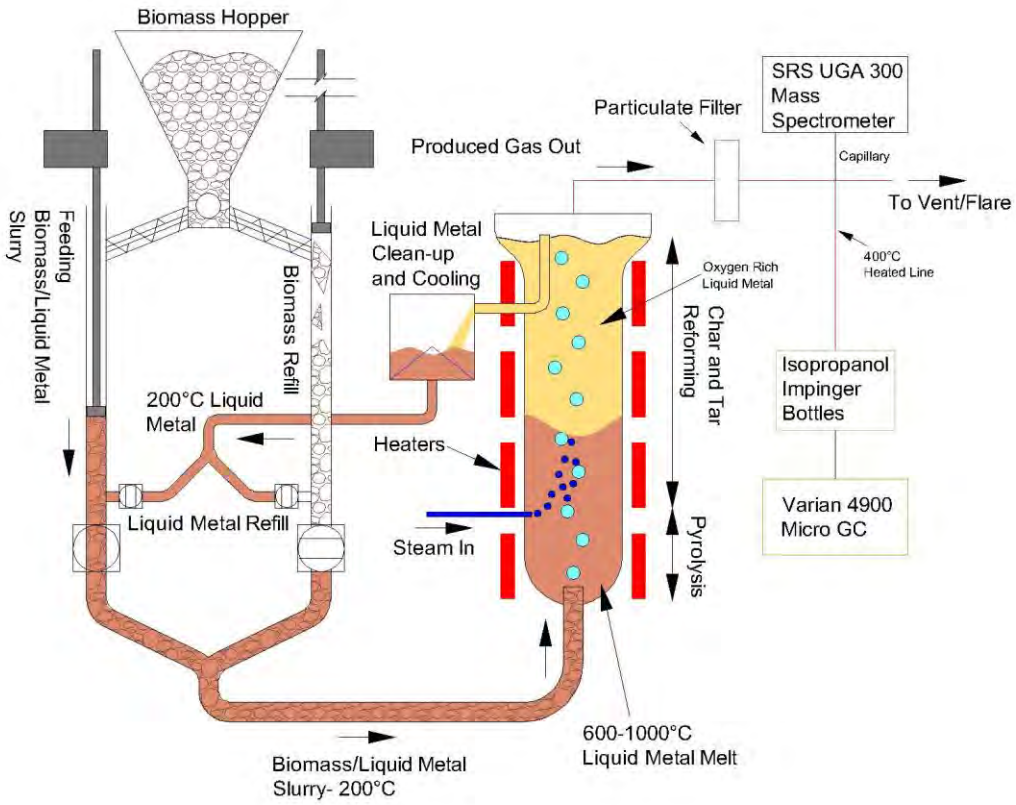

Figure 2.1- Schematic of proposed molten metal gasifier

The feed system will consist of screw driven plungers which reciprocate such that one of the plungers will feed biomass while the other is refilling so that the system will be continuously fed. A typical feed sequence will start with the plunger retracting past the biomass inlet with the valve at the bottom of that feed tube being closed. Then, wet biomass will be fed into the tube from a hopper by an auger. When the appropriate amount of biomass is in the pipe, the plunger will retract below the biomass feed inlet, sealing the biomass from the outside environment. Next, 200°C molten metal will be allowed into the tube and will mix with the wet biomass. The wet biomass and the hot

metal will interact to dry the biomass forming steam, which will react with the molten tin to form hydrogen gas and tin dioxide. The hydrogen gas and leftover steam will be collected for further use or vented. The outside of the feed pipe will be lined with heaters to maintain the temperature above the melting point of the tin-bismuth. When the biomass-tin reaction stops releasing gas, this feed tube will be ready to feed, and will wait for the other to complete its cycle. When the other feed tube has completed its cycle, the valve below the full tube will open, and the plunger will begin to advance at the set feed rate. The plunger will continue until it is at the end of its stroke at which point the valve will close and the plunger will retract to make ready for its next filling cycle. Meanwhile the other cylinder will have been filled and will begin feeding.

The slurry of molten metal and woodchips will be pushed by the feeding system through a junction of the two feed tubes, and into the bottom portion of the reactor. The bottom of the reactor is designed to be made of 304ss, and held to less than 800°C. In this stainless steel piece, the incoming slurry will be heated from its feeding temperature of 200°C up to the reactor temperature or 800°C, whichever is less. The majority of the temperature change must take place here to minimize the thermal stresses on the high temperature reactor walls which will probably be a refractory material such as alumina.

As the slurry reaches the bottom of the reactor it will rise buoyantly from the bottom of the reactor to the top. While it is rising it will be rapidly heated to the reactor temperature, up to 1000°C. The biomass should then pyrolyze and release large amounts of gas. At various points in the reactor, steam, hydrogen or other gases may be inserted to aid

in the gasification of the biomass char and adjust the composition of the produced gases. Also, the tin dioxide that was produced while drying the biomass may help gasify the char.

Due to material compatibility issues associated with molten tin, and the severe heat and moderate pressures required, the reactor body will need to be made of a refractory material such as alumina or mullite. However, further material selection tests need to be performed. The reactor is designed to attach to the feed system by means of a compression seal. The ports at the top will be similar. It is estimated that the reactor will need approximately 20kW of electric heat to supply the required energy to heat up the incoming biomass-metal slurry as well as to provide adequate energy to drive the pyrolysis and gasification reactions and offset any parasitic heat losses as predicted by a simple heat and mass transfer model.

It is expected that by the time the biomass reaches the top of the reactor it will have fully gasified, however, some ash and possibly some char may remain. These solids, as well as enough molten metal to maintain the systems height will flow out of the top of the reactor and into the cooling and clean-up loop. There will be a large vessel maintained at approximately 300°C. This vessel will be used to separate the molten metal from the remaining solids by means of floatation. Since char as well as all of the ash components will float on molten tin-bismuth, as long as sufficient molten metal is maintained in the cooling vessel, clean metal can be drawn off the bottom. This vessel will periodically need to be opened and have the solids manually removed. In larger versions, this step may be automated, but cost and complexity requires that this be done manually at this stage.

From the cooling and clean up vessel, clean metal will be further cooled in a heat exchanger to 200°C. This metal will then be recycled into the feed system.

2.2 Problem Statement

There are several fundamental questions that need to be answered before the design of this continuous flow pyrolysis and gasification system can be completed. As noted previously in the literature review, very little kinetic data can be found regarding the reaction of biomass, producer gas or char with tin-bismuth. Also, little data can be found regarding the role that tin oxide will play in these reactions. This information is required to determine the required residence time, and thus the height of the reactor, as well as advantageous places in the reactor to insert additional gases like steam or hydrogen to aid in gasification of the char. For this reason, a study was proposed to determine key reaction rates in molten tin-bismuth at the expected operating conditions of this continuous system.

The primary reactions of interest are oxidation of tin-bismuth by water or air, reduction of tin-bismuth by hydrogen and carbon monoxide, decomposition of methane in the presence of pure tin-bismuth and in the presence of tin oxide. Furthermore, this experiment will allow for experience to be gained in working with high temperature molten tin-bismuth on a smaller and less expensive scale than the proposed gasification experiment allowing for materials and methods to be tested.

3. Facility

A system has been designed to allow for various gas reactions to take place in a bubble rising through a column of molten tin-bismuth which can be heated up to 1000°C. The system is divided into several subsystems that meter the desired reactants into the reactor, contain and control the flow of the molten tin-bismuth, collect and analyze the gases produced from the reactions and collect all manner of data concerning the entire process. A description of the design and function of this system follows.

3.1 Required Measurements

There are 5 fundamental measurements that need to be made to determine the kinetic rates of reactions occurring among the gases and molten metal.

1. The gas composition entering the reactor
2. The residence time of the gas in the molten metal
3. The gas composition exiting the reactor
4. The size of the interface between the gas and metal
5. Temperature of the reaction
6. Pressure of the reaction

The composition of the gas entering and exiting the reactor is measured with a combination of a quadrapole mass spectrometer and a relative humidity meters. Large amounts of water vapor are not readily measured with a mass spectrometer, so relative humidity meters along with the necessary temperature sensors are utilized to determine

the water content of the gas, before the water is removed and the gas sampled by the mass spectrometer.

The temperature of the reaction is assumed to be the same as the temperature of the molten metal. The temperature of the metal is measured with a K-type thermocouple inserted into the melt.

According to simple hydrostatics the pressure of the reaction will vary linearly with the height of the bubble in the molten metal. The pressure at the bottom of the molten metal melt is approximated as the pressure of the gas in the line entering the bottom of the reactor, which is measured with a pressure transducer. The pressure above the melt is measured in a similar manner. Then the pressure of the reaction is linearly interpolated based on the location of the bubble in the melt.

The measurement of the residence time of the gas bubble in the melt is somewhat more complicated. The problem is confounded by the opacity of the molten metal, which makes simple optical measurements impossible. As noted in the literature review there have been several different methods developed for measuring the velocity of bubbles in liquids. The most simple and promising technique noted in the literature review is the use of microphones to detect the departure of the bubble from the orifice and the arrival of the bubble at the melt surface. The current study use a two microphone system very similar to the one used by Fu, Xu and Evans as described in section 1.3.2. This system includes a microphone located above the melt which detects both the bubble departures from the

orifice and their arrivals at the top, and a second microphone located in the gas supply line that detects the bubble departures from the orifice.

To determine the accuracy of the microphone system a simplified version of the molten metal kinetic experiment was built that used water instead of molten metal, and a clear plastic tube instead of ceramic tube. This facilitated the use of optical measurements to determine the timing of the bubble release from the orifice and arrival at the top surface as compared to microphone signals in the input line and above the melt. Different placements of the microphone were tested to arrive at an optimal location to hear the signals. It was found that with the microphone located above the surface, a peak occurred in the microphone signal when the bubble left the orifice, and when the bubble hit the surface another, smaller peak occurred in the signal. Similar results are found with a microphone in the orifice line, but with different relative magnitudes. The timing of these peaks with the release and arrival of the bubble was verified through imaging with a high speed camera operating up to 1000 frames per second. It was determined that the release peak occurred within 1 frame or 1/1000 of a second of the bubble release, and similarly for the arrival. When this microphone setup is transferred to a liquid metal melt, it was found to produce similar peak patterns. The association between the microphone peaks and the bubble release and arrival is assumed to be the same. The residence time of the bubble is then determined by measuring the amount of time between release and arrival peaks in the microphone signal, which is described in further detail in section 4.1.1.

The size of the interface between the gas and the molten metal is calculated based on several measurements and assumptions. The gas flow rates entering the system are measured by rotameters. The temperature and pressure are measured at the rotameter and at the entrance to the reactor. This data allows for the calculation of the volumetric flow rate of gas into the bubble. The microphone measurements allow for the calculation of the bubble release frequency. The volume of each bubble can then be calculated from the volumetric flow rate and the bubble release rate. The equivalent spherical diameter and surface area of the bubble area are then calculated. These assumptions and measurements are discussed further in section 4.1.

Based on making these 5 measurements a test setup was developed as can be seen in figure 3.1. Due to the high temperature and pressure of the molten metal system and the use of explosive gases, the reactor and molten metal handling system are all held in a room separated by a concrete wall from the room containing the controls and operator of the experiment. The system can be divided into 4 sub-systems:

1. Gas Preparation
2. Reactor
3. Gas Analysis and Venting
4. Molten Metal Handling

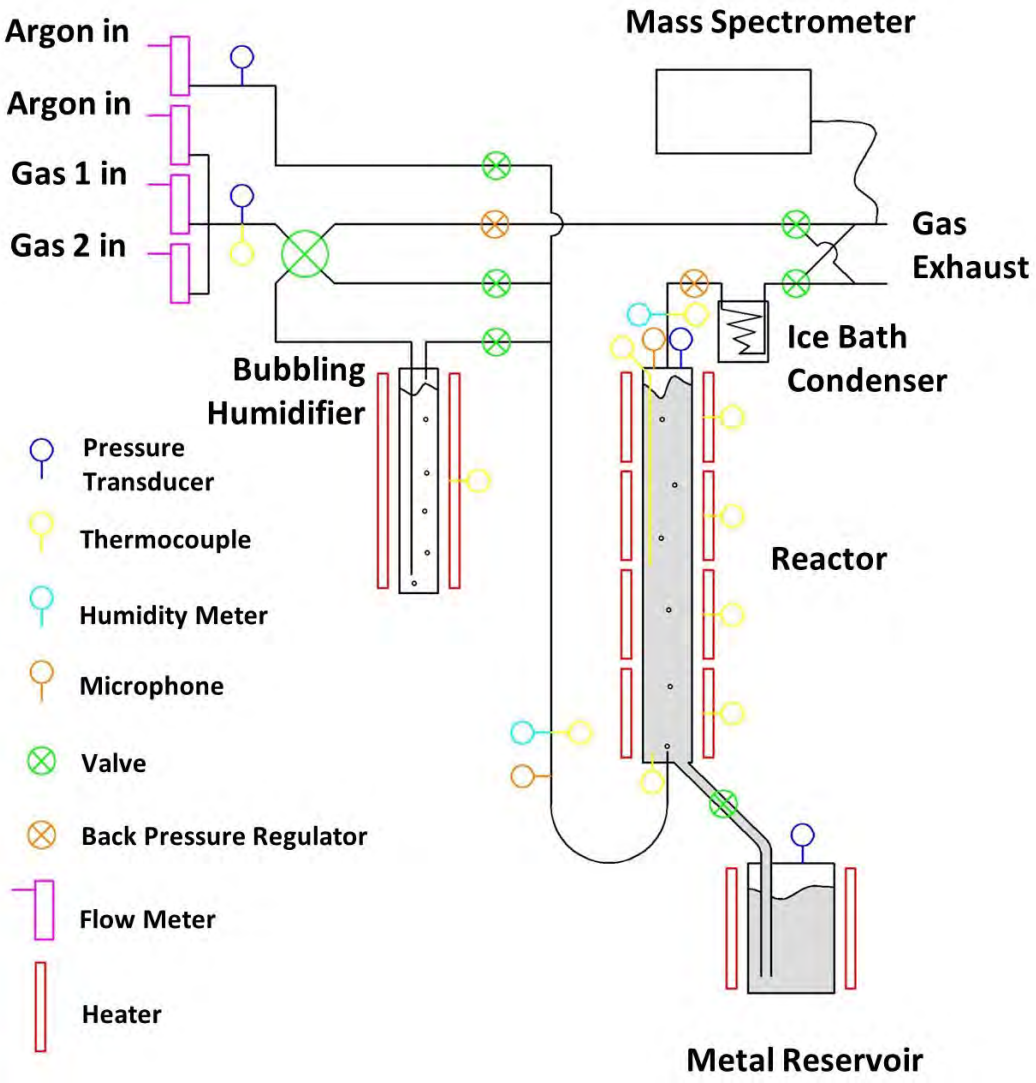

Figure 3.1- Schematic of facility

3.2 Gas Preparation

The gas preparation subsystem regulates the flow of the different gases into the system and diverts the flow to different locations. When molten metal is in the reactor, there must be a constant flow of gas through the bubble injector to prevent it from clogging. For this reason there must be multiple gas circuits that can run independently so

that smooth transitions may be made between different gas mixtures and sources. One circuit allows pure argon gas to be sent directly to the bubble injector in the bottom of the reactor, or through the bubbling humidifier and then to the bubble injector. The bubbling humidifier is simply a column of heated water through which the gas stream is bubbled. Adjusting the temperature of the water controls the water vapor pressure in the exiting gas stream. The second gas circuit contains a mixture of gases. The mixture of the gas is controlled by rotameters in each gas line. After passing through the rotameters, the gases are mixed, pass by a thermocouple and pressure transducer, then go through a diverting valve. The diverting valve can send the mixed gas directly to the sampling circuit, directly to the bubble injector in the bottom of the reactor, or through the bubbling humidifier and then to the bubble injector. Remotely controlled valves control the flow of the input gas. When the bubbling humidifier is in use, the section of tube carrying gas from the exit of the humidifier to the bottom of the injector is heated to above the temperature of the humidifier to prevent condensation of the vapor. Just prior to entering the reactor the gas passes by a relative humidity meter and thermocouple so that the water vapor content of the mixture is known prior to reaction.

3.3 Reactor

The reactor wall is a mullite (alumina oxide and silicon dioxide) tube. The tube has an inner diameter (ID) of 20 mm, an outer diameter (OD) of 26 mm and a length of approximately 890 mm. The ends of the tube are fitted with custom made 316 stainless steel compression fittings utilizing graphite packing. Welded directly to the fittings are all of

the required ports for gases, molten metal transport and measurement devices. The bottom fitting has a port that accepts the bubble injector, one for a thermocouple that measures the metal temperature near the bubble formation point, and a port to transfer molten metal in and out of the reactor. At the top of the reactor the fitting has ports for the gases to exit the reactor, cooling gas to enter the reactor, a thermocouple to measure the gas temperature above the melt, the top microphone, a sensor to measure the height of the metal in the reactor and a thermocouple to measure the metal temperature.

The geometry of the bubble injector can be seen in figure 3.2. The injector is made of 3.2 mm outer diameter 316 stainless steel tube with an inner diameter of 1.8 mm. The tip of the injector is sharpened to avoid interfering with the bubble formation process.

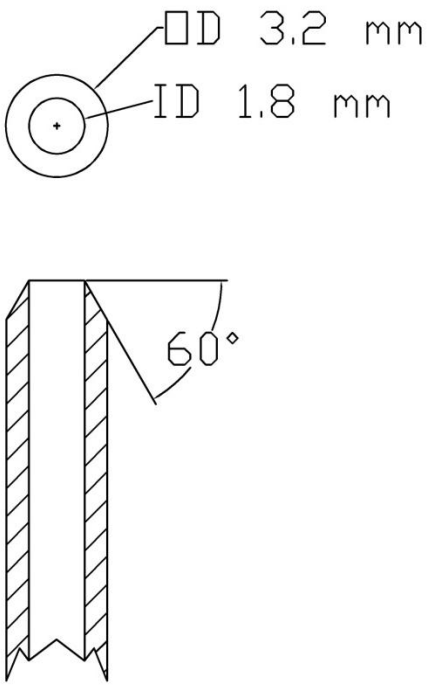

Figure 3.2- Geometry of bubble injector

A custom sensor to measure the location of the top of the molten metal in the reactor had to be developed because of a lack of appropriate commercially available sensors. This simple sensor is a 3.2mm ceramic tube with four small axial holes. A small diameter steel wire is run through each axial hole and out a radial hole bored at different distances from the end. A small voltage is placed between the molten metal and each of the 4 wires so that when the wire contacts the metal a small electrical current travels through a 10 kohm resistor across which the voltage is measured as can be seen in the schematic in figure 3.3. By measuring the change in voltage across each resistor it is

possible to detect which wires are in contact with the metal and determine the height of the metal relative to the position of the wires.

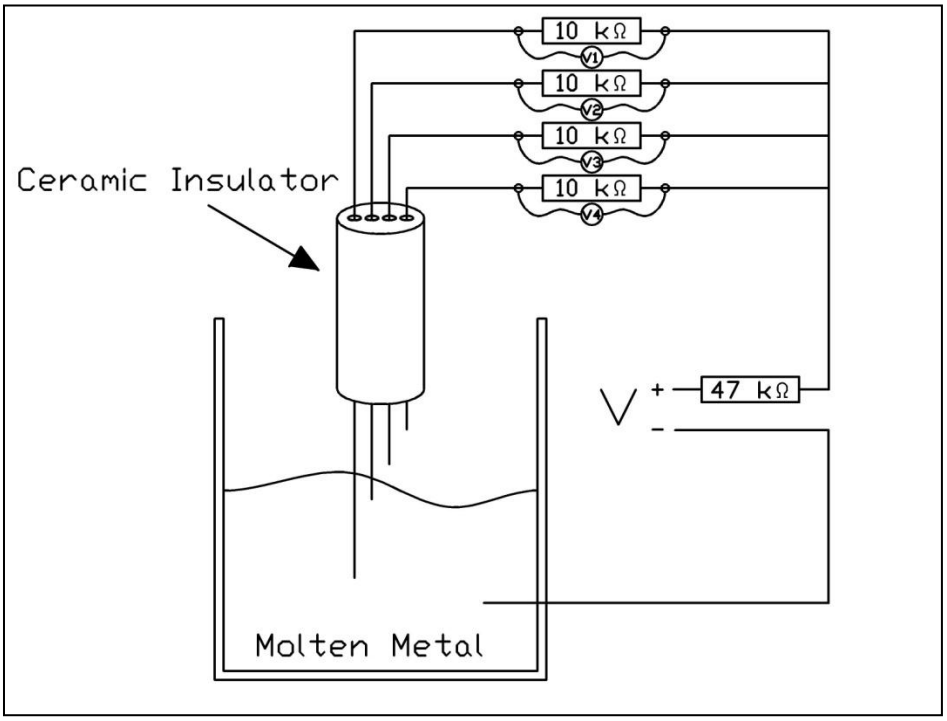

Figure 3.3- Schematic of height sensor probe. V = applied voltage, V1 tIn this instance V1 and V2 would be a measureable voltage, while V3 and V4 would measure approximately 0V indicating that the first two wires are in contact with the grounded molten metal and the third and fourth circuits are open.

The reactor is surrounded by 4 cylindrical radiant heaters. Each heater is 425 W and is powered by 120 V AC power. The temperature of each heater is measured by a thermocouple centered in the air space between the heater and the reactor. These heaters are controlled by a PID controller in LabView. The heaters have a maximum temperature of 1100°C, which allows them to easily heat the reactor and its contents to 1000°C. The

heaters and reactor are wrapped in 2 inches of ceramic wool insulation and an aluminum facing to reduce heat loss.

3.4 Gas Analysis and Venting

The gas lines that exit the reactor are heated to prevent any water vapor present in the gas from condensing. The gas exiting the reactor passes by a relative humidity meter and thermocouple so that the water vapor content may be known prior to the gas being dried by passing through an ice bath condenser. Prior to the ice bath there is a back pressure regulator that maintains the pressure in the gas above the reactor at a predefined set point. After passing through the condenser the gas can either be diluted with air and vented to the outside, or sampled by the mass spectrometer and then vented to the outside. Likewise, as mentioned earlier, gas coming directly from the mixed gas distribution valve can be either vented or sampled through these same gas circuits. The line coming from the gas distribution valve to the gas sampling and venting circuits also has a backpressure regulator so that the gases can be mixed under the same pressure that they must enter the bottom of the melt, and then sampled to determine the gas composition entering the melt.

The mass spectrometer is a UGA 300 made by Stanford Research Systems which is discussed further in section 3.6. In either the case of the gas coming directly from the mixing circuit, or from the top of the reactor, the gases are sampled by the mass spectrometer at atmospheric pressure to simplify the sampling setup and reduce condensation problems. This mass spectrometer draws gas through a capillary and into a

small chamber before passing through the bypass pump and being vented. In the small chamber there is an orifice that allows a small portion of the sampled gas to enter the high vacuum region of the RGA. This sampling method reduces the response time of the instrument compared to a system without a separate bypass gas circuit. Because all of the gases expected to be in the system are simple gases with the largest being argon (atomic mass~=40) the mass spectrometer is setup to scan from 1 to 65 AMU every 30 seconds and record the mass spectra for later analysis.

3.5 Liquid Metal Handling

To reduce the possibility of breaking the non-elastic ceramic tube that makes up the reactor wall it is necessary to prevent the molten metal from freezing in the reactor. So there is a 304 stainless steel reservoir below the reactor in which the metal may be frozen, melted and stored. This reservoir is heated by a 624 W heater tape and wrapped on all sides by 2 inches of ceramic wool insulation. The reservoir, heater and insulation are all contained within a steel pressure vessel that contains a nitrogen atmosphere to prevent oxidation of the tin-bismuth. There is a thermocouple in the metal, as well as on the outside of the reservoir, and a pressure transducer attached to the pressure vessel. A 316 stainless steel tube connects the bottom of the reactor to the bottom of the reservoir to transfer the molten metal. The regular melting and reactor filling cycle consists of the following steps:

1. Melt the metal in the reservoir and heat to 200°C. Heat the reactor and metal transfer line to 200°C to prevent freezing of the metal and thermal shock on the ceramic reactor walls.

2. Make sure gas is flowing through the bubble injector to prevent it from clogging with metal. Then, slowly increase the pressure in the pressure vessel by adding nitrogen gas through a precision regulator from a high pressure gas bottle. As the pressure in the pressure vessel increases, metal is forced up the transfer tube and into the reactor. Keep increasing the pressure slowly until the metal height sensor discussed above registers the desired height, near the top of the reactor. This measurement can be verified by the pressure difference between the reservoir and the top of the reactor, and independently by the gas pressure bubbling through the reactor.

3. Close the remotely controlled valve in the transfer line to prevent further metal transfer.

4. Heat the reactor and metal contained to the desired temperature and perform the required experiments.

5. Allow the reactor and metal to cool to 200°C, then open the transfer valve and slowly reduce the pressure in the reservoir until all of the metal is out of the reactor.

3.6 Data Acquisition System

The only measurements that are not recorded automatically by the data acquisition system are the flow meter readings. These measurements along with the time and the position of relevant valves are recorded by hand. All other data is recorded automatically. The three main components of the data acquisition system are the National Instruments

CompactDAQ system, the Stanford Research Systems UGA 300 and a standard Windows PC which allows the operator to interface with the two systems. All relevant model and serial numbers can be found in the appendix.

3.6.1 Temperature, Pressure, Voltage

The National Instruments CompactDAQ system is a modular system that has interchangeable modules for acquiring thermocouple data and different ranges of voltages as well as the ability to produce output voltages and many other functions. The system interfaces with a PC via a USB connection and in this case National Instruments LabView software.

All thermocouple measurements utilize one of two NI 9213, 13 channel thermocouple input modules with built in cold junction compensation for the CompactDAQ. All of the thermocouples are type K, chromel-alumel. Thermocouples that measure the outer surface temperature of components or the room air temperature were made in house from K type thermocouple wire. All other thermocouples are 1/8” diameter, ungrounded stainless steel sheathed thermocouples. All extension wire is K type thermocouple grade wire. All of the thermocouples and wire were supplied by Omega Engineering.

The system has four Omega Engineering PX309 pressure transducers with 0-5 V output. A schematic of their wiring can be seen in figure 3.4. Relative humidity is measured by two Honeywell HIH 5031 humidity sensors whose wiring is represented in figure 3.5. The

two microphones used to detect bubbles are PUI Audio condenser microphones whose wiring can be seen in figure 3.6. The output signal from the liquid metal height sensor, which was discussed in section 3.3, consists of four separate voltage measurements across 1kOhm resistors. All of these voltages are measured by a NI 9205 32 channel analog input module with common mode noise rejection for the CompactDAQ.

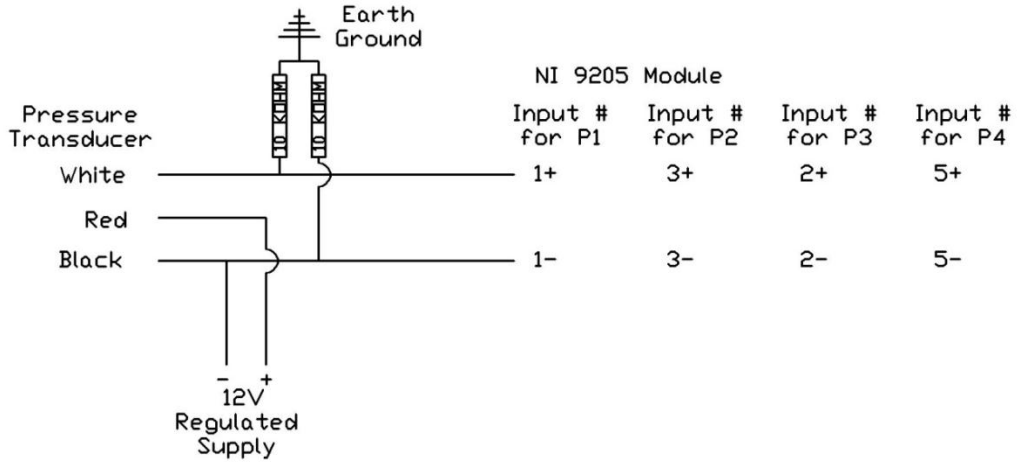

Figure 3.4- Wiring diagram for pressure transducers

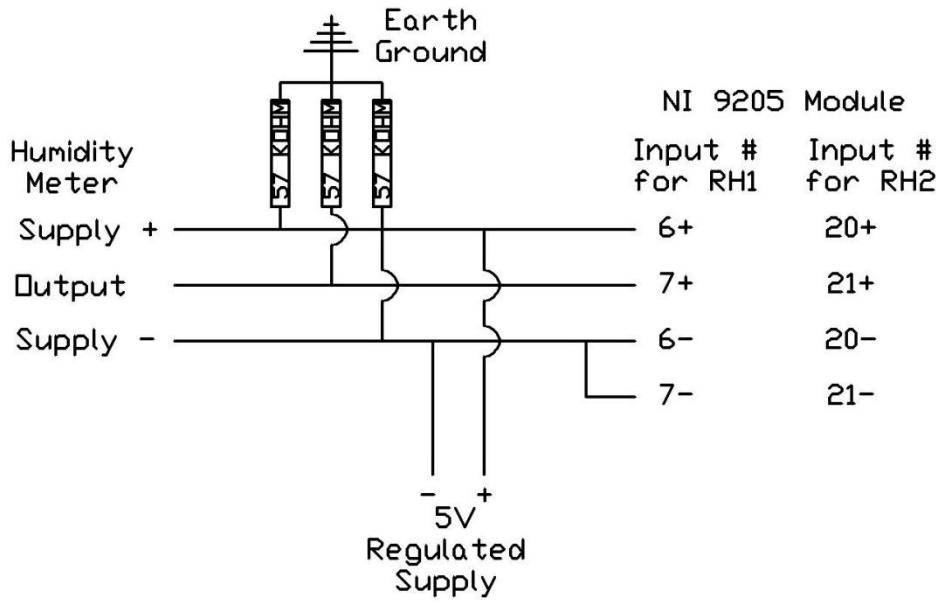

Figure 3.5- Wiring diagram for relative humidity sensors

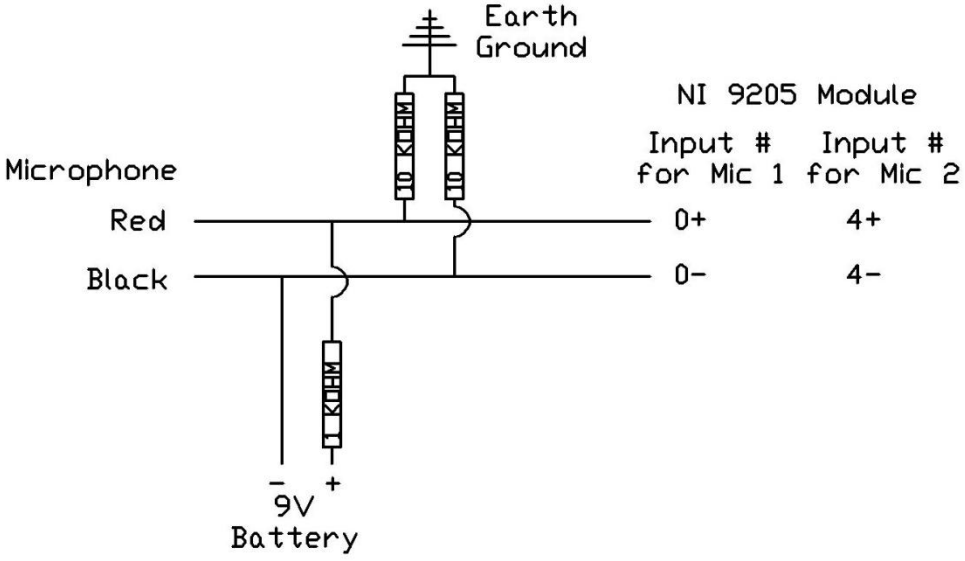

Figure 3.6- Wiring diagram for microphones

The CompactDAQ system interfaces via USB with a Dell Optiplex 960 computer with Windows XP operating system. National Instruments LabView version 9.0 software running on the computer provides graphical user interface with the CompactDAQ system. A custom LabView program was written that imports data from the DAQ, and records all data to a text file every ten seconds. If a subprogram is initiated by the user, LabView recording resources are re-allocated to recording only the time and two microphone signals to a separate text file in 20 second increments at a rate of 5 kHz. This is to allow for higher frequency measurements that are necessary to capture the bubbles signal from the microphones. The LabView program also controls all of the heaters via a NI 9403 digital in-out module for the compact DAQ which sends 0 or 5 volt signals to solid state relays to control the heaters.

3.6.2 Partial Pressure

As mentioned earlier, partial pressures of the gas system are measured using a Stanford Research Systems UGA 300. The UGA 300 system contains all of the vacuum and support systems necessary to run a built-in RGA 300, a quadruple mass spectrometer. The RGA 300 is capable of measuring a mass spectrum with a mass to charge ratio from 1 to 300 amu. Two pieces of software control the system, one which controls the vacuum pumps and valves, UGA 1.0, and another which controls the RGA and records the partial pressure measurements, RGA 3.1, both sold by Stanford Research Systems. For each scan, the RGA software outputs a text file with one column being the mass to charge ratio and a second

column being the corresponding ion current. More information on how the mass spectrometer works and how the mass spectrum is interpreted can be found in section 4.2 below.

4. Calculations

All calculations except equilibrium compositions were performed using MATLAB R2011a. The MATLAB scripts and functions used to do the calculations can be found in the appendix. Equilibrium compositions were calculated using a program called STANJAN version 3.89, written by W.C. Reynolds.

4.1 Bubble Calculations

The calculations involving the bubble transit time, velocity and diameter were all done independently of the partial pressure and other reaction calculations. The bubble calculations rely on time and flow rate data recorded by hand as well as data files generated by the LabView program, described in section 3, which contain temperature, pressure, height and microphone data.

4.1.1 Bubble Transit Time

In this study, chemical reactions are taking place inside or on the surface of a bubble that is rising through the molten metal melt. To determine the rate of the reaction, the change in chemical composition in the bubble and the time over which these changes occur need to be known. In this system that time is equal to the time it takes the bubble to rise though the melt. This transit time can be measured with the microphone system which was mentioned in section 3. It consists of two condenser microphones, one in the gas line near the inlet to the melt, the other located in the gas space above the melt. The microphone

signal in the input line shows large peaks at the instant the bubble is released from the orifice, and the microphone at the top shows a peak when the bubble is released, followed by another peak when the bubble hits the surface. The time difference between a release peak and its corresponding hit peak represents the time it takes the bubble to transit the molten metal melt from orifice tip to the top surface.

When the time between bubble releases, the release period, is shorter than the bubble transit time, determining which bubble hit peak corresponds to which bubble release peak can be difficult. Two methods were used to determine the transit time of the bubble from the microphone signals. The first method involves finding the locations of each peak in the signal and using a simple algorithm to determine the most likely transit time. The second method uses an autocorrelation procedure on the top microphone signal to look for a correlation between the two sets of peaks corresponding to the transit time. Because the transit time should not be a function of release rate over a small range of release rates, the correlation corresponding to the transit time should not change with bubble release frequency.

Individual Peak Method

A data set of voltage versus time for both the top microphone (mic 1) and the bottom microphone (mic 2) is required to find the transit time using this method. This data is recorded at 5 kHz for 20 seconds producing 100,000 data points per data set. The data is recorded at a specified melt temperature, pressure and gas flow rate. For each

temperature and pressure combination, several data sets are recorded over a range of gas flow rates.

The microphone voltage and time data is analyzed using a Matlab script named "*peaks_new.m"* (see appendix) which was written to determine the locations of the peaks associated with the release of the bubble from the orifice and the bubble hitting the top surface of the melt, and associate the release of one bubble with its hit peak. After these peaks are organized, the transit time and velocity of each bubble can be determined. This task is complicated by the fact that in most cases, several bubbles are released before the first bubble reaches the surface.

The first step in determining which release peaks go with which hit peaks is to get an estimate of the transit time by plotting and analyzing the data set with the lowest flow rate. Care is taken while acquiring the data to ensure that the data set with the lowest flow rate does not have more than one bubble in the melt at a time. This ensures that there will be no overlap in release and hit signals: the release signal and the following hit signal will be from the same bubble. From this plot, the release and hit peaks can easily be determined, and the approximate transit time for this data set estimated.

The microphone voltage signals for each data set are imported into MATLAB from the text file in which they were recorded. The voltages are then normalized according to equation 4.1 and 4.2, and $v_{2,norm}$ is shifted down 2 units so that both signals can easily be plotted on one graph without overlap and on similar scales.

$$v_{1,norm} = \frac{V_1 - \bar{V}_1}{V_{1,diff}}$$

Equation 4.1- normalization of V_1 with: $V_{1,diff}$ = maximum of $\left|V_{1,max} - \bar{V}_1\right| \; and \; \left|V_{1,min} - \bar{V}_1\right|$, $\bar{V}_1$= arithmetic mean of V_1, $V_{1,max}$ = maximum value of V_1, and $V_{1,min}$ = the minimum value of V_1

$$v_{2,norm} = \frac{V_2 - \bar{V}_2}{V_{2,diff}} - 2$$

Equation 4.2- normalization of V_2 with: $V_{2,diff}$ = maximum of $\left|V_{2,max} - \bar{V}_2\right| \; and \; \left|V_{2,min} - \bar{V}_2\right|$, $\bar{V}_1$= arithmetic mean of V_2, $V_{2,max}$ = maximum value of V_2, and $V_{2,min}$ = the minimum value of V_2. Two is subtracted so $v_{2,norm}$ will not overlap with $v_{1,norm}$ for ease of plotting.

Both $v_{1,norm}$ and $v_{2,norm}$ are then plotted versus time on one plot. The user of the program then must graphically input the approximate location of each release peak in the plot of $v_{2,norm}$. The release peaks can easily be differentiated from the hit peaks in $v_{2,norm}$ because the release peaks are much larger than the barely visible hit peaks in the $v_{2,norm}$ signal. Previously noted experiments with a similar microphone system and a high speed camera that imaged the releases and hits of bubbles in water showed this relationship was true for a microphone in the input line. The hit and release peaks can be seen in figure 4.1 which is a segment of data set 18 taken on 2-23-2011. The entire data set can be seen in figure 4.2.

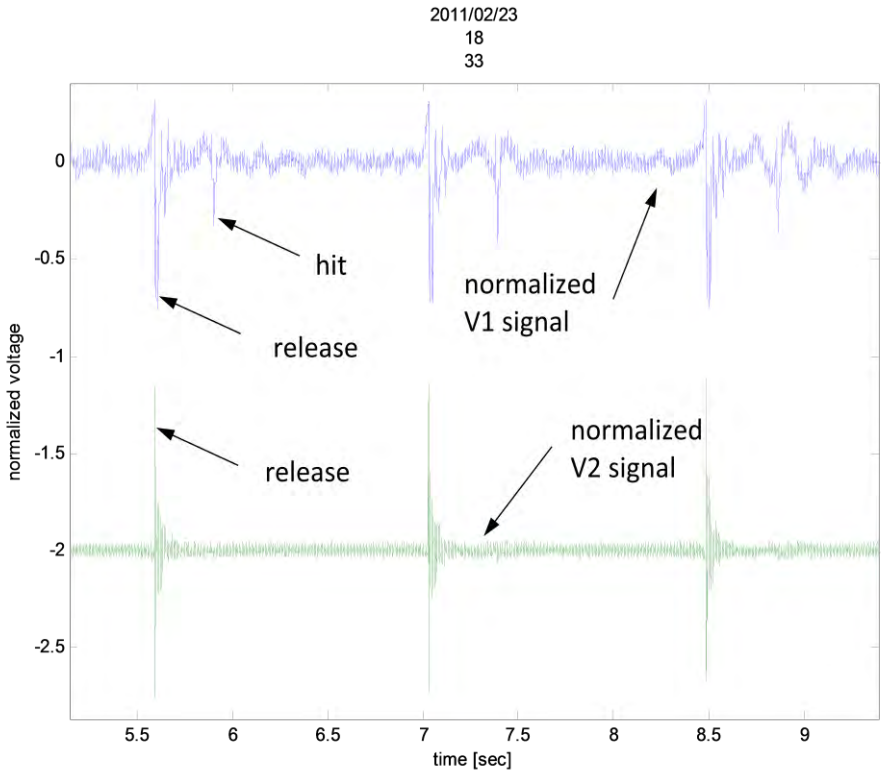

Figure 4.1- magnified view of figure 4.2 indicating one set of hit and release peaks.

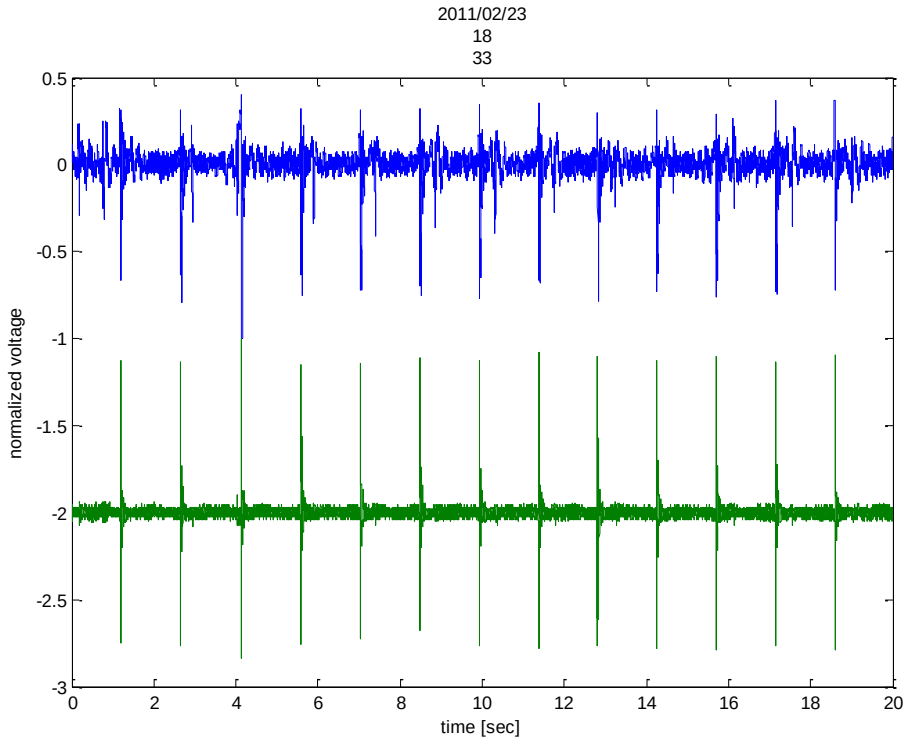

Figure 4.2- Data set recorded on 2-3-2011 at a flow setting of 33 mm, reactor temperature of 200°C, pressure of 1.7 atm, with a 1.8 mm orifice, used as an example for describing calculations

When the approximate locations of the $v_{2,norm}$ peaks are input graphically, the MATLAB script searches within a 0.2 second window centered on each estimate for a minimum value of the $v_{2,norm}$ signal. The time of this minimum is then taken to be the time of the bubble release and is stored for later use. The "*peaks_new.m*" MATLAB script then uses the estimate of the transit time obtained from the lowest flow rate along with the measured release times to estimate where the hit peaks should be and plot a marker at that estimate on the normalized voltage versus time plot as can be seen in figure 4.3. The user then interprets this information and graphically inputs estimated locations of each release

and hit pair in the $v_{1,norm}$ signal, skipping releases for which the data is unclear. The exact times at which the peaks occur are then found with a similar minimum searching procedure as described for the releases. The transit time for each measured bubble can then be calculated directly from the release and hit pairs according to equation 4.3.

$$t_{hit}-t_{release}=t_{transit}$$

Equation 4.3- Transit time calculation from hit and release times obtained from individual peak method

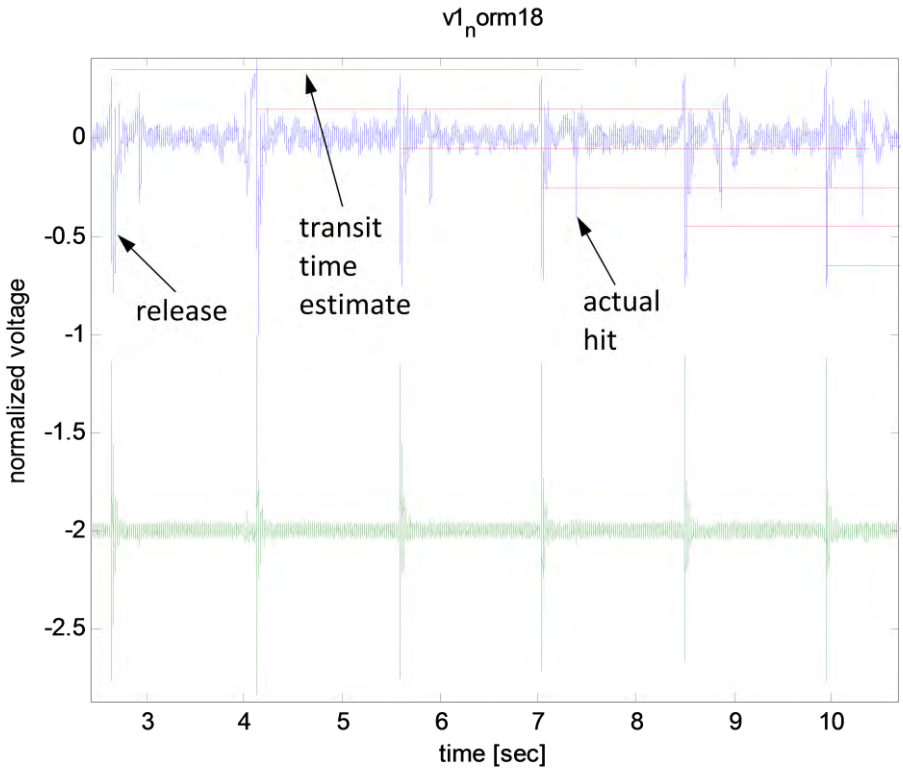

Figure 4.3- Magnified view of figure 4.2 indicating release peak, transit time estimate, and actual hit peak for specified release

Autocorrelation Method

The same data set is required for the autocorrelation method as for the individual peak method; however the bottom microphone signal is only used qualitatively to determine which peaks in the upper microphone signal are release peaks. Each data set is shifted by the mean of the set so that it is centered about zero volts to enable the autocorrelation function to work properly. The *xcorr* function in MATLAB was used to calculate the autocorrelation of the top microphone signal. The *xcorr* function computes the cross correlation of two vectors, g and h, according to equation 4.4 where j is the index in the vectors, N is the length of the vector and k is the lag. When this equation is applied to each point in a vector the result is a vector of the correlation of each point over the range of lags k from 0 to N [39]. When g and h are the same vectors, this computation results in the autocorrelation of the vector over a range of lags from 0 to N. Large positive values of autocorrelation at a particular lag indicate that segment of the vector is periodic with a period corresponding to the lag at which high autocorrelation occurs. Negative values of autocorrelation indicate a relationship between positive and negative peaks in the original signal. These relationships are outlined in figure 4.4. There is a very large peak at zero lag because the signal matches perfectly with itself when compared without any shift.

$$xcorr(g,h) = \sum_{k=0}^{N-k-1} g_{j+k} h_k$$

Equation 4.4- Cross correlation function. If g ≡ h the function becomes the autocorrelation function [39]

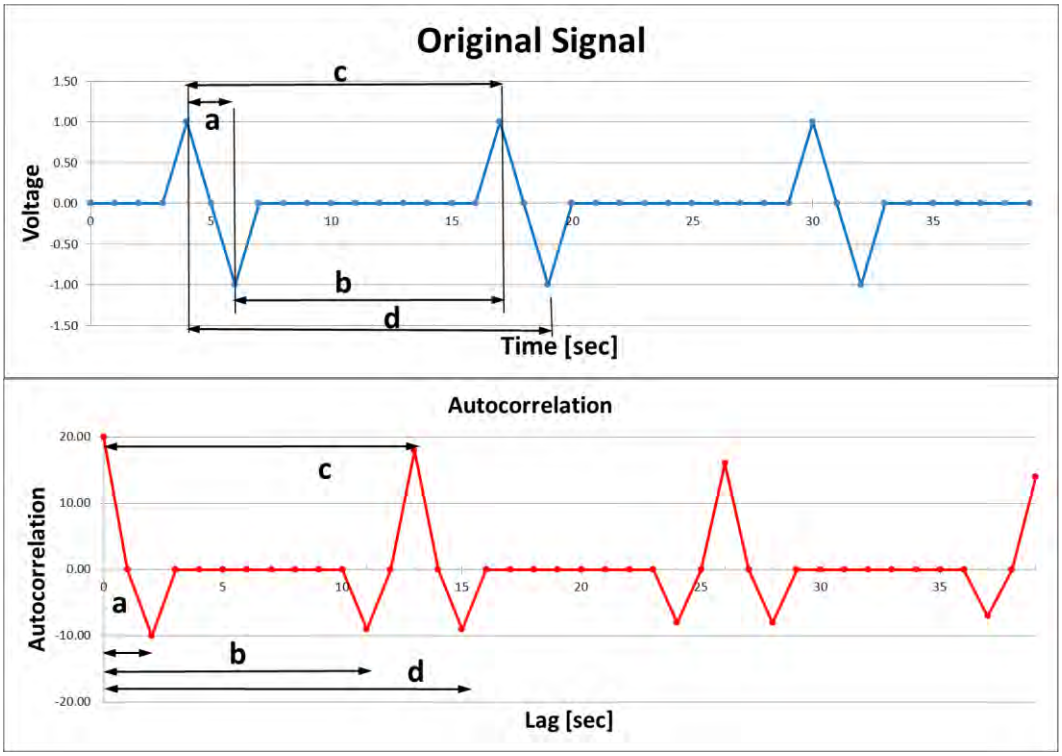

Figure 4.4- Plots of simple periodic signal (top) and autocorrelation of signal (bottom) with dimensional relationships shown: **a** = distance from positive peak to next negative peak, **b** = distance between negative peak and next positive peak, **c** = period of signal and **d** = distance from positive peak to second negative peak. Subsequent peaks in autocorrelation plot represent similar distances between further peaks.

The results can be more difficult to interpret when applied to a real signal because noise and small variations in frequency in the signal transfer through the autocorrelation function. When autocorrelation is applied to an actual top microphone signal the frequency of the signal is more easily discernible than the transit time, as can be seen in figure 4.5.

Figure 4.5 is a plot of a portion of both microphone signals with microphone 1 (top microphone) plotted in blue and averaging about 8.6 volts and microphone 2 (bottom microphone) plotted in green and averaging about 8.48 volts. The releases are clearly discernible in the microphone 2 signal as well as the microphone 1 signal, occurring near 5.6, 7.0, 8.5, and 9.9 seconds. The hit peaks are also marked and are near 5.9, 7.4, and 8.9 seconds. It is expected that autocorrelation of the microphone 1 signal should have peaks associated with the overall period of the cyclic signal (1.45 sec) as well as one or more associated with the relationship between the release peaks and the hit peaks. Using logic derived from the analysis done on the simplified signal above, it is expected to find peaks in the auto correlation signal near 0.36 sec and 1.09 sec corresponding to the distance from a release to the next hit, and from a hit to the next release respectively, and at these values plus some multiple of the overall period. Because both the release and hit signals have their larger departure from the mean in the negative direction, the expected autocorrelation peak between them should be positive. As can be seen in the plot of the autocorrelation of the signal, bottom of figure 4.5, there are several smaller positive peaks between the overall period peaks, but none line up well with 0.36 or 1.09 sec lags, or their multiples. One or more of the peaks may be associated with these lags of interest, but it is not altogether obvious which.

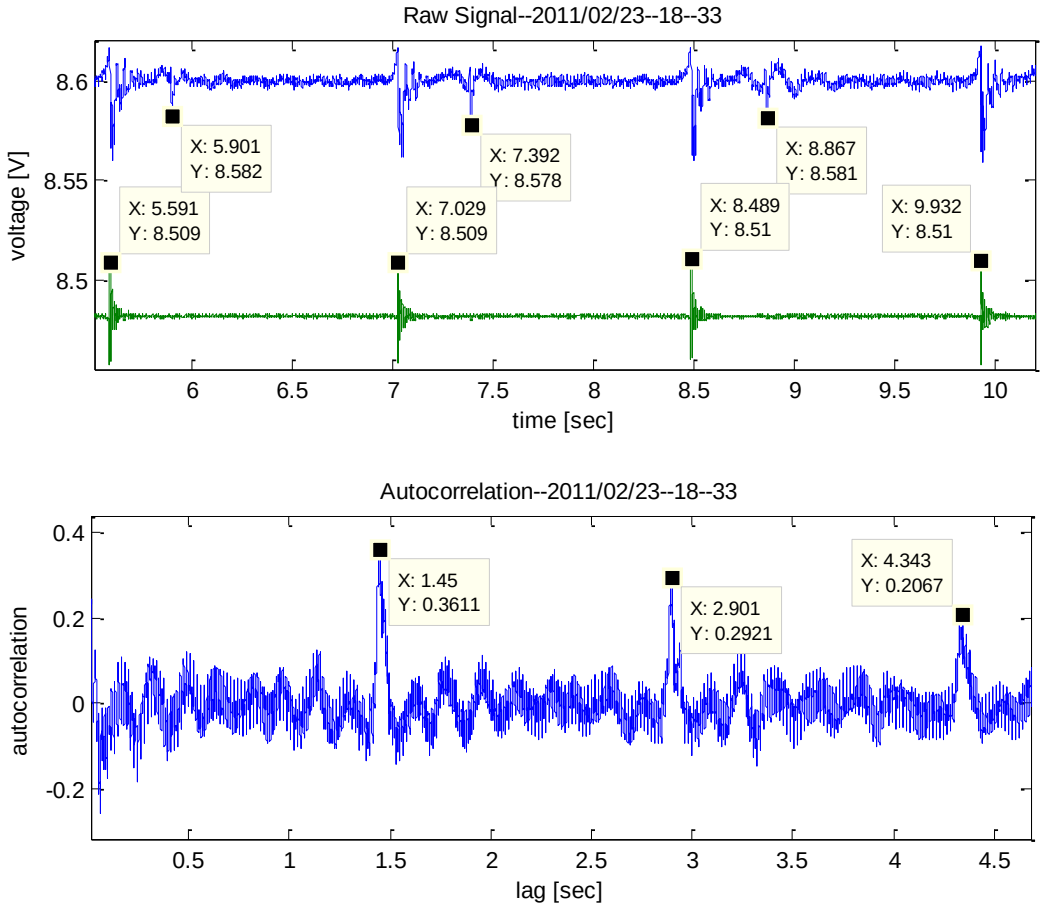

Figure 4.5- Original microphone signals (top) microphone 1 in blue and microphone 2 in blue, and autocorrelation of microphone 1 signal (bottom) showing first few major peaks.

The minor peaks in the autocorrelation signal appear to emanate from the oscillating noise in the microphone signal. The hit peaks in the raw signal are narrow compared to both the release peaks and the noise oscillations, which means that they have low power, and is probably why they do not have strong peaks in the autocorrelation plot. Some other data sets had stronger peaks that appeared to be associated with the hit peaks. However, because of the generally weak autocorrelation between release and hit peaks this

is not the ideal method for finding the transit time. It is probable that further tuning of the microphone system will result in larger hit peaks with less noise, which would make the autocorrelation method more desirable. If that could be accomplished, more of the data analysis associated with finding the transit time could be automated rather than using the manual method described above. This, however, will be left to future work because the manual method produces more easily interpreted data, and the relatively small amount of data needed does not make the manual method prohibitively time consuming.

4.1.2 Bubble Velocity

While knowing the velocity of the bubble is not necessary for calculating reaction rates if the transit time is known, it is helpful for comparing the experimental data to literature data and for calculating various dimensionless parameters. The average velocity can easily be calculated from the measured transit time discussed above and the height of the melt above the orifice as shown in equation 4.5. The calculated average velocity includes the time while the bubble is accelerating, so it is slightly lower than the terminal velocity. However, a simple experiment that varied the height of the melt while measuring the velocity of the bubble, showed that the average measured velocity of a 5.3mm diameter bubble did not change significantly if the height of the melt was varied from 0.09 m to 0.68 m, figure 4.6. This suggests that the acceleration of the bubble occurs in a distance significantly less than 0.09 m.

$$V_{average} = \frac{tt}{h}$$

Equation 4.5- average velocity ($V_{average}$) calculated from bubble transit time (tt) and height of melt (h)

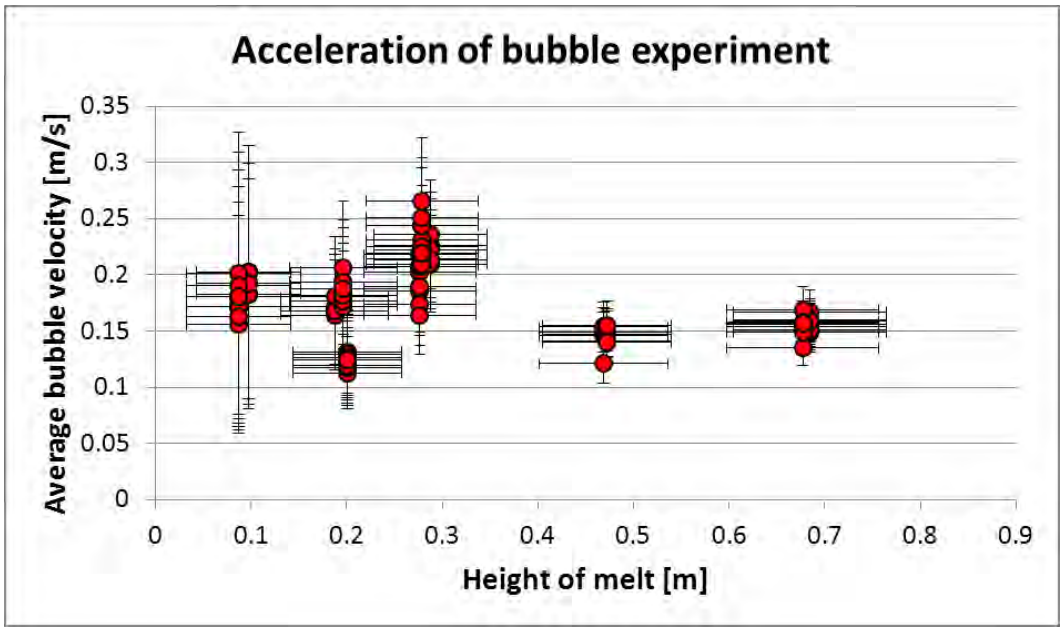

Figure 4.6- Results from test to determine acceleration distance of bubble. The test was done in tin-bismuth alloy at approximately 200°C with an average bubble diameter of 5.3mm.

4.1.3 Bubble Diameter

It is necessary to estimate the surface area of the bubble when considering reactions between the gases and the molten metal that are taking place while the bubble rises through the melt. Knowing the diameter or equivalent spherical diameter is also convenient when comparing to literature data. The calculation of equivalent spherical diameter is simple with the hit and release data mentioned earlier in the Section 4.1.1. The bubble frequency may be calculated as the reciprocal of the time between bubble releases

as seen in Equation 4.6, and the volume flow rate of the gas at the orifice is calculated from the orifice pressure, the orifice temperature, the known input gas composition and the mass flow rate measured with the rotameters, as can be seen in equation 4.7. The bubble volume can be calculated from the bubble frequency and volumetric flow rate as in equation 4.8. The equivalent spherical diameter is then calculated from equation 4.9.

$$F_b = \frac{1}{(R_i - R_{i-1})}$$

Equation 4.6- The bubble frequency, F_b, is given with R_i-R_{i-1} being the difference in time between two successive bubble release peaks

$$\dot{V}_o = \dot{m}\frac{\bar{R}\,T}{P\,mw}$$

Equation 4.7- The volumetric flow rate at the bubble orifice,$\dot{V}_o$, calculated from the gas mass flow rate, $\dot{V}_o$, the universal gas constant, $\bar{R}$, the orifice temperature, T, the orifice pressure, P, and the molecular weight of the gas, mw

$$V_b = \frac{\dot{V}_o}{F_b}$$

Equation 4.8- The bubble volume, V_b, calculated from the volume flow rate at the orifice, $\dot{V}_o$, and the bubble frequency, F_b

$$D_b = 2\left(\frac{V_b}{\pi}\,\frac{4}{3}\right)^{\frac{1}{3}}$$

Equation 4.9- The spherical equivalent bubble diameter (D_b) calculated from the bubble volume (V_b) from equation 4.8

4.2 Partial Pressure Calculations

As described in section 3.6.2, the output from the mass spectrometer is a mass spectra consisting of values of ion current for a range of mass to charge ratios (m/z). For the experiments at hand, ion currents for mass to charge ratios ranging from 1 to 65 in 0.1 increments were recorded. These mass spectra were analyzed to obtain the partial pressures of the gases sampled.

The data from the residual gas analyzer (RGA) was interpreted by Stanford Research Systems (SRS) RGA software. The software has the capabilities to interpret the spectra produced by the RGA and convert it to partial pressure data for several gases using a least squares fit to the spectra data. However, for greater control over the analysis and greater precision, a separate analysis of the spectra data was completed using MATLAB. The RGA software analysis was used only for reference while running the experiments as the MATLAB analysis could not be completed in real time.

4.2.1 Calibration of the Mass Spectrometer

Proper analysis of the mass spectra begins with calibration of the mass spectrometer. The mass scale, pressure reduction factor, fragmentation factors and sensitivity factors were all calibrated to the operating conditions of each experiment.

To calibrate the mass scale two reference gases are needed. Hydrogen was used as a low mass reference and argon was used as a high mass reference. Each gas was allowed into the mass spectrometer and measured, and then calibration parameters were adjusted

to place the largest hydrogen peak at a mass to charge ratio (m/z) of 2 and another set of parameters was adjusted to set the largest peak from argon at a m/z of 40. A separate set of parameters was used to adjust the mass scale resolution such that the width of these peaks was less than 1 atomic mass unit (amu) at 10% of the peak value. The calibration of the mass spectrum for other m/z values was then interpolated from the values at 2 and 40 amu.

The next calibration procedure performed finds the pressure reduction factor (PRF) which accounts for the pressure reduction between where the sample is drawn into the capillary to the ion chamber. This calibration was carried out by letting a known pressure of argon into the sampling area and measuring the pressure in the ion chamber with the mass spectrometer operating. The pressure measured by the mass spectrometer was then compared to the known pressure in the sampling area and the PRF was adjusted until the two pressures matched. This value varied with setup and different gases but for this series of experiments was generally found to be approximately 1.39×10^{9} amp/torr.

As described later, analysis of the mass spectra to obtain the partial pressures of sampled gases requires that the fragmentation factors of each gas be known for all significant peaks created in the mass spectrum by that gas. Standard values of these fragmentation factors can be found tabulated in databases, including a library in the RGA software, but more accurate results may be gained from measuring these factors for the gases of interest with the mass spectrometer operating at the typical operating conditions of the experiment. To measure the fragmentation factors the gas of interest must be

sampled either as a pure gas or as a mixture with a gas whose fragmentation factors are known. A spectrum is produced and from it a background spectrum is subtracted. The background spectrum is produced by taking a reading of the gases still present in the ion chamber with the sample valve closed after it has been pumped down to below about $5x10^{-8}$ torr or lower. This accounts for the gases that are always present in the ion chamber which account for a small amount of each produced spectrum. If the gas of interest was introduced in a mixture, the other components of the mix are subtracted in a similar fashion as to the background subtraction. The values of the remaining spectrum at each m/z value are then put in a vector. The sum of all of these values is found, and then each value is divided by the sum to normalize the spectrum so that the sum of all of its parts is equal to one. These values represent the fragmentation factors for the gas at each mass. In practice only the major peaks are used as fragmentation factors, generally so they add up to more than 0.999 for each gas. For instance, if pure argon gas was sampled and a background subtraction performed, there may be only three significant peaks at 40, 20 and 37 with values of 684, 68.4 and 7.6 torr respectively. Summing these values gives 760 torr, and dividing each peak height by the sum give 0.9 for 40 amu, 0.09 for 20 amu and 0.01 for 37 amu. Therefore, for this example the fragmentation factors for argon would be:

$$\alpha_{Ar,40} = 0.9$$

$$\alpha_{Ar,20} = 0.09$$

$$\alpha_{Ar,37} = 0.01$$

With these other calibrations completed the sensitivity factors of each gas may be determined. These factors adjust for differences in the way the different gases ionize and are read by the mass spectrometer operating at specific conditions. They are similar to the pressure reduction factor and cannot be physically separated from it, but are applied to each gas individually. For instance, the PRF could be set to 1 and the sensitivity factors calculated to account for the PRF as well as individual gas differences, but this is awkward with the RGA software. The PRF may be thought of as a rough adjustment accounting for the pressure reduction system, while the sensitivity factors are a fine adjustment that accounts for ionization efficiencies and other gas specific properties. To find the sensitivity factor for a gas, a mixture of the gas is needed in which it is at a partial pressure similar to what is expected in the experiment. The sensitivity factor may not be valid over a range of more than one order of magnitude change in the mole ratio of the gas. It is important that the other gases in the calibration mixture not have significant peaks that overlap or the sensitivity factor may be skewed. After the mixture is sampled, the partial pressure of the gas of interest is calculated from the mass spectrum and compared to the known partial pressure in the mixture. The sensitivity factor is then adjusted until the calculated partial pressure and the known partial pressure match. The range of applicability of the sensitivity factor should then be tested by measuring mixtures of different known concentrations of the gas.

4.2.2 Interpretation of the mass spectrum

With the mass spectrometer properly calibrated the spectra that it produces can be analyzed to determine the partial pressure composition of the gas that was sampled. The mass spectrum is a list of ion currents produced over a range of mass to charge ratios. With the mass to charge ratio on the x-axis and the ion current on the y-axis, a plot of the mass spectrum would have peaks in the ion current at values of m/z corresponding to ions present at the collector. For instance, the two biggest peaks in a spectrum produced from measuring argon gas would be at m/z values of 40 and 20 corresponding to Ar^{+1}, Ar^{+2}. If there is more than one gas present then the spectrum produced would be a linear combination of the spectrums from each gas. The height of the peak at each mass, m, can be described by equation 4.10.

$$H_m = \sum_{i=1}^{g} \alpha_{i,m} P_g$$

Equation 4.10- Equation for the height (H) of the peak associated with mass to charge ration (m) where g is the number of gases, alpha is the fragmentation factor of gas i at m/z= m, and P_g is the partial pressure of the gas g.

The system of equations to be solved to get the partial pressures of each gas can be written more concisely in matrix form, as shown in equation 411.

$$A\,P = H$$

Equation 4.11- Matrix equation where is H a (m x 1) vector of peak values at each m/z value, A is a (m x g) matrix of fragmentation factors, most of which are zeros, P is a (gx1) vector of partial pressures which have not had their gases sensitivity factor applied, g is the number of gases being analyzed, and m is the maximum m/z value

If there are more peaks being considered than gases, the system of equations to solve for the partial pressures of the gases is over-specified because there will be m equations and g unknowns, with m larger than g. To solve these equations a Least Squares solution is found using Singular Value Decomposition (SVD) whose format is shown in equation 4.12. If the error is defined as $x = (A P - H)^2$, and U, w and V are found from the singular value decomposition of A such that $A=U\,w\,V^T$, and w_r is calculated from the matrix w, as described in equation 4.13, then the minimal error will occur at the solution of equation 4.12 [39].

$$P = V\,w_r\,U^T\,H$$

Equation 4.12- Matrix equation result from SVD of equation 4.11

$$w_{r\,i,j} = \begin{cases} 1/w_{i,j} & if\ w_{i,j} > s \\ 0 & if\ w_{i,j} \leq s \end{cases} with\ s\ being\ a\ small\ number$$

Equation 4.13- Calculation of w_r from w matrix described above

Once the values of P are found using the MATLAB function *SVD*, all that remains is to multiply each component of P by its corresponding sensitivity factor to obtain the partial

pressure of each gas as shown in equation 4.14. Examples of the MATLAB code used in these calculations may be found in the appendix.

$$Pp_{(i)}=P_{(i)}*SF_{(i)}$$

Equation 4.14- Calculation of partial pressure (Pp) from matrix P, described in equation 4.12 and a vector of gas sensitivity factors (SF)

4.3 Gas Composition Calculations

4.3.1 Equilibrium Compositions

The thermodynamic equilibrium composition of each reaction performed was calculated for three reasons. First, by knowing the thermodynamic equilibrium composition of a system it is possible to predict the direction that a certain reaction will precede. Second, the equilibrium composition serves as a bound, past which a reaction is not expected to take. In this sense, knowing the thermodynamic equilibrium is useful as a tool for trouble shooting unexpected results. Third, when comparing measured data to literature data, it is important to know if the measured reaction approaches equilibrium because kinetic rates found in literature data are generally measured far from equilibrium and different rates would be expected close to equilibrium.

All equilibrium calculations were performed using STANJAN version 3.89 written by W.C. Reynolds, which uses thermodynamic data from the NIST-JAANAF tables [11]. This program uses what is known as the Element Potential Method to solve for the equilibrium

composition of a system containing a known population of elements given a set of product compounds. The element potential is a property of the system, and each independent atom in the system has its own element potential [40]. For example, in a system that contains water (H_2O) and methane (CH_4), there will be defined one element potential for the element hydrogen (H), one for oxygen (O) and one for carbon (C). This method assumes that the system consists of ideal gases and ideal mixtures.

The Gibbs function for the system can be defined as in equation 4.15, with the partial molar Gibbs function for each species defined as in equation 4.16. The atomic population of the system can be described as in equation 4.17, which simply means that the population of each element in the system is calculated from the sum of the number of that atom in each species present in the system.

$$G = \sum_{j=1}^{s} \bar{g}_j \, N_j$$

Equation 4.15- Gibbs function of a system with variables defined in table 4.1 and equation 4.16 [40]

$$\bar{g}_j = g_j(T, P) + R\,T \ln(x_j)$$

Equation 4.16- Partial molar Gibbs function for species j at temperature (T) and pressure (P) with variables defined in table 4.1 [40]

$$P_i = \sum_{j=1}^{s} n_{i,j} \, N_j \quad for\ i = 1\ to\ a$$

Equation 4.17- Atomic population constraints for each element (i) in a system with a elements, with variables described in table 4.1 [40]

With the system describes as such, the thermodynamic equilibrium composition of the system is the distribution of the moles of each species present (N) when the Gibbs function of the system (G) is minimized. This constrained minimization problem can be solved using the method of LaGrange Multipliers which will not be discussed here, but whose results can be found for this system in equation 4.18 [40]. The LaGrange multipliers in equation 4.18 (λ_i) are the element potentials discussed earlier.

$$x_j = exp\left(-\frac{g_j(T,P)}{R\,T} + \sum_{i=1}^{a} \lambda_i\, n_{i,j}\right)$$

Equation 4.18- Formula for mole fraction of species j, the result of applying method of LaGrange Multipliers to minimization problem with variables defined in table 4.1 [40]

With the addition of equation 4.19, equations 4.18 and 4.19 make up a problem set that STANJAN uses to iteratively solve for the unknown element potentials and mole fractions of each species [40].

$$\sum_{j=1}^{s} x_j = 1$$

Equation 4.19- Final constraint equation for element potential method, the sum of mole fractions of each element, in each phase must add to 1, with variables defined in table 4.1

Variable	Description	Variable	Description
s	Number of species in system	T	Temperature of system
j	Species index	P	Pressure of system
a	Number of elements in system	P_i	Population of i elements in system
i	Element index	R	Universal gas constant
G	Gibbs function of system	x_j	Mole fraction of species j in phase
$\overline{g_J}$	Partial molar Gibbs function of species j	$n_{i,j}$	Number of moles of element I in species j
g_j	Gibbs function of pure species j	λ_i	Element potential of element i
N_j	Number of moles of species j in system		

Table 4.1- Definition of variables used in equations 4.16 to 4.20

4.3.2 Measured Gas Compositions and Rates

All of the calculations mentioned in this section were carried out in a MATLAB script called “reaction_analysis.m” which can be found in the appendix. This program requires several input files in which the raw data is held, which are all kept in the same directory named in the script. The first input file is named “fdata.txt” and contains all of the information required to assemble the file names of the log files from the mass spectrometer

which contain the raw ion current and mass to charge ratio outputs discussed in section 4.2. The second file required is called “flowdata.txt” and contains all of the flow meter reading vs. time data recorded by hand. The third file is called “inputs.txt” and contains information regarding the setup of the experiment such as which reactor was used and the reactant gases used. The fourth file is named “Rec” followed by the date of the experiment. This data records all of the pressure, temperature and other data read by the data acquisition system. The program also reads the mass spectrometer log files mentioned earlier.

The program first determines the partial pressure before and after reaction by the method described in section 4.2. From the partial pressures the mole fractions of each gas are determined using equation 4.20. The mole fractions of water are found from equation 4.21 using the appropriate recorded relative humidity and temperature data.

$$mf_i = \frac{Pp_i}{\sum_{i=1}^{n_g} Ppi}$$

Equation 4.20- Calculation of the mole fraction of gas i, with Pp_i = the partial pressure of gas i, and n_g = the number of gases analyzed

$$mf_{H2O} = exp\left(\frac{T\ (17.3)}{T + 238} + 6.416\right)\frac{RH}{P}$$

Equation 4.21- Calculation of the mole fraction of water from the relative humidity (RH), pressure at the relative humidity meter (P) and temperature at the relative humidity meter (T). For the input reading RH_{in}, T21, and P4 are used, for the output use RH_{out}, T20 and P1. Equation is given in Honeywell HIH3031 RH meter data sheet.

The mass flow rate of the gas into the reactor is calculated from the recorded flow setting using the calibration equation appropriate to the setup and gas. The total molar flow rate into the reactor is determined from the mass flow rate, mole fraction of each gas in and molecular weight of each gas as seen in equation 4.22. With the total molar flow rate in to the reactor known, the molar flow rate of each gas can be calculated as in equation 4.23.

$$\dot{mol}_{in,t} = \frac{\dot{m}}{\sum_{i=1}^{n_g} mf_{in,i}\, mw_i}$$

Equation 4.22- Calculation of total molar flow rate in from mass flow rate ($\dot{m}$), and the sum of each gas in the analysis of the mole fraction of that gas in ($mf_{in,i}$) and the molecular weight of that gas(mw_i)

$$\dot{mol}_i = mf_i\, \dot{mol}_t$$

Equation 4.23- Calculation of the molar flow rate of gas i from the mole fraction of gas i (mf_i) and the total molar flow rate ($\dot{mol}_t$). Can be used for either the input or output gas by using the appropriate total molar flow rate.

The total molar flow rate of the gas out is calculated based on the assumption that the carrier gas, either argon or helium, is inert and therefore constant. Using this assumption the total molar flow rate out is calculated as shown in equation 4.24, and the individual molar flow rates out may be calculated using equation 4.23 again.

$$\dot{mol}_{out,t} = \frac{\dot{mol}_{in,c}}{mf_{out,c}}$$

Equation 4.24- Calculation of the total molar flow rate out based on the assumption that the flow rate of the inert carrier gas is constant, from the molar flow rate in of the carrier gas ($\dot{mol}_{in,c}$) and the mole fraction out of the carrier gas ($mf_{out,c}$)

The calculation of the residence time of the gas in the reactor is different for the empty reactor compared to the molten metal reactor. For the molten metal reactor the residence time is simply calculated by dividing the height measured by the height sensor by the velocity measured previously in the bubble calculations section. The residence time for the empty reactor is calculated by dividing the volume of the reactor by the average volumetric flow rate as is shown in equation 4.25.

$$t_{res} = \frac{L_{reactor} Ax_{reactor}}{\left(\frac{\dot{mol}_{in,t} + \dot{mol}_{out,t}}{2}\right)\frac{\bar{R}\, T_{avg}}{P_{avg}}}$$

Equation 4.25- Calculation of the residence time of the gas in the empty reactor from the length of the reactor ($L_{reactor}$), cross sectional area of the reactor ($Ax_{reactor}$), molar flow rate in and out ($\dot{mol}_{in,t}$, $\dot{mol}_{out,t}$), universal gas constant ($\bar{R}$), average temperature and average pressure in the reactor (T_{avg}, P_{avg})

With the molar flow rates in and out of each gas and the residence time known, the observed rate of increase of each gas can be calculated as shown in equation 4.26.

$$rate_i = \frac{\dot{mol}_{out,i} - \dot{mol}_{in,i}}{t_{res}}$$

Equation 4.26- Calculation of rate of increase of each gas i ($rate_i$), from the molar flow rate in and out of each gas ($\dot{mol}_{in,i}$, $\dot{mol}_{out,i}$) and the residence time of the gases in the reactor (t_{res})

4.4 Experimental Uncertainty Calculations

There will always be some inaccuracies in experimental measurements do to unpredictable variation in measurement parameters. In an attempt to quantify these variations experimental uncertainties have been calculated for all pertinent measured or calculated values. The propagation of measured uncertainties into calculated values was predicted with equation 4.27 [41]. The experimental uncertainties are based on a 95% confidence region, assuming a normal distribution of error.

$$s_Y = \sqrt{\left(\frac{\partial Y}{\partial X}\right)^2 s_X^2 + \left(\frac{\partial Y}{\partial Z}\right)^2 s_Z^2 + \cdots + \left(\frac{\partial Y}{\partial X}\right)\left(\frac{\partial Y}{\partial Z}\right) s_{XZ}^2 + \cdots}$$

Equation 4.27- For the function f described by: Y=f(X,Z,…), where s_n is the standard deviation of s and s_{Xz} is the square root of the estimated covariance between X and Z. The covariance terms are set to zero if the X and Z terms are known or assumed to be independent. [41]

4.4.1 Bubble Velocity Uncertainty

In this analysis, the standard deviation estimates come from three different sources. One source is the uncertainty of an instrument as predicted by the manufacturer based on their measurements and calculations; these are shown in table 4.2. Some instruments, most notably the gas flow meters, had to be calibrated in house for specific conditions, so the standard deviation of these measurements was estimated with MATLAB's "*regstats*" function. In the case where there are not enough repeated measurements to get an accurate estimate, the standard deviation was taken to be ½ of the smallest measurement scale of the instrument. One instance where this estimate was used was with the readings from the bubble flow meter used to calibrate the gas flow meters. In this case it is a conservative estimate of the standard deviation.

Variable	Uncertainty	Units	Source of Estimate
reactor temperature	5	C	heater control tolerance
tin bismuth density	711	kg/m^3	literature: Moser, Gasior and Pstrus
metal density parameter A	211	kg/m^3	literature: Moser, Gasior and Pstrus
metal density parameter B	0.851	kg/m^3-K	literature: Moser, Gasior and Pstrus
metal viscosity parameter A	0.009	N/m	literature: Moser, Gasior and Pstrus
metal viscosity parameter B	1.00E-05	N/m-K	literature: Moser, Gasior and Pstrus
time (microphone measurements)	0.004	sec	from high speed camera calibration
flow setting	0.5	mm	1/2 of smallest scale
height (using height sensor)	0.0046	m	from height sensor geometry
pressure	2	%	component data sheet
temperature	0.75	%	component data sheet
mass flow rate	20	%	mass flow meter calibration

Table 4.2- Sources of measurement error in bubble calculations

The uncertainty associated with finding the mass flow rate of gases out of each flow meter was the most complicated. Because the experiment takes place at conditions outside of the factory calibration of the rotameter, a calibration curve is required for each pressure and gas combination for each flow meter. To obtain this curve a bubble flow meter is used as a reference. The bubble flow meter consists of glass tube graduated in 0.2 ml divisions through which gas flows. Soapy water is introduced over the gas inlet, which is at the bottom of the bubble flow meter, allowing a soap bubble to form. The progress of this bubble is then timed with a stopwatch as it advances up the tube past graduation marks. By measuring the time between two volume marks, the flow rate may be found by dividing the volume between the marks by the time for the bubble to travel that volume. The setup for this calibration is shown in figure 4.7. The gas pressure upstream and downstream of the flow meter is set with the gas bottle regulator and the backpressure regulator. The temperature of the gas is also measured and recorded for conversion from volumetric flow rate to mass flow rate. Downstream of the backpressure regulator, the system is at atmospheric pressure, and the entire setup is at room temperature.

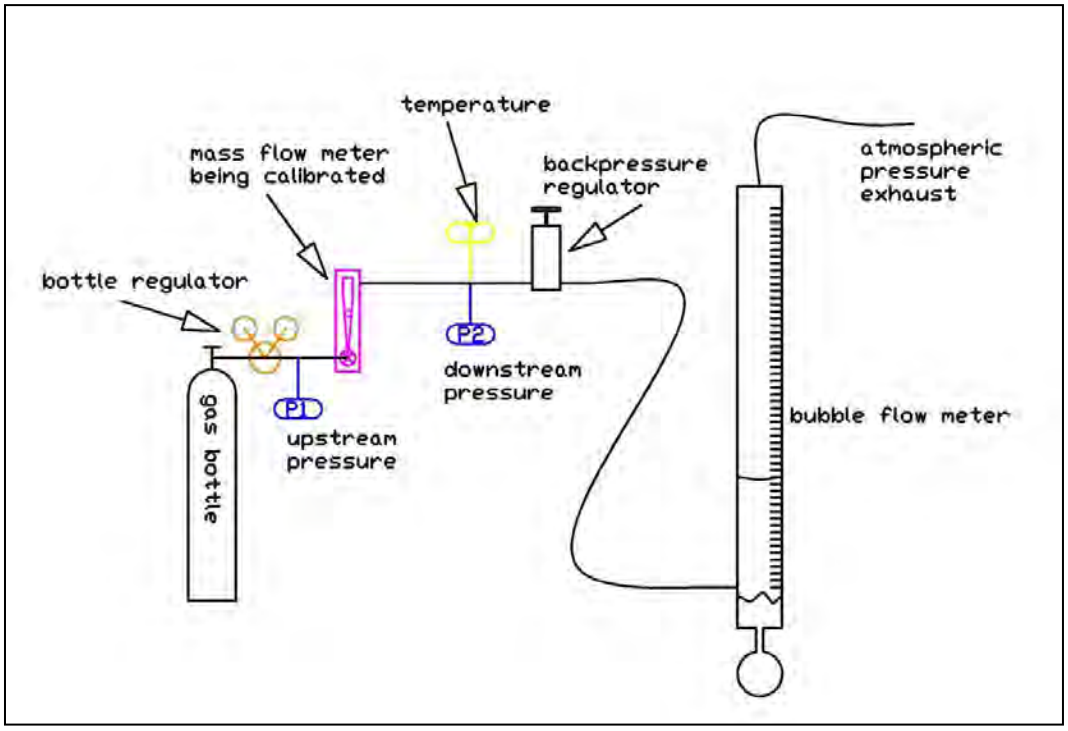

Figure 4.7- Flow meter calibration setup

Measurements of the volumetric flow rates according to the bubble flow meter are recorded at several flow settings over the entire range of the flow meter being calibrated. Each volumetric flow rate is then converted to a mass flow rate using the recorded temperature and pressure of the gas along with its known composition and the ideal gas law. A second order polynomial is then fit to the data using a least squares fit with the mass flow rate as the dependent variable and the setting on the scale of the flow meter as the independent variable. The result is a curve such as can be seen in figure 4.8 which shows the individual measured points, the fit curve and an equation for that curve. A 95% confidence region for each calibration curve is calculated using MATLAB's *regstats* function.

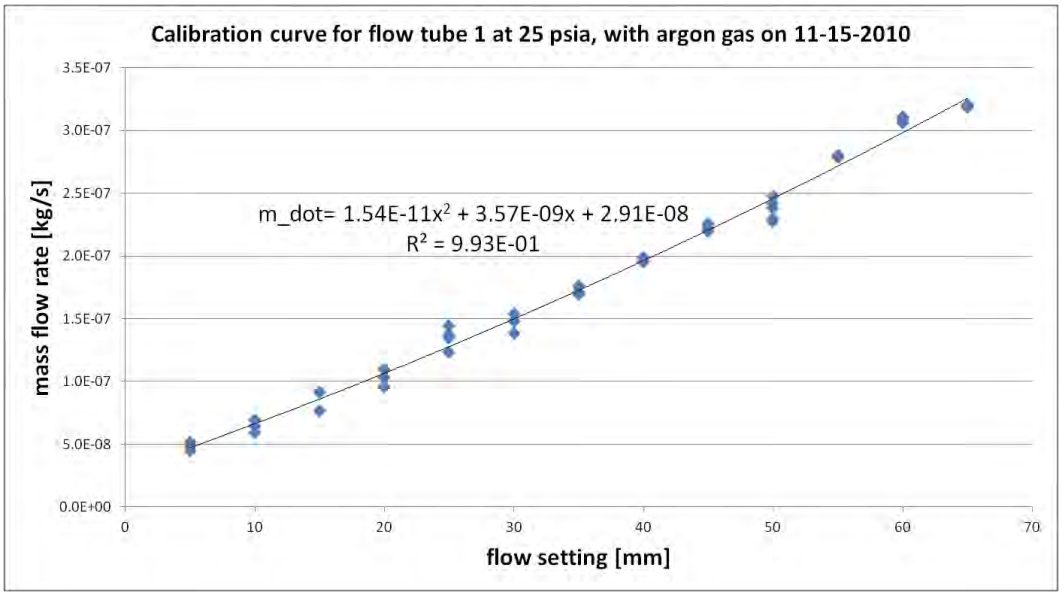

Figure 4.8- Example of flow meter calibration curve

4.4.2 Partial Pressure Uncertainty

There are several sources of uncertainty associated with the measurements of the partial pressure. As described in the section 4.2, the partial pressure measurement goes through several steps. First, a known gas is measured with the mass spectrometer and the output is used to calculate a partial pressure for each gas using a sensitivity factor equal to 1, using a least squares fit procedure, then a calibrated sensitivity factor is calculated by comparing the measured partial pressure with the known partial pressure of the gas components. With a valid calibration, an unknown gas may be measured with the mass spectrometer and analyzed in the same manner, but with the calibrated sensitivity factors.

The four major sources of error in this procedure are the calibration, the mass spectrometer, the fragmentation factors used in the least squares fit, and the least squares fit. The error in the calibration is due to the error in the composition of the known gas, and the errors associated with the calculation of the un-calibrated partial pressure, which are similar to those being described. The errors associated with the mass spectrometer include how small changes in the ion chamber pressure and measurement errors in the machine affect the output ion current. The fragmentation factors are gathered from library values. These library values do not generally cite uncertainties but it is known that their values are dependent upon the specific mass spectrometer and conditions under which the gases are sampled. For this reason, high precision analysis requires the measurement of the fragmentation factors for each gas under the specific conditions of sampling, which is costly and time consuming and not possible for an exploratory experiment set such as this. The errors associated with the least squares fit stem from the fact that it is attempting to fit a linear model onto a real world physical measurement that contains some random variation, however these errors are easily quantified with standard deviations estimated from model parameters.

The uncertainty of the least squares fit was estimated using equation 4.28 below. As described in section 4.2, the partial pressures were fit using a least squares procedure called singular value decomposition in which the partial pressures are calculated from the matrix equation, $P = V w_r U^T H$, equation 4.12 found in section 4.2, with the components described earlier. With those matrices already in place it is simple to calculate the variance and

covariance of the fitted parameters (the partial pressures P) according to equations 4.28 and 4.29.

$$\sigma^2(P_j) = \sum_{i=1}^{m} \left(\frac{V_{j,i}}{w_i}\right)^2$$

Equation 4.28- Variance of partial pressure values calculated from matrices used in equation 4.12. P, V and w are the same matrices as in equation 4.12, and m is equal to the number of gases under consideration [39].

$$Cov(P_j, P_k) = \sum_{i=1}^{m} \left(\frac{V_{j,i}V_{k,i}}{w_i^2}\right)$$

Equation 4.29- Covariance of two partial pressures (P_j and P_k) with the variables the same as equation 4.28 [39].

Using equations 4.28 and 4.29 on a typical mass spectrum of 5% methane in argon, the uncertainty of the fit on each partial pressure, with the uncertainty being approximated as twice the square root of the variance, was found to be between 0.5 and 1 torr which amounts approximately ±3% error for the fit to methane and less than 0.3% error for argon. Inspection of the covariance matrix allows for insight into how the components interact in the least squares fit. A high value of covariance means that the two parameters share significant defining peaks in the mass spectrum as described in section 4.2 and it may be difficult to actually tell which gases are causing the peaks. An example of the covariance matrix is plotted in figure 4.9. The plot shows a small ridge along the line x=y due to the fact that each parameter will have a covariance with itself, and peaks associated with combinations of gases 3,9,10 and 11, which are CO, C_2H_2, C_2H_4 and C_2H_6. These gases all

share peak 28, and the C_2 hydrocarbons share many others, which cause the high covariance.

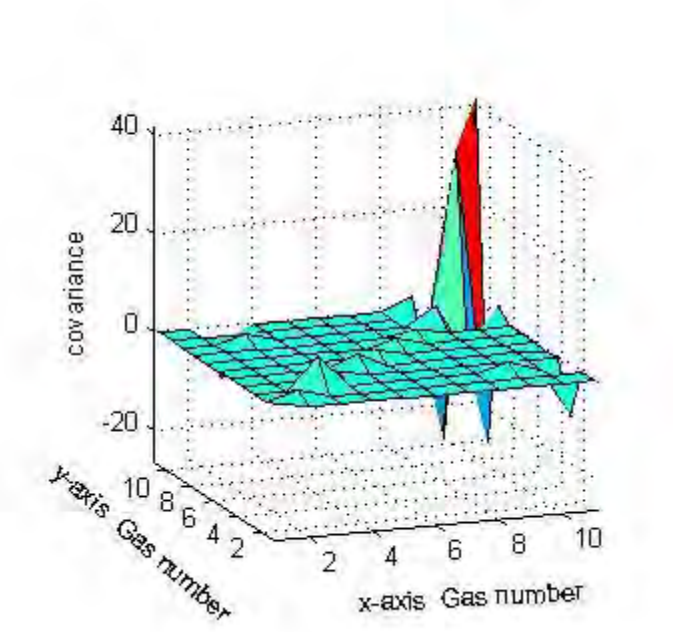

Figure 4.9- Plot of partial pressure covariance. Gas numbers 1 to 11 on the x and y-axes correspond to: Ar, CO_2, CO, H_2, CH_4, O_2, H_2O, He, C_2H_2, C_2H_4 and C_2H_6, with Ar being 1 and C_2H_6 being 11.

Because the uncertainty of the mass spectrometer measurements and the fragmentation factors are unknown, the overall partial pressure uncertainty is estimated from a series of measurements taken of known gas compositions using different calibrations. It was found that repeated measurements of the same gas under conditions that vary as in the course of a typical experiment produce partial pressures that may vary by up to 15%. This number includes all of the uncertainty resulting from varying mass spectrometer pressures, the least squares fit and the calibration. On a given day, with the mass spectrometer operating at near constant pressure, measuring a gas near the composition at which the calibration was performed the variation drops to near 3%, which

is similar to the predicted error of the least squares fit. Unfortunately, there is not currently a means to make a better prediction of the overall partial pressure measurement error, so the larger of ± 15% or twice the standard deviation calculated in equation 4.28 will have to be used.

4.4.3 Uncertainty of Other Calculations

The experimental uncertainties of several other parameters were estimated using equation 4.27 above, assuming zero covariance between variables. These parameters include the molar flow rate of each gas in and out of the reactor, the mole fraction of each gas in the mixture going in and out of the reactor, the residence time in the reactor, the rate of conversion. Several measurement uncertainties were estimated and are shown in table 4.3. Unfortunately, two of the most important variables, partial pressure and mass flow rate, have high uncertainty values. The reason the partial pressure uncertainty is high is discussed above, while the reason for the high mass flow rate uncertainty is simpler. Flow rates of less than 10 sccm, which are needed to produce individual bubbles in the molten metal experiments, are difficult to work with. More accurate flow meters were unavailable, so low cost rotameters were used. Higher quality flow meters as well as dual stage pressure regulators on the gas bottles may make it possible to achieve lower uncertainty values for mass flow rate. With the results from this study, it is possible to better predict the output compositions of the gases, and thus calibrate to those conditions which should reduce the partial pressure uncertainty.

Due to the propagation of these errors through the calculations, the errors associated with variables calculated from multiple combinations of mass flow rate and partial pressures are very high. In the case of the rates of conversion, in some cases the error is so large that the rate becomes meaningless. For this reason, the majority of the results will be shown in as near to the measured states as possible, with other variables like rates shown only for comparison.

Variable	Uncertainty	Units	Source of Estimate
reactor temperature	5	C	heater control tolerance
tin bismuth density	711	kg/m^3	literature: Moser, Gasior and Pstrus
height (using height sensor)	0.0046	m	from height sensor geometry
height (empty reactor)	0.03	m	from heater geometry
inner diameter of baseline reactor	0.0002	m	measurement error
partial pressure	15	%	Partial Pressure Uncertainty Section
relative humidity	3	%	component data sheet
pressure	2	%	component data sheet
temperature	0.75	%	component data sheet
mass flow rate	20	%	mass flow meter calibration

Table 4.3- Measurement uncertainties used in calculations.

5. Results

5.1 Bubble Measurement Results

A set of experiments was done to determine key parameters regarding the bubble of gas which moves up through the tin-bismuth melt in the reaction experiments. Argon gas was used in these bubble measurement experiments. As described in greater detail earlier, argon gas was metered into the bottom of the reactor through a 1.8 mm inner diameter stainless steel tube. The tin-bismuth at the bottom of the reactor, where the bubble forms, is held to between approximately 200 and 300°C, while the rest of the metal was heated to 200, 400, 600 or 700°C. Two microphones are used to determine the time between the bubble leaving the orifice and its arrival at the top surface of the tin-bismuth. The microphones are also used to determine the bubble release frequency which is used along with the flow rate to determine the bubble volume, and equivalent spherical diameter. Multiple flow rates were tested at each temperature.

A model suggested by Mendelson to predict the velocity of a bubble in molten metal was discussed in section 1.3.2 and shown in equation 1.19, which is repeated below. The velocity predicted by this model can be seen in figure 5.1 along with the measured average bubble velocities. It should also be noted that the model for the terminal velocity is affected very little by the temperature of the metal. This is because the density and surface tension of the metal change very little with temperature [18].

$$U_T = \sqrt{\frac{\sigma}{\rho\, r} + r\, g}$$

Equation 1.19- Model suggested by Mendelson for terminal velocity of bubble in molten metal calculated from the metal surface tension (σ), metal density (ρ), bubble radius (r), and gravitational constant (g) [25]

Mendelson's model for the terminal velocity of the bubble appears to be in good agreement with the measured data. Although the measured data is actually the average velocity of the bubble, the acceleration time of the bubble was found to be short, so the terminal velocity should be a good approximation for the measured average velocity. From this data the average velocity over these conditions was found to be 0.21 [m/s], with a standard deviation of 0.03 or about 14%. This is the velocity used in the reaction experiment calculations to determine the time of reaction between the gas bubble and the molten metal. Figure 5.2 is shown as an example of the experimental errors associated with this data.

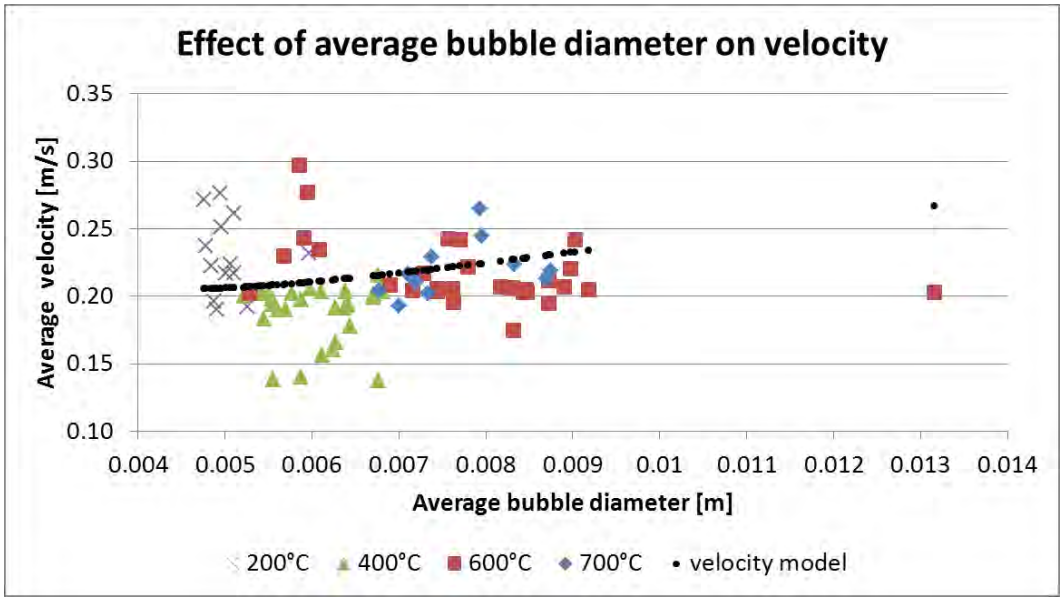

Figure 5.1- Plot comparing the measured average bubble velocity as a function of average bubble diameter with the terminal velocity predicted by Mendelson's model in equation 1.19

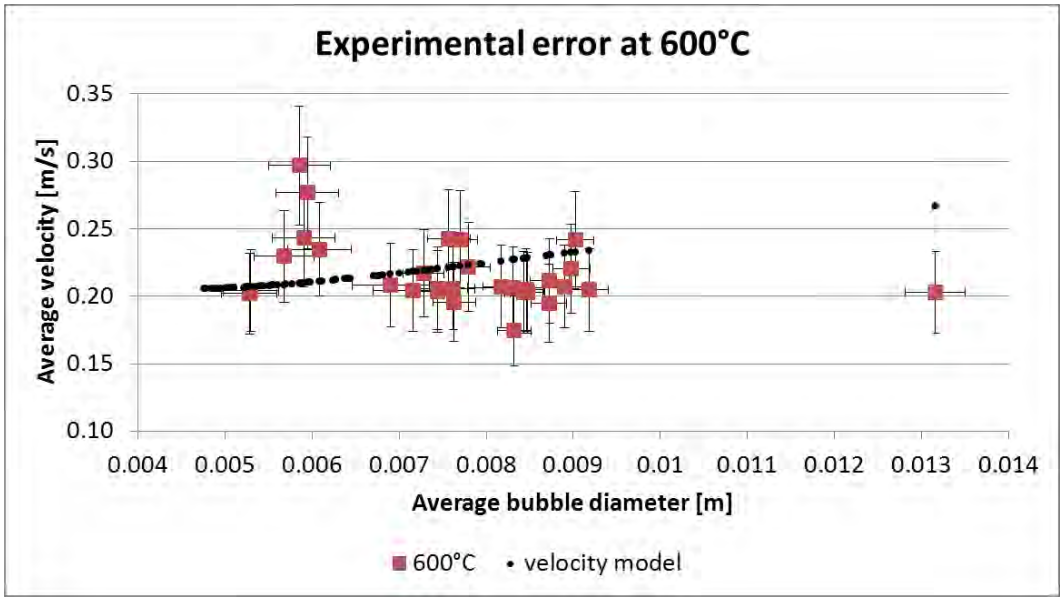

Figure 5.2- Average bubble diameter versus average bubble velocity at 600°C showing estimated experimental error

The mass flow rate has a slight positive correlation with the average bubble velocity as can be seen in figure 5.3. This suggests that inertial and momentum forces are significant in the bubble formation force balance. Although the mass flow rate has a positive correlation with diameter and Mendelson's model suggests a slight positive correlation between diameter and velocity, the correlation between mass flow rate and bubble diameter cannot be seen in the measured data, figure 5.4.

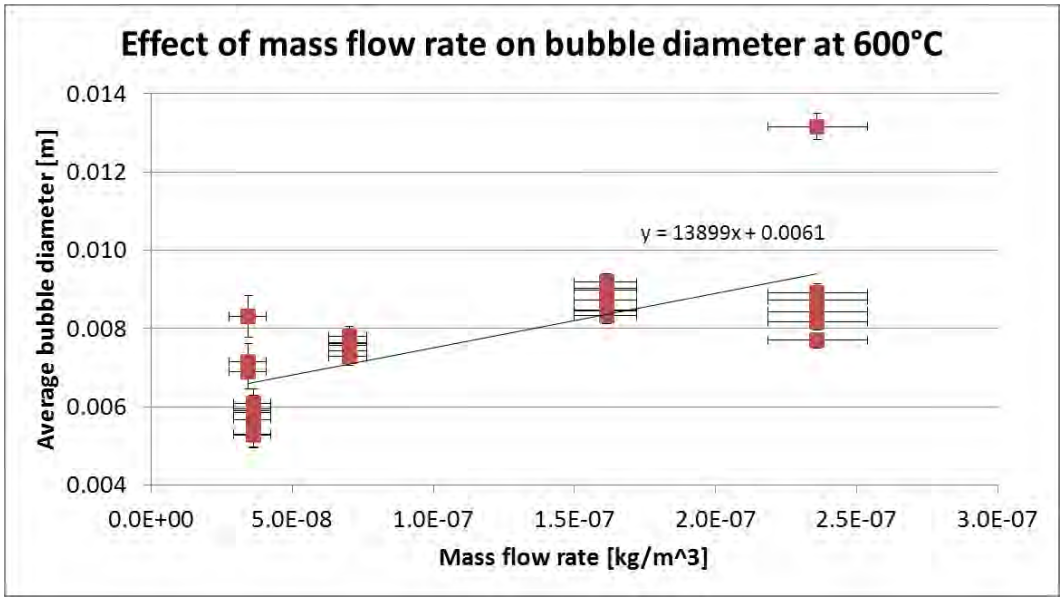

Figure 5.3- Effect of mass flow rate on the average bubble diameter with a best fit linear trend line.

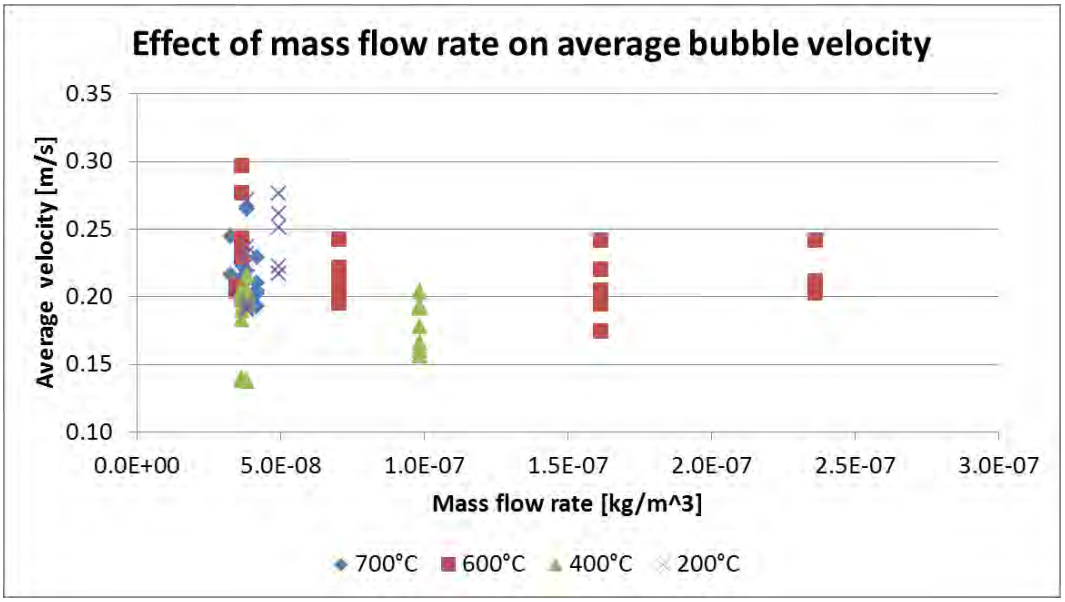

Figure 5.4- The effect of mass flow rate on average bubble velocity. Mass flow rate appears to have little effect on velocity.

Figure 5.5 below shows that the temperature of the metal has no apparent effect on the average velocity of the bubble. This is in agreement with the model, as noted earlier, the temperature of the metal effects the surface tension and density very little.

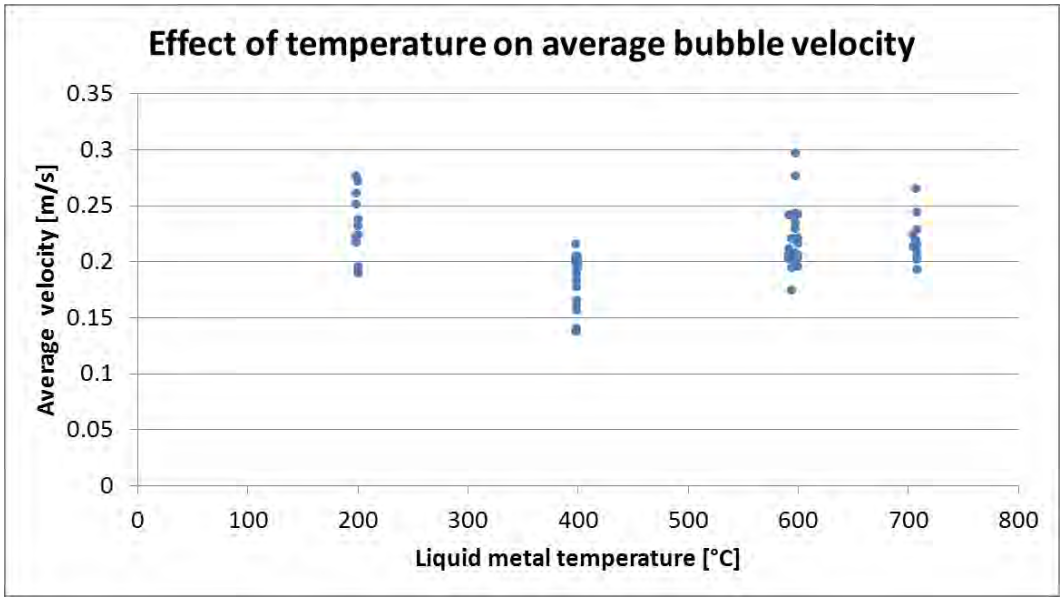

Figure 5.5- Effect of temperature on average bubble velocity.

5.2 Chemical Reaction Results

A list of all of the reactions and the conditions at which they were performed can be found below in table 5.1. These experiments were performed in two different reactors as described previously; an empty, small diameter alumina reactor for the gas only reactions and a mullite reactor filled with molten tin-bismuth alloy. The pressure in the empty reactor was held approximately constant near 170 kPa, while the pressure in the molten metal reactor varied from about 170 kPa at the bottom to 101 kPa at the top due to the hydrostatic pressure of the metal. The residence time of the gas in the empty reactor is determined from the reactor geometry and the flow rate, while the residence time in the molten metal reactor is determined by the height of the metal and the bubble velocity which was found to be approximately 0.21 [m/s].

The purpose of performing reactions in the empty reactors is to enable direct comparison between the reaction taking place with and without the tin-bismuth metal present so that the effect of the molten metal can be determined. In these experiments methane was used as a very simple model for wood and hydrocarbons formed during wood pyrolysis. Experiments 1-5 compare the effects that combinations of tin-bismuth, water and tin-dioxide have on methane reforming. The experiments with the 6 gas mixture compare how methane reforming is effected by other components that may be present in a real gasifier producer gas such as CO, CO_2, H_2 as well as determining how O_2 will interact with the molten tin-bismuth. Finally, because water and oxygen gas were found to easily oxidize tin to form tin dioxide (SnO_2), experiments 9 and 10 were performed to determine if H_2 or CO could be used to reform tin-dioxide back to pure tin under these conditions.

Experimental Conditons				
Exp. Number	Reactants	Temperatures [°C]	Average Pressure [kPa]	Residence Time [sec]
1	CH4	25 to 1000	173	6.0 to 27.0
2	CH4+SnBi	200 to 700	134	3.1 to 3.3
3	CH4+SnBi+SnO2	200 to 800	137	3.1 to 3.4
4	CH4+H2O	70 to 1000	175	5.5 to 22.6
5	CH4+H2O+SnBi	200 to 400	141	4.0
6	CH4+O2+CO+CO2+H2	38 to 1000	172	6.2 to 25.9
7	CH4+O2+CO+CO2+H2+SnBi	200 to 980	135	3.0 to 3.4
8	CO	200 to 1000	172	5.5 to 24.1
9	CO+SnBi+SnO2	200 to 800	137	3.0 to 3.8
10	H2+SnBi+SnO2	200 to 800	138	3.2 to 3.5

Table 5.1- List of experiments and the range of conditions at which they were performed

5.2.1 CH4 Reforming

The rates of methane decomposition in the empty reactor measured in this work appear to be in good agreement with rates given by Palmer obtained from un-catalyzed thermal decomposition of methane experiments. A comparison of the measured composition from experiment 1 and the composition predicted by Palmer can be seen in figure 5.6, where Palmer's rate constant (equation 5.1) and first order rate law (equation 5.2) were used to calculate the composition at the conditions at which experiment 1 was performed as well as at conditions representative of taking place in the tin-bismuth reactor if the tin-bismuth were inert.

$$k = \exp\left[14.6 - \frac{22.5 \times 10^8}{T}\right]$$

Equation 5.1- Rate constant of thermal methane decomposition proposed by Palmer with k having units 1/sec and T being temperature in Kelvin [31]

$$[CH_4] = -kt + \ln([CH4]_0)$$

Equation 5.2- First order rate law giving concentration of CH4 with [CH4]o being the initial concentration of methane, k being the rate constant described in equation 5.1, and t being the time of the reaction in seconds

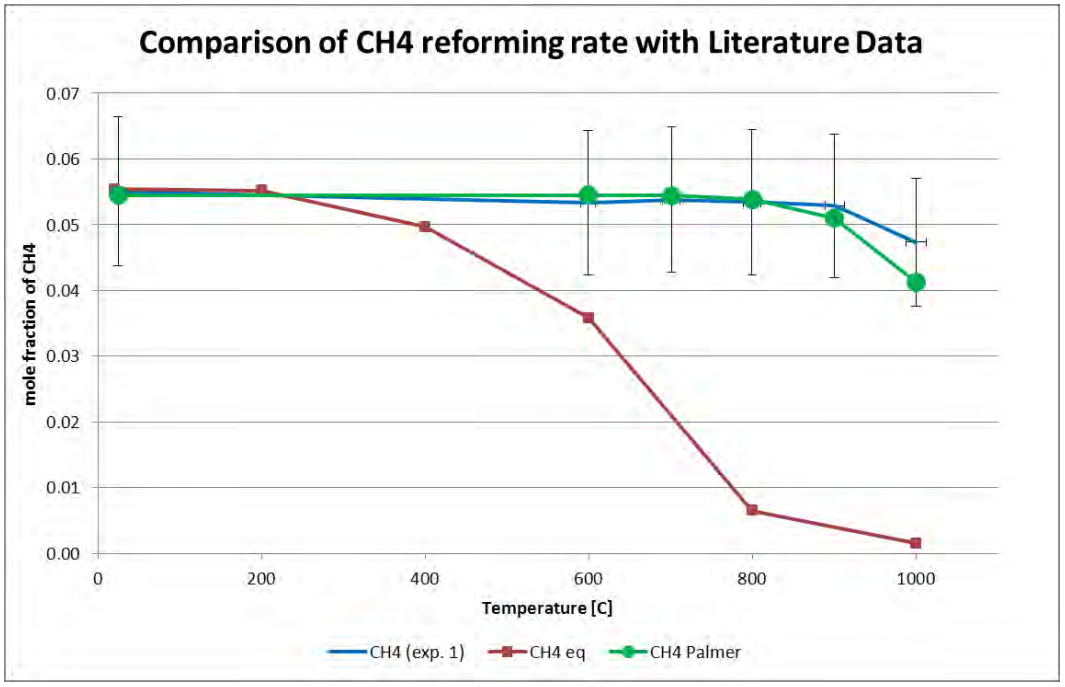

Figure 5.6- Comparison of CH4 decomposition measured in experiment 1 (CH4 (exp.1)), the predicted equilibrium concentration of CH4 in experiment 1 (CH4 eq) and the composition predicted by equation 5.1 and 5.2 at experiment 1 conditions (CH4 Palmer)

Additionally, figure 5.6 shows that the input composition of experiment 1 was at equilibrium, but the equilibrium shifted lower at temperatures higher than 200°C. The measured methane composition lagged the equilibrium composition due to the kinetics of the reactions, and did not achieve equilibrium values even at 1000°C.

The differences in methane decomposition in experiments 6 and 7 appear to be small suggesting that tin-bismuth has little effect on methane decomposition when CO, CO_2, O_2 and H_2 are present, as can be seen in figure 5.7. The results of experiments 4 and 5 in figure 5.7 show that no methane decomposition is occurring in the molten metal at temperatures below 400°C, in the presence of water. As discussed in section 5.2.2, the hydrogen production seen in figure 5.8 for experiment 5 is the result of water decomposition.

Inspection of figures 5.7 and 5.8 below will reveal that in experiments 2 and 3, an increase in methane and hydrogen was observed. The apparent increase in methane is probably due to another hydrocarbon gas forming in the system that is not being considered in the analysis. The peaks at mass to charge ratios of 14, 15 and 16 are common to methane and many other hydrocarbons. If multiple gases form the same peaks in a mass spectrum, and at least one of the gases is not properly identified, the partial pressure of the other gases sharing those peaks will be erroneous. This is discussed further in section 5.2.4.

Assuming the methane data for experiments 2 and 3 are erroneous as discussed above, formation of hydrogen can be used as an indication of methane decomposition. Figure 5.8 shows that in experiments 2 and 3, methane decomposition occurred at a lower temperature in tin-bismuth than in an empty reactor, experiment 1.

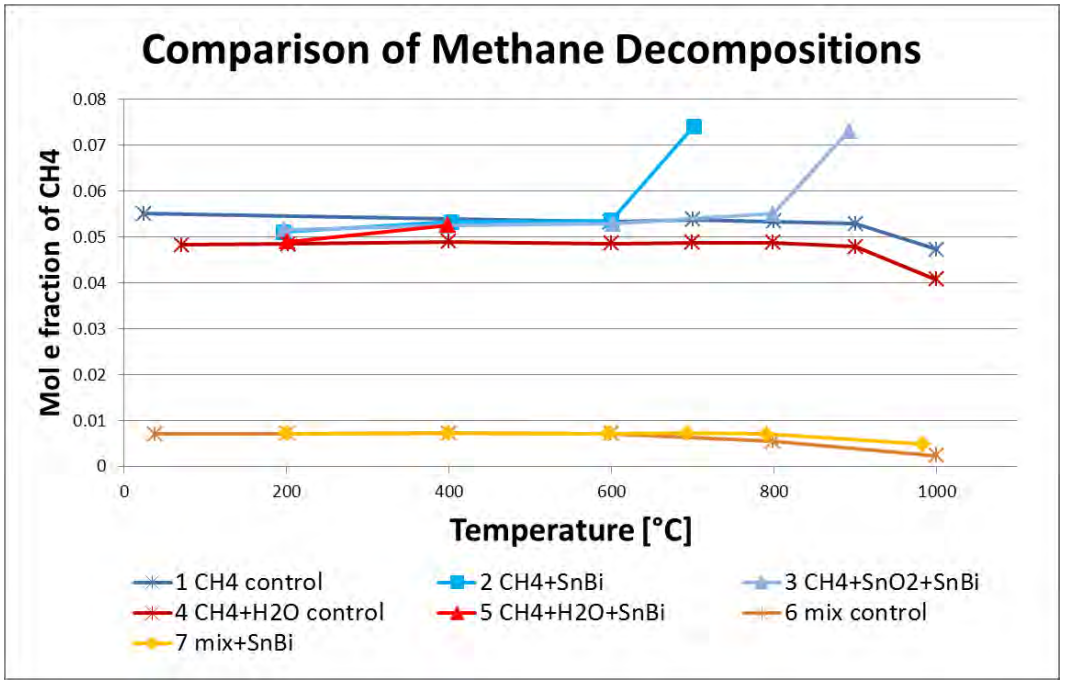

Figure 5.7- Comparison of methane decomposition over different conditions. The number indicates the experiment number in table 5.1 above.

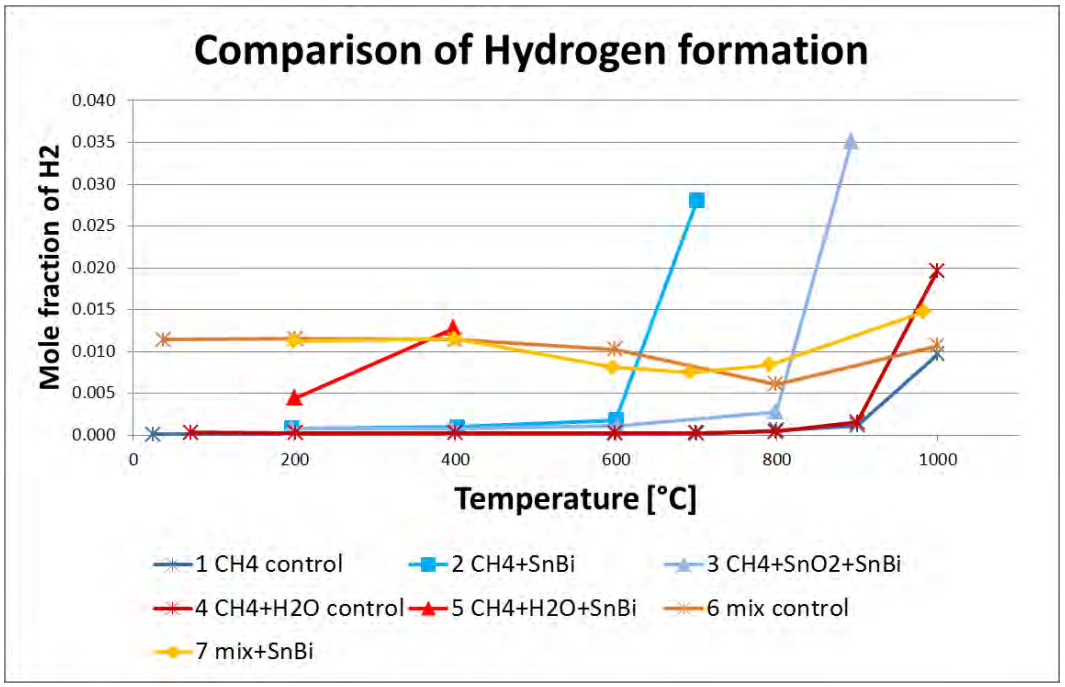

Figure 5.8- Comparison of the hydrogen formation at different reaction conditions.

Comparing figures 5.7 and 5.9 reveals that none of the methane experiments reached equilibrium at any temperature, but most started to approach equilibrium above about 800°C. This comparison also shows that the results of experiments 2 and 3 appear to show the methane composition moving farther from the equilibrium composition. This is an indication that there is something wrong with the analysis of experiments 2 and 3 as discussed above.

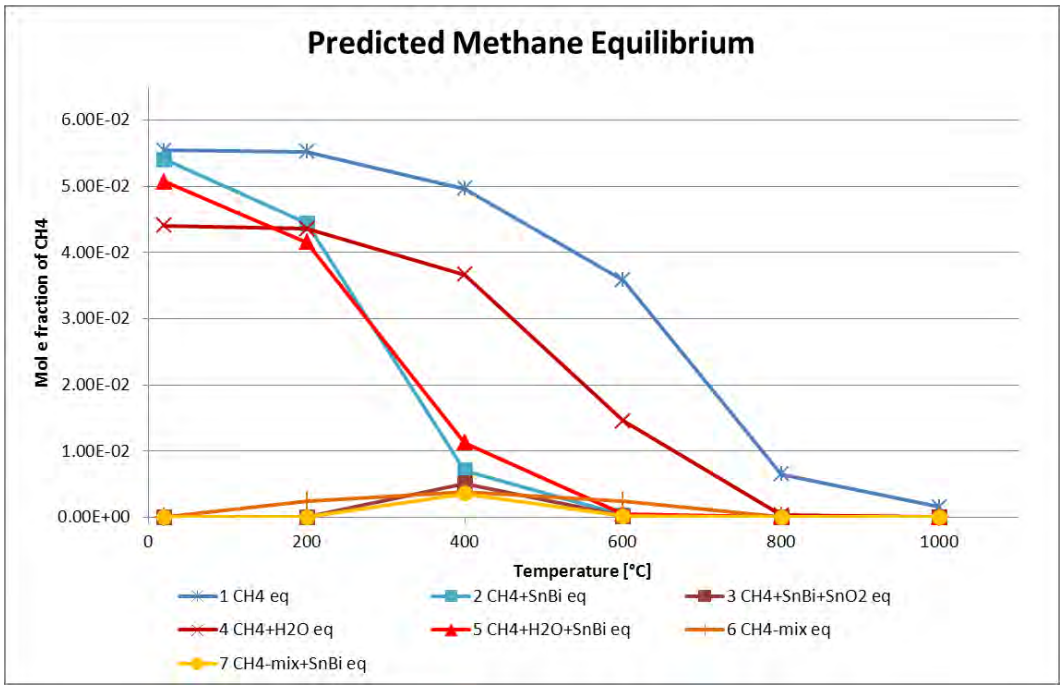

Figure 5.9- Equilibrium composition of methane as predicted by STANJAN calculations

5.2.2 Metal Oxidation

In many of the reactions it is apparent that some of the tin-bismuth is being oxidized. After experiments which took place in the molten tin-bismuth involving either water or oxygen as a reactant, a dark grey scale was found near the top of the reactor at the level of the molten metal surface. In some instances, such as experiment 5, this scale was formed in enough quantity to completely block gases from exiting the reactor, forcing the experiment to cease. It was determined that the only possible sources of this scale are the reactants and the tin-bismuth melt. A review of literature suggests that tin dioxide (SnO_2) and bismuth trioxide (Bi_2O_3) are the only tin and bismuth oxides that will form and are stable under the conditions of these experiments [34] [20]. Comparing the Gibbs free energy of formations of the two oxides suggests that tin dioxide will form preferentially over bismuth trioxide because the free energy of formation of tin dioxide is lower at all temperatures involved with these experiments, see figure 5.10. Furthermore, tin dioxide is known to be grey in color, while bismuth trioxide is yellow [42]. Although no testing was done on the actual scale formed, it appears with relative certainty that it is primarily tin dioxide with little or no bismuth oxides present.

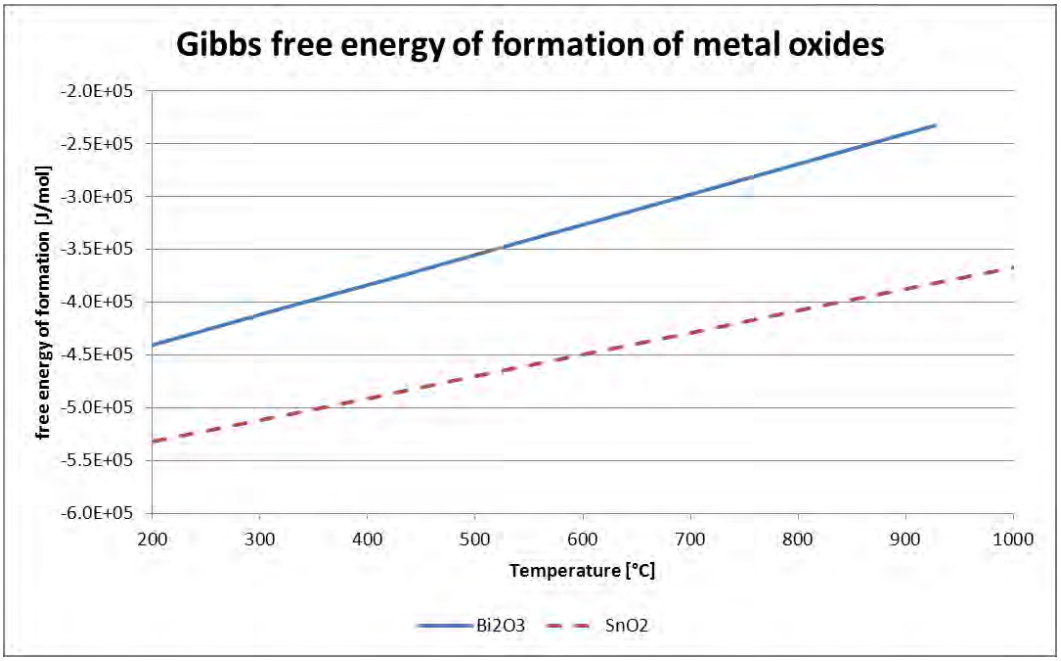

Figure 5.10- Free energy of formation of tin dioxide and bismuth trioxide, calculated from data by Kurchania and Kishimoto respectively [16] [19]

Experiments 5 and 7 can be used to determine the conditions under which the metal in the melt will be oxidized by water and oxygen gas respectively. It the case of experiment 5, it is easiest to represent the oxidation of the metal by water as being proportional to the evolution of hydrogen gas. Because there is no apparent decomposition of methane during this experiment, and no evolution of any gas components that contain oxygen, it is reasonable to assume that any hydrogen gas formed comes from the reaction described in equation 5.3. Thus, for every H_2 molecule formed, there will be one SnO_2 molecule formed.

$$H_2O + Sn + Bi \leftrightarrow H_2 + SnO_2 + Bi$$

Equation 5.3- Decomposition of water in molten tin-bismuth

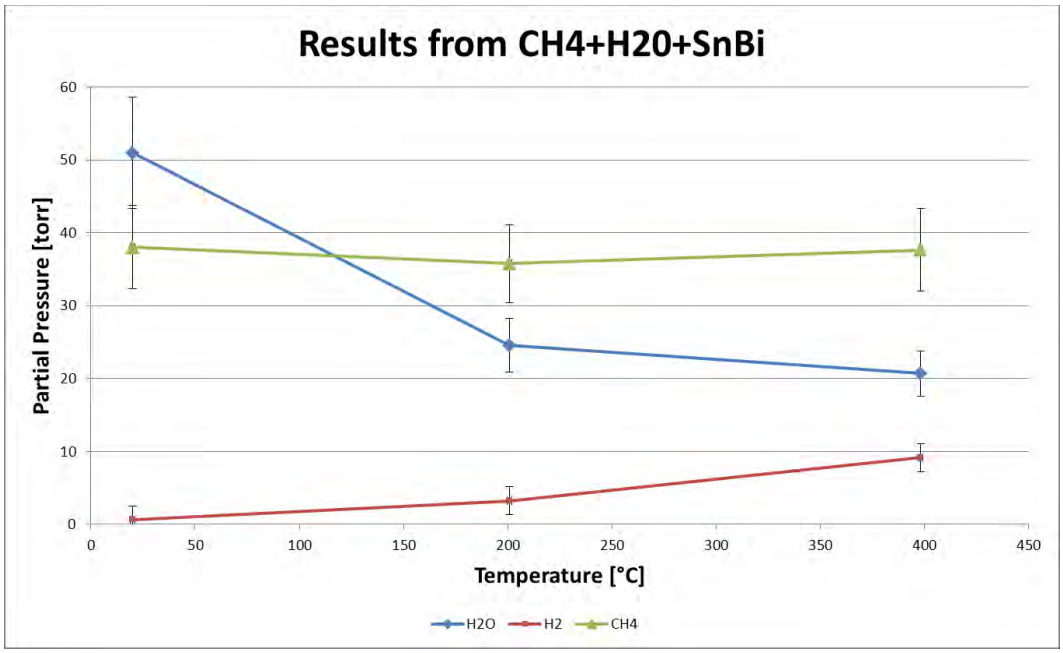

Figure 5.11- Component partial pressures results from experiment 5, showing the production of hydrogen and from the decomposition of water. The data at 20°C is the input gas composition, the metal is solid below 138°C and no reaction is assumed.

From the results of experiment 5, figure 5.11, and the discussion above it becomes apparent that water is decomposing to form hydrogen gas and tin dioxide at a significant rate at temperatures between 200 and 400°C. It was not possible to perform this experiment at higher temperatures because the tin dioxide plugged the reactor, but, literature data from Otsuka et al. suggest that the rate of water decomposition will continue to increase up to at least 700°C [43].

The results of experiment 7 also show significant apparent oxidation of tin, but over a wider temperature range and by oxygen gas rather than water. A plot of the mole fraction of oxygen in the product stream, figure 5.12, shows that nearly all of the oxygen is reacted at temperatures at or above 400°C when in the presence of tin-bismuth during experiment 7. The results of experiment 6, the same reactants as 7 but without tin-bismuth, show that the oxygen content of the gas is only lowered significantly at temperatures above 600, and oxygen is not entirely eliminated until 1000°C is reached.

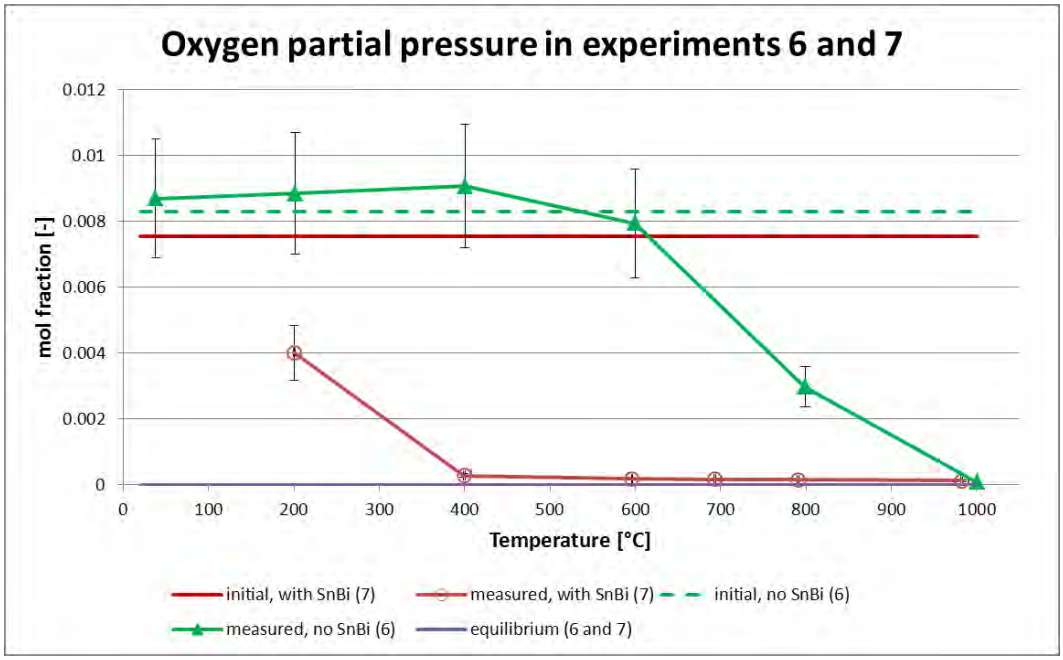

Figure 5.12- Oxygen partial pressures measured during experiments 6 and 7 comparing measured mole fraction of oxygen to the input mole fraction. Experiment 6 took place in an empty reactor, while experiment 7 took place in tin-bismuth. In both cases the equilibrium oxygen concentration was predicted to be very near zero for the entire temperature range.

There are several other oxygen containing compounds present in both of these experiments, so it is necessary to examine the changes in all of the compounds to determine if tin-dioxide is being formed, figure 5.13 and 5.14. An element balance was performed, summing all of the moles of each element that enter and exit the reactor, subtracting the value out from the value in to determine if there are significant amounts of any element remaining in the system. In the case of oxygen, it is suggested that any oxygen found to be remaining in the system, is in the form of tin dioxide. As such, the molar formation rate of tin dioxide can be calculated as one half of the unaccounted elemental oxygen flow rate.

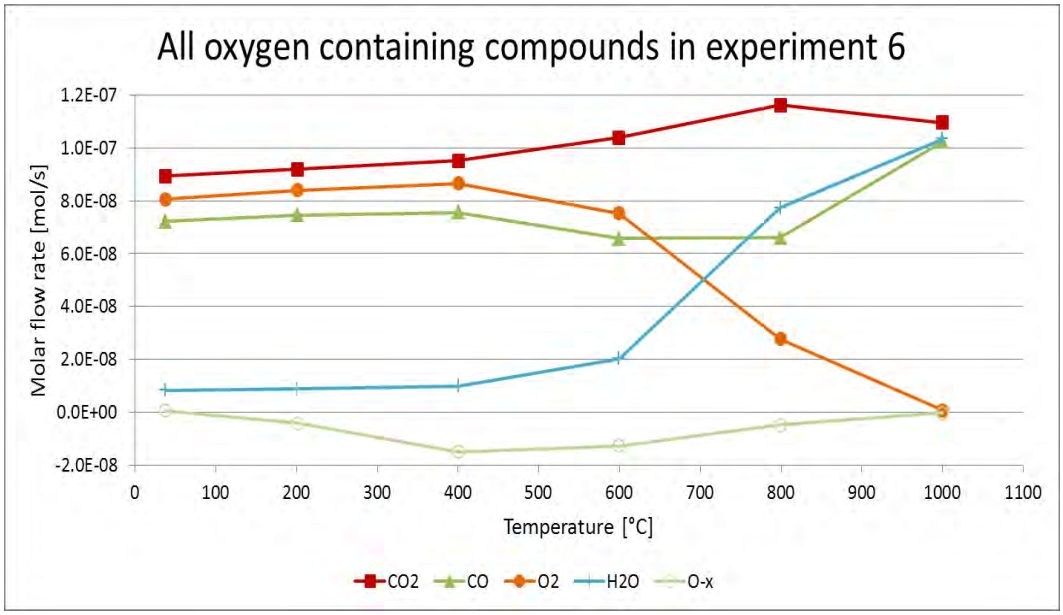

Figure 5.13- Results from experiment 6 (6 gas mixture in empty reactor) showing all of the oxygen containing compounds present. Also shown is the unaccounted for oxygen (O-x) as determined by an element balance on the molar flow rates in and out of the reactor.

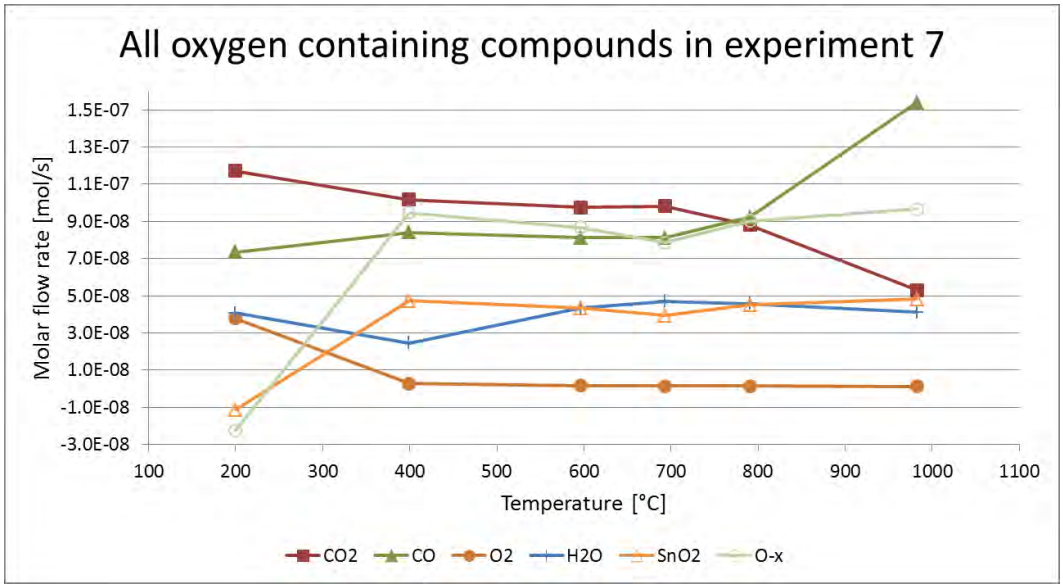

Figure 5.14- Results from experiment 7 (6 gas mixture in tin-bismuth) showing all of the oxygen containing compounds and unaccounted for oxygen (O-x) as in Figure 5.13. Also shown is the molar formation rate of tin dioxide (SnO2) as calculated from the otherwise unaccounted for oxygen.

In the case without tin-bismuth present, it appears as though the oxygen that reacts forms primarily water and carbon monoxide, with very little oxygen unaccounted for in the element balance. Comparatively, the case with tin-bismuth present shows lower water production, and much oxygen unaccounted for in an element balance, which is assumed to form tin dioxide.

5.2.3 Reduction of Oxidized Metal

It is apparent that the liquid tin-bismuth melt is easily oxidized over a wide range of conditions by both oxygen and water, apparently forming tin dioxide. This tin dioxide has been shown in literature to be useful as a catalyst for combustion of CH_4, H_2 and CO [37]

[13]. Experiments 9 and 10 were carried out in an attempt to determine the rates at which CO and H_2 will reduce tin-dioxide. Both experiments involved oxidizing some of the tin by first running argon and water through the melt, then purging with argon until all of the produced hydrogen gas was removed. After the purge, the reducing agent, CO in experiment 9 or H_2 in experiment 10, was bubbled through the partially oxidized tin-bismuth at a variety of temperatures.

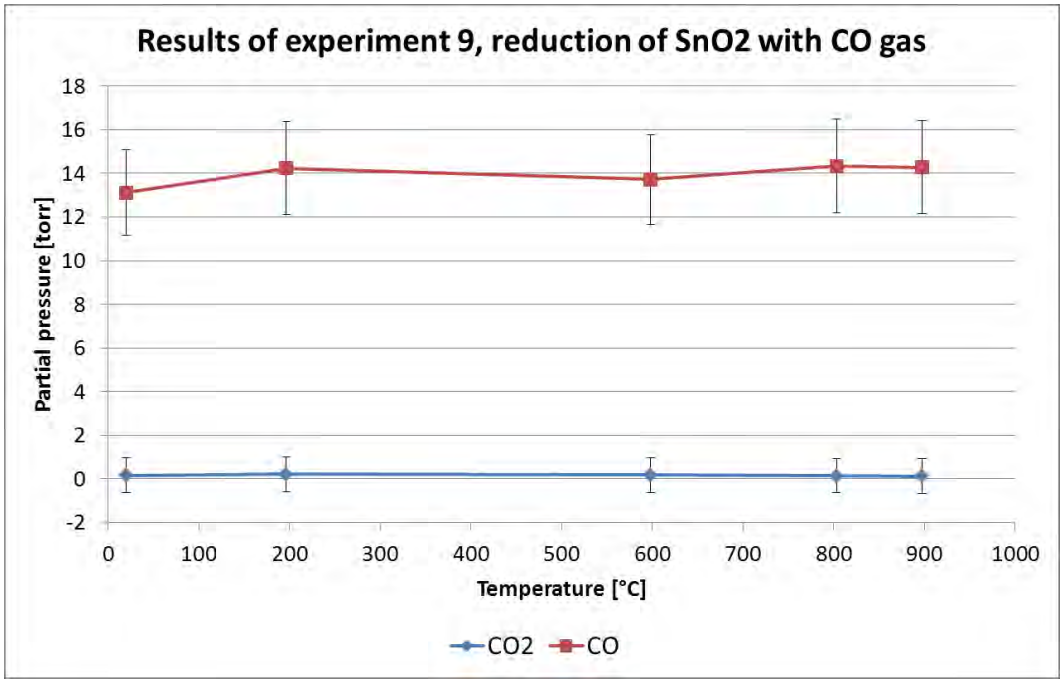

Figure 5.15- Results of reduction of SnO2 with CO gas. No measurable reaction took place.

The reaction that was expected to take place in the case of experiment 9 is shown in equation 5.4, as suggested by Fuller and Warwick. Furthermore, the metastable tin monoxide (SnO) is expected to reform into tin dioxide and pure tin as seen in equation 5.5

[44]. The change in Gibbs free energy for the overall reaction on the basis of forming one CO_2 molecule was calculated using data from the NIST-JANAF Thermochemical Tables and from Kurchania et al. [11] [16]. As can be seen in figure 5.16 the change in Gibbs free energy is negative under all conditions of these experiments so, thermodynamically the reactions should proceed to form CO_2 and tin. However, the results of experiment 9 show no detectable reaction taking place up to 900°C, as can be seen in figure 5.15.

$$CO + SnO_2 \leftrightarrow CO_2 + SnO$$

Equations 5.4- Reduction of tin dioxide by carbon monoxide as suggested by Fuller and Warwick [33]

$$2\,SnO \leftrightarrow SnO_2 + Sn$$

Equations 5.5 – Reformation of metastable tin monoxide into tin dioxide and liquid tin [44]

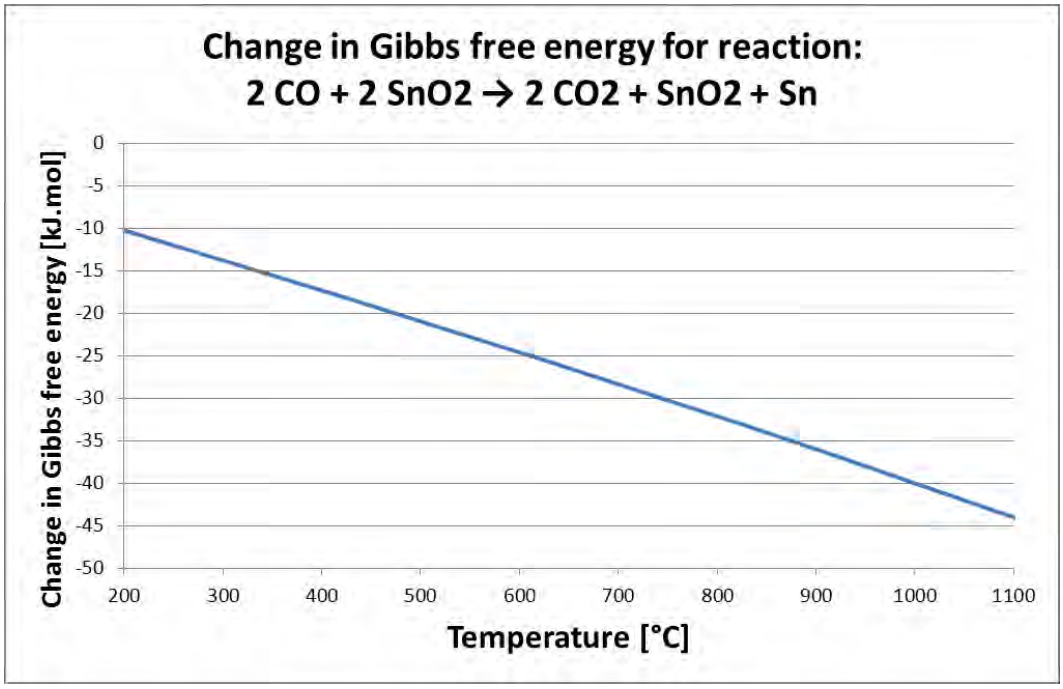

Figure 5.16- Calculated change in Gibbs free energy for the reduction of SnO_2 by CO [11] [16]

The lack of reaction is probably due to a combination of two factors. First, the kinetic rate of reaction may be limited, so that although the reaction is taking place it is so slow that was not observed. Literature suggests that this reaction is not very fast, even at higher temperatures [36]. The second probable factor limiting the reaction is that the tin dioxide floats on top of the tin-bismuth melt in a thin layer, which severely limits the contact time with the gas. The reaction described in equation 5.4 is known to take place in the smelting of tin from cassiterite (tin ore, primarily SnO_2) [36]. Van Deventer measured the production of CO_2 at a significant rate from this process between 780°C and 1160°C, with the rate increasing with temperature [36]. The geometry of the reaction in this work

compared to Van Deventer's is considerably different. Van Deventer's reactor was a packed tube filled with graphite and SnO_2 designed for long residence times, while the interaction between the CO and SnO_2 in this work is very short.

The results of experiment 10 show that there may be a small amount of reaction taking place between tin dioxide and hydrogen gas to form water (figure 5.17). However, literature data disagrees with these results, showing increasing reaction rate from 500 to 750°C, where no reaction was measured in this work [32]. It is possible that the water was not produced by any reaction, but was left over in the system from the oxidation stage of the experiment. In any case, the rate of reaction was very low and a significant amount of the metal oxide was not removed. It is probable that the lack of reaction in experiment 10 had the same cause as in experiment 9, too low of a reaction rate at these temperatures and too short of a reaction time between the gas and solid oxide.

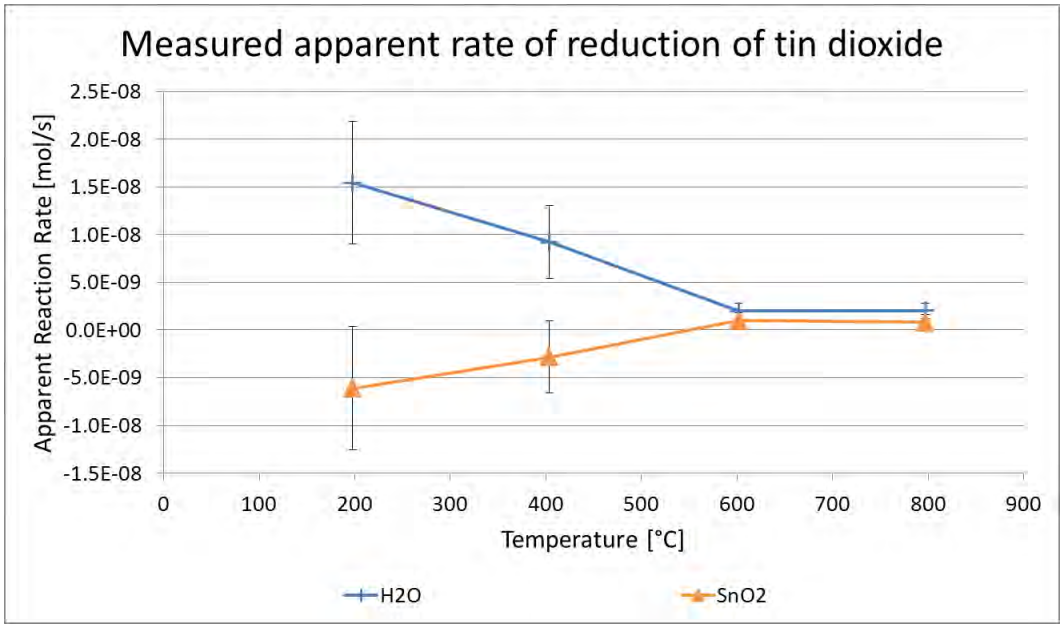

Figure 5.17- Results of experiment 10, the measured apparent rates of reduction of tin dioxide and formation of water from reaction proposed in equation 5.6.

$$SnO_2 + 2\,H_2 \leftrightarrow Sn + 2\,H_2O$$

Equation 5.6- Reduction of tin dioxide by hydrogen [32]

5.2.4 Unidentified Mass Spectrum Peaks

Noted previously in this chapter, a number of the experiments produced a gas or gases that caused peaks on the mass spectrum that are not used in the partial pressure analysis. These peaks cannot be accurately used in the analysis unless the gases that cause them are identified. Table 5.2 shows the conditions at which these unidentified peaks were found to occur.

Experimental Conditons						
Exp. Number	Reactants	Temperatures [°C]	Average Pressure [kPa]	Residence Time [sec]	Temperature at which unidentified peaks occur [°C]	Notes
1	CH4	25 to 1000	173	6.0 to 27.0	1000	barely detectable
2	CH4+SnBi	200 to 700	134	3.1 to 3.3	700	highest level
3	CH4+SnBi+SnO2	200 to 800	137	3.1 to 3.4	-	
4	CH4+H2O	70 to 1000	175	5.5 to 22.6	900-1000	barely detectable
5	CH4+H2O+SnBi	200 to 400	141	4	-	
6	CH4+O2+CO+CO2+H2	38 to 1000	172	6.2 to 25.9	-	
7	CH4+O2+CO+CO2+H2+SnBi	200 to 980	135	3.0 to 3.4	200-400	lower at 400° than 200°C
8	CO	200 to 1000	172	5.5 to 24.1	-	
9	CO+SnBi+SnO2	200 to 800	137	3.0 to 3.8	-	
10	H2+SnBi+SnO2	200 to 800	138	3.2 to 3.5	-	

Table 5.2- List of experiments with conditions that produced mass spectrums with unidentified peaks noted

From inspection of table 5.2, it appears as though there is little consistency among conditions at which unidentified peaks occur in the mass spectrum. They occur over a wide range of temperatures, at different residence times and with different reactants. One common factor is methane in the reactants. However, there are several cases where methane is used and unidentified peaks do not occur. The relative size and locations of these peaks also changes with conditions. These facts suggest that there may be multiple causes of these peaks.

Although the unidentified peaks are not always the same, they appear to follow a general pattern: they occur in groups of roughly 3 to 8 separated from each other by 1 atomic mass units (amu) with the groups separated by approximately 12 amu. This pattern can be seen in figure 5.18, which is an example of a mass spectrum that has unidentified peaks compared with a spectrum without unidentified peaks.

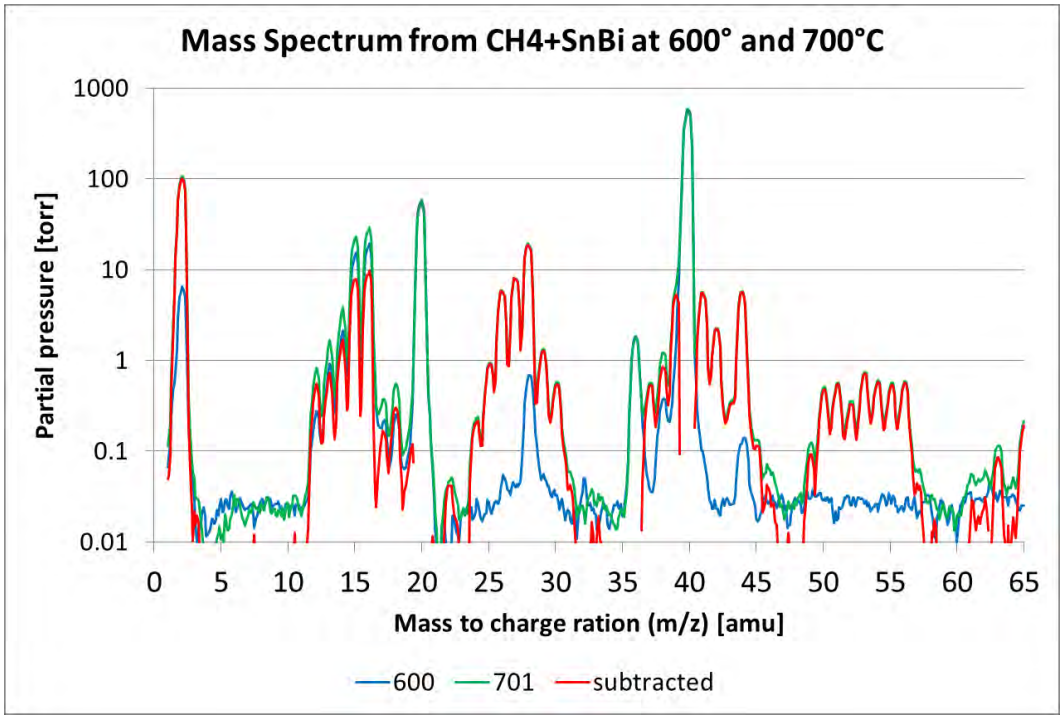

Figure 5.18- Comparison of mass spectra with (700) and without (600) unidentified peaks from the experiment 2. Also shown is the result of a subtraction of the two spectra.

This pattern of peaks mentioned above is common to most hydrocarbon molecules. This makes identification of the gas or gases that are causing these peaks very difficult with a quadrapole mass spectrometer. However, from comparing the subtracted spectra to library spectra of various hydrocarbons it appears as though the unidentified gases that cause the peaks in the range 49-57 amu are at least 4 carbons long, and peaks higher than that are probably caused by gases 5 or more carbons long.

Assuming that the unidentified gas is a mixture of hydrocarbons, one possible source is the decomposition of methane. A study by Olsvik, Rokstad and Holmen suggest that methane decomposition can be described by a stepwise dehydrogenation, as in equation 5.7. That study suggests that at high temperatures there are several intermediate steps in

methane decomposition that produce C_2 hydrocarbons and hydrogen, and that given enough time to react, the only products will be solid carbon and H_2 gas. If, however the reaction time is limited, the product gas will contain C_2 intermediates as well as secondary products formed from the C_2 hydrocarbons, such as benzene [45]. The experimental results of Olsvik et al. showed that the major products of methane pyrolysis at 1 atm and from 1200 to 1600°C are ethene, acetylene, benzene, hydrogen and carbon with several other hydrocarbons listed as minor products. These experiments took place with residence times between approximately 0.01 and 0.6 seconds. As can be seen in figure 5.19, the gases suggested by Olsvik et al. create many of the unidentified peaks seen in figure 5.18, but not all.

$$CH_4 \rightarrow C_2H_6 + H_2 \rightarrow C_2H_4 + H_2 \rightarrow C_2H_2 + H_2 \rightarrow 2\,C + H_2$$

Equation 5.7- Methane decomposition suggested by Olsvik et al. [45]

Another possible source of the hydrocarbons that are forming the unidentified peaks is contamination of the experimental system. Hydrocarbons such as machining oil may have gotten into the system, but this is not likely the cause because bake outs of the reactor to 1000°C were performed each time the reactor was re-assembled. It is also possible that larger hydrocarbons were formed in some experiments, but condensed in the system, only to be re-volatilized and show up in the mass spectra of another experiment.

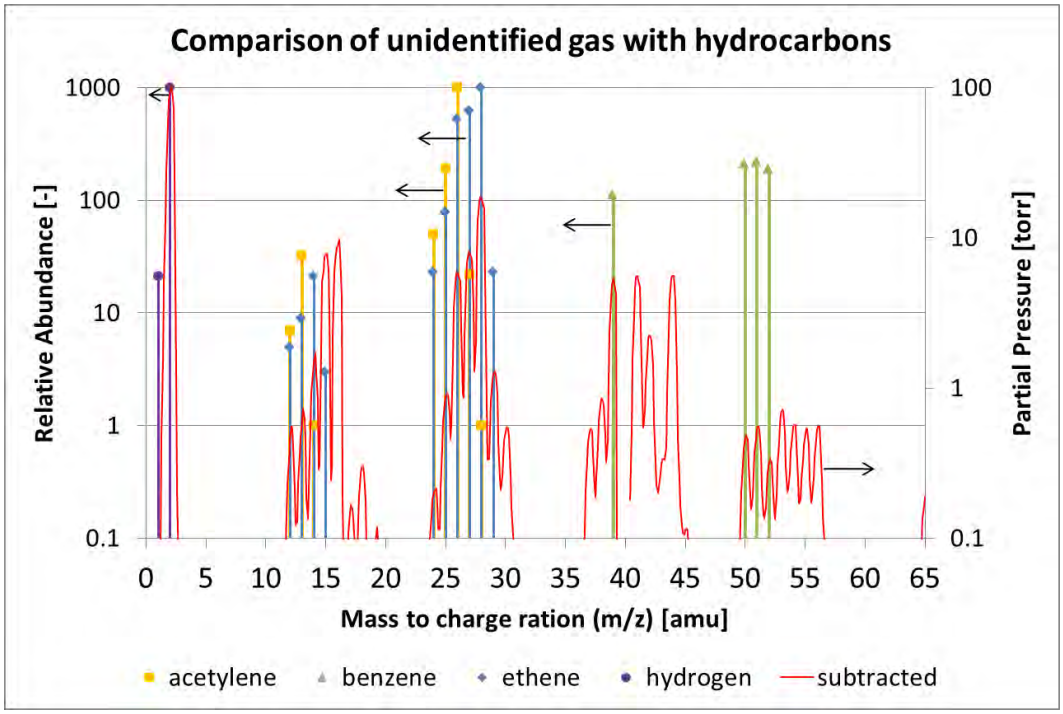

Figure 5.19- Comparison of subtracted mass spectrum from figure 5.18 with mass spectra of gases suggested by Olsvik et al. [45]

Further investigation of this matter is required to draw more definite conclusions. The addition of a carefully calibrated gas chromatograph to the gas analysis system may aid in the identification of these unknown gases and their source.

6. Conclusions

6.1 Bubble Measurements

The results of the bubble velocity experiments showed that the experimental results utilizing a two microphone bubble detection system are in good agreement with Mendelson's model for the terminal velocity of a bubble rising through a liquid. The conditions studied were 200-700°C tin-bismuth between 1 and 1.7 atmospheres with an average bubble diameter of 6.7 mm. Under these conditions the average velocity was approximately 0.21 m/s. The main factor with which the velocity varies is the bubble diameter, however this variation was small. The diameter of the bubble is most greatly affected by the gas mass flow rate.

A new method was developed to determine the velocity of a bubble in a molten metal from microphone data. Previous experiments described in the literature measured the bubble velocity by shutting off the flow and measuring the time between the last bubble release and the last bubble reaching the surface. The current work uses a method which allows the measurement to take place without shutting off the flow. This method determines the bubble velocity in a steady state flow using an estimate of the transit times. The new method agrees well with literature results.

In the future, improvements may be made to the microphone system to make the signals from the bubbles stronger compared to the background noise. If the improvements are sufficient enough to improve the power associated with each bubble peak, it may be

possible to analyze the bubble data with an autocorrelation method rather than the manual peak finding method used in the current analysis. This would be a great improvement which would decrease the time it takes to analyze the data while increasing the accuracy of the measurement. Further improvements to accuracy could be obtained by using higher accuracy mass flow meters.

6.2 Chemical Reactions

The chemical reaction experiments compose a fairly broad overview of the reactions important to a tin-bismuth pyrolysis and gasification system. As such they are not entirely complete and leave many questions unanswered. The unexpectedly high errors associated with partial pressure and mass flow measurements made the uncertainty in calculated rate values too high for the rates to be statistically significant. But, conclusions can be drawn from the partial pressure data when compared to literature data. Even with these noted problems, the results suggest several important trends and some areas of research that may produce interesting results in future work.

The measured decomposition rate of methane in a reactor without liquid tin-bismuth was similar to literature data. The rate of methane decomposition appears to be accelerated when bubbled through tin-bismuth in the temperature range of 600-900°C. This increase in rate may be due to the improved heat transfer to the reaction provided by the thermally conductive liquid metal. Furthermore, the products of this decomposition are uncertain, but appear to hydrogen, carbon and hydrocarbon chains between 2 and at least

4 carbons long formed in a similar fashion to the decomposition reaction described by Olsvik in equation 5.7 [45]. This increased decomposition of methane did not appear when the mixture of 1% of each CO, CO_2, CH_4, H_2, O_2 and 95% argon was heated in the presence of tin-bismuth up to 1000°C. This suggests that the unknown methane decomposition reaction may be inhibited by CO, CO_2, H_2, O_2 or a mixture of these compounds.

Tin was found to be oxidized rapidly by oxygen gas at temperatures between 200 and 1000°C. Near complete conversion of oxygen in the above described 6 gas mixture was observed at 400°C with a residence time of approximately 3.2 seconds in tin-bismuth, with almost all of the oxygen being used to form tin dioxide. Water was found to readily form tin dioxide and hydrogen at temperatures between 200 and 400°C. Higher temperatures were not able to be tested due to the build-up of tin dioxide in the reactor.

Reduction of tin dioxide in this reactor was less successful. Carbon monoxide did not appear to be effective at reducing tin dioxide at temperatures between 200 and 800°C, while hydrogen may have reduced a detectable, but insignificant amount of tin-dioxide at 200 and 400°C. However, the apparent reduction of tin dioxide by hydrogen disagrees with literature data and may have been caused by water left in the system from a previous test.

The effect that tin-bismuth appears to have on methane decomposition warrants more study to confirm these results and to identify the reaction taking place and its products. This study may be further extended to larger hydrocarbons or solids such as

cellulose or wood. The addition of a gas chromatograph to the gas analysis train may help in the identification of the hydrocarbons being produced.

Further study into the reduction of tin dioxide is needed. Literature suggests that CO and H_2 are more successful at reducing tin dioxide at higher temperatures, up to 1500°C, and with longer residence times. Because tin-bismuth so readily oxidizes and appears difficult to reduce, the proposed gasification system may need to be reconsidered. The system should either be re-designed so that the molten metal does not come into contact with any oxidizing agents like O_2 or H_2O, or a different molten material be found that will not oxidize so readily.

7. Works Cited

[1] R. Perlack and B. Stokes, "U.S. Billion-Ton Update: Biomass Supply for a Bioenergy and Bioproducts Industry," U.S. Department of Energy, OakRidge, Tn, 2011.

[2] A. V. Bridgewater, D. Meier and D. Radlein, "An overview of fast pyrolysis of biomass," *Organic Geochemistry,* vol. 30, pp. 1479-1493, 1999.

[3] M. Puig-Arnavat, J. Bruno and A. Coronas, "Review and analysis of biomass gasification models," *Renewable and Sustainable Energy Reviews,* vol. 14, no. 9, pp. 2841-2851, 2010.

[4] D. Mohan, C. U. J. Pittman and P. H. Steele, "Pyrolysis of wood/biomass for bio-oil: a critical review," *Energy and Fuels,* vol. 20, pp. 848-889, 2006.

[5] A. Kumar, D. Jones and M. Hanna, "Thermochemical biomass gasification: A review of the current status of the technology," *Energies,* vol. 2, pp. 556-581, 2009.

[6] Food and Agriculture Organization Forestry Department, "Wood gas as and engine fuel," Food and Agriculture Organization of the United Nations, Rome, Italy, 1986.

[7] W. Lin, L. O. Pordesimo, A. Haryanto and J. Wooten, "Co-gasification of hardwood chips and crude glycerol in a pilot scale downdraft gasifier," *Biosource Technology,* vol. 102,

pp. 6266-6272, 2011.

[8] Diversified Energy, "HydroMax-Advanced Gasification Technology," [Online]. Available: http://www.diversified-energy.com/index.cfm?s_webAction=hydromax. [Accessed 18 August 2011].

[9] T. H. Crane, H. Ringer and D. Bridges, "Production of gaseous fuel by pyrolysis of municipal solid waste, NASA CR-141791," National Aeronautics and Space Administration, Houston, 1975.

[10] R. Eatwell-Hall, V. Sharifi and J. Swithenbank, "Hydrogen production from molten metal gasification," *International Journal of Hydrogen Energy,* vol. 35, pp. 13168-13175, 2010.

[11] M. W. Chase, Jr., "NIST-JANAF Thermochemical Tables-Fourth Editions, Parts 1 and 2," American Chemical Society, American Institute of Physics and the National Insititue of Standards and Technology, Woodbury, New York, 1998.

[12] G. Sikha, W. A. McPhee, Q. Zhang, M. T. Koslowske, T. T. Tao and R. White, "One-dimensonal modeling of a liquid tin anode solid oxide fuel cell," *ECS Transactions,* vol. 17, no. 1, pp. 161-173, 2009.

[13] T. T. Tao, W. A. McPhee, M. T. Koslowske, L. S. Bateman, M. J. Slaney and J. Bentley, "Advancement in liquid tin anode-solid oxide fuel cell technology," *ECS Transactions,* vol. 12, no. 1, pp. 681-90, 2008.

[14] X. Chen, K. Khor and S. Chan, "Identification of O2 reduction processes at yttria stabilized zirconia/doped lanthanum manganite interface," *journal of Power Sources,* vol. 123, pp. 17-25, 2003.

[15] T. Tao, M. Slaney, L. Bateman and J. Bentley, "Anode Polarization in Liquid Tin Anode Solid Oxide Fuel Cell," *ECS Transactions,* vol. 7, no. 1, pp. 1389-1397, 2007.

[16] R. Kurchania and G. M. Kale, "Oxygen potential in molten tin and Gibbs energy of formation of SnO2 employing an oxygen sensor," *Journal of Materials Research,* vol. 15, no. 7, pp. 1576-1582, 2000.

[17] E. Bilek, K. E. Skog, J. Fried and G. Christensen, "Fuel to burn : economics of converting forest thinnings to energy using BioMax in southern Oregon," U.S. Department of Agriculture, Forest Service, Forest Products Laboratory, Madison, Wi, 2005.

[18] Z. Moser, W. Gasior and J. Pstrus, "Surface Tension Measurements of the Bi-Sn and Sn-Bi-Ag Liquid Alloys," *Journal of Electronic Materials,* vol. 30, no. 9, pp. 1104-1111, 2001.

[19] A. Kishimoto, A. Wada, T. Michimoto, T. Furukawa, K. Aoto and T. Oishi, "Solubility and activity of oxygen in Pb-Bi melts," *Materials Transactions,* vol. 47, no. 1, pp. 122-128, 2006.

[20] R. Ganesan, T. Gnanasekaran and R. Srinivasa, "Determination of standard molar gibbs free energy of formation ofBi2O3 over a wide temperature range by EMF method,"

Chem. Thermodynamics, vol. 35, pp. 1703-1716, 2009.

[21] N. Geary and R. Rice, "Bubble size prediction for rigid and flexible spargers," *AIChE Journal,* vol. 37, no. 2, pp. 161-168, 1991.

[22] S. Nafaei, T. Borca-Tasciuc and D. Wen, "Theoretical and experimental investigation of quasi-steady-state bubble growth on top of submerged stainless steel nozzels," *Colloids and Surfaces A: Physicochemical and Engineering Aspects,* vol. 369, pp. 11-19, 2010.

[23] J. Hernandez-Aguilar, R. Cunningham and J. Finch, "A test of the Tate equation to predict bubble size at an orifce in the presence of frother," *International Journal of Mineral Processing,* vol. 79, no. 2, pp. 89-97, 2006.

[24] R. Andreini, J. Foster and R. Callen, "Characterization of Gas Bubbles Injected into molten metals under laminar flow conditons," *Metallurgical Transactons B,* vol. 8, no. 4, pp. 625-631, 1977.

[25] H. D. Mendelson, "The prediction of bubble terminal velocities from wave theory," *A.I.Ch.E. Journal,* vol. 13, no. 2, pp. 250-253, 1967.

[26] K. Schwerdtferger, "Velocity of rise of argon bubbles in mercury," *Chemical Engineering Science,* vol. 23, no. 8, pp. 937-938, 1968.

[27] C. Zhang, S. Eckert and G. Gerbeth, "Experimental study of singel bubble motion in a

liquid metal column exposed to a DC magnetic field," *International Journal of Multiphase Flow,* vol. 31, no. 7, pp. 824-842, 2005.

[28] Q. Fu and J. Evans, "A capacitance probe for measurement of bubbles in molten metals," *ISIJ International,* vol. 39, no. 4, pp. 309-318, 1999.

[29] M. Schneider and J. Evans, "A novel probe for detecting gas bubbles in liquid metals," *Metallurgical and Materials Transactions B,* vol. 37, no. 3, pp. 333-337, 2006.

[30] Q. Fu, D. Xu and J. Evans, "Chlorine fluxing for removal of magnesium from molten aluminum: Part 1. Laboratory-scale measurements of reaction rates and bubble behavior," *Metallurgical and Materials Transactions B-Process Metallurgy and Materials Processing Science,* vol. 29, no. 5, pp. 971-978, 1998.

[31] H. B. Palmer, J. Lahaye and K. c. Hou, "On the kinetics and mechanism of the thermal decomposition of methane in a flow system," *The Journal of Physical Chemistry,* vol. 72, no. 1, pp. 348-353, 1968.

[32] B.-S. Kim, J.-c. Lee, H.-S. Yoon and S.-K. Kim, "Reduction of SnO2 with hydrogen," *Materials Transactions,* vol. 52, no. 9, pp. 1814-1817, 2011.

[33] M. J. Fuller and M. E. Warwick, "The catalytic oxidation of carbon monoxide on tin(iv) oxide," *Journal of Catalysis,* vol. 29, pp. 441-450, 1973.

[34] D. W. Yuan, R. F. Yan and G. Simkovich, "Rapid oxidation of liquid tin and its alloys at 600 to 800°C," *Journal of Materials Science,* vol. 34, pp. 2911-2920, 1999.

[35] B. Risold, D. Hallstedt, L. Gauckler, H. Lukas and S. Fries, "The bismuth-oxygen system," *Journal of Phase Equilibria,* vol. 16, no. 3, pp. 223-234, 1995.

[36] J. Van Deventer, "The effect of admixtures on the reduction of cassiterite by graphite," *Thermochimica Acta,* vol. 124, pp. 109-118, 1988.

[37] P. T. Wierzchowski and L. W. Zatorski, "Kinetics of catalytic oxidation of carbon monoxide and methane combustion over alumina supported Ga2O3, SnO2 or V2O5," *Applied Catalysis B: Environmental,* vol. 44, pp. 53-65, 2003.

[38] M. A. Dietenberger and M. H. Anderson, "Method and apparatus to protect synthesis gas via flas pyrolysis and gasification in a molten liquid". United States of America Patent 7875090, 25 January 2011.

[39] W. H. Press, B. P. Flannery, S. A. Teukolsky and W. T. Vetterlling, Numerical Recipes in C: the Art of Scientific Computing 2nd ed., Cambridge, Uk: Cambridge University Press, 1992.

[40] W. C. Reynolds, "The element potential method for chemical equilibrium analsysi: Implementation in the interactive program STANJAN version 3," Department of Mechanical Engineering, Stanford University, Stanford, 1986.

[41] C. Croarkin and P. Tobias, "NIST/SEMATECH e-Handbook of Statistical Methods," NIST/SEMATECH, [Online]. Available: http://www.itl.nist.gov/dic898/handbook/. [Accessed 5 December 2011].

[42] Web Elements, "Compounds," [Online]. Available: http://www.webelements.com/compounds. [Accessed 25 April 2012].

[43] K. Otsuka, S. Murakoshi and A. Morikawa, "Hydrogen production from water by reduced tin oxide," *Fuel Processing Technology,* vol. 7, pp. 213-223, 1983.

[44] P. Charvin, S. Abanades, F. Lemont and G. Flamant, "Experimental study of SnO2/SnO/Sn thermochemical systems for solar production of hydrogen," *AIChE Journal,* vol. 54, no. 10, pp. 2759-2767, 2008.

[45] O. Olsvik, O. A. Rokstad and A. Holmen, "Pyrolysis of Methane in the Presence of Hydrogen," *Chemical Engineering Technology,* vol. 18, pp. 349-358, 1995.

8. Appendix

8.1 Equipment list

Part	Manufacturer	Model	Serial Number / Version
Computer	Dell	Optiplex 960 Intel Core Duo CPU	D982RK1
Computer Operating System	Microsoft	Windows XP Professional	Version 2002 SP3
Labview DAQ Software	National Instruments	Labview 2009 (32 bit)	Version 9.0 f3
CompactDAQ	National Instruments	NI cDAQ-9172	13FBDE7
cDAQ TC module 1	National Instruments	NI 9213	14483C5
cDAQ TC module 2	National Instruments	NI 9213	14483BA
cDAQ voltage module	National Instruments	NI 9205	140E319
cDAQ DIO module	National Instruments	NI 9403	13E593B
Mass Spectrometer	Stanford Research Systems	UGA 300	91022
UGA Software	Stanford Research Systems	UGA Control Software	UGA 1.0
RGA Software	Stanford Research Systems	RGA Control Software	RGA 3.1
Flow Tube 1	Aalborg	042-07-N	247988-36
Flow Tube 2	Aalborg	012-10-N	252765-34
Flow Tube 3	Aalborg	042-07-A	284592-1
Flow Tube 4	Aalborg	042-07-N	292477-44
Pressure Transducer 1	Omega Engineering	PX309-2005V	071507I138
Pressure Transducer 2	Omega Engineering	PX309-2005V	101407I007
Pressure Transducer 3	Omega Engineering	PX309-2005V	071507I146
Pressure Transducer 4	Omega Engineering	PX309-2005V	060210I044
Microphones	PUI Audio, Inc.	AOM-6545P-R	N/A
RH meters	Honeywell	HIH-5031-001	N/A

8.2 MATLAB scripts and functions

8.2.1 “inputs_2.m”

```
%%%%%%%%%%%%%%%%%%%%%%%%%%%%%%%%%%%%%%%%%%%%%%%
%   inputs_2.m
%   collects input variables from sources and
%   saves into input.mat file for use by other
%   scripts
%
%   k.bourne
%%%%%%%%%%%%%%%%%%%%%%%%%%%%%%%%%%%%%%%%%%%%%%%
clear all

directory='C:\Documents and Settings\kjbourne\Desktop\Bubble Analysis\heated_injector\3-15-
12\'
```

```
fast_name='fast_031512_1.lvm';
slow_name='rec03_15_12_1.txt';
flow=[1 3.5 2.5 2 15 14.5 35.5 61 61];    %flow settings
num_f=9;      %number of fast records


doe=0.069;     %orifice diameter in inches
D_o=doe*.0254;   %in meters
flow_cal=1;     %1 is 0-5.77fm in argon meter, 2 is 0-5.77 in mix meter3, ch4 in fm4
l_reactor_e=35;         %length of reactor in inches
l_reactor=l_reactor_e*0.0254;    %length of reactor 35 8-6-10 to 3-15-11
                  %34 3-16-11 to 6-10-11, 35 6-14-11 to 6-15-11
hs_n=3;    %height sensor number 1 for 11/3/10-5/3-11, 2 for 5/4/11 to 6/14/11, 3 for 2/22/12 on

if doe==0.040
   injector_offset=0.017;  %17mm offset
elseif doe==0.070
   injector_offset=0.015; %15mm offset
elseif doe==0.125
   injector_offset=0.017;  %17mm offset
elseif doe==0.069
   injector_offset=0.015;  %injector installed 3-6-12
%    injector_offset=0.11;   %dip tube offset
end

if hs_n==1         %get heigh sensor offsets based on spec. dimensions
   hs1o=0.0151;
   hs2o=0.0060;
   hs3o=0.0028;
   hs4o=0.0008;
elseif hs_n==2
   hs1o=0.0163;
   hs2o=0.0083;
   hs3o=0.0055;
   hs4o=0.0020;
elseif hs_n==3
   hs1o=0.0222;
   hs2o=0.0095;
   hs3o=0.0079;
   hs4o=0.0048;
end

if num_f~=length(flow);
   msgbox('wrong number of files or flow readings')
end
```

```
%xxxxxxxxxxxxxxxxxxxxxxxxxxxxxxxxxxxx
%gets date
date_V=textread([directory fast_name],'%s',2,'headerlines',9);
date=date_V(2);

%gets times
%gets first start time, hr, min, sec
start=textread([directory fast_name],'%s',2,'headerlines',10);
S=start(2);
V=datevec(S, 13); %time and date vector
hr1=V(4);
min1=V(5);
sec1=V(6);
fast_start=3600*hr1+60*min1+sec1;   %time in seconds since midnight of fast start

%gets first stop time for length of record
stop=textread([directory fast_name],'%s',2,'headerlines',16);
st=stop(2);
v2 = datevec(st, 13);
hr2=v2(4);
min2=v2(5);
sec2=v2(6);

record_time=round((hr2-hr1)*3600+(min2-min1)*60+(sec2-sec1));   %length of time per record

%xxxxxxxxxxxxxxxxxxxxxxxxxxxxxxxxxxxxxxxxxxxxxxxxxxxxxxxxxxxxxxxxxxxxxxxxxxxxxxxxxxx

[tt,m1,m2]=textread([directory fast_name],'%f %f %f','headerlines',23);
num_p=length(tt); %gives number of recorded points
dt=tt(2)-tt(1);

time=zeros(num_f,1);
for f=1:num_f
   row_fast=1+round((num_p/num_f)*(f-1));
   time(f)=tt(row_fast);
end

s_s=textread([directory slow_name],'%s',2,'headerlines',10);
% S=start(2);
slow_v= datevec(s_s(2), 13); %time and date vector
hr_slow=slow_v(4);
min_slow=slow_v(5);
sec_slow=slow_v(6);

slow_start=3600*hr_slow+60*min_slow+sec_slow;   %time in seconds since midnight of slow start
```

```
times_slow_mid=(fast_start+time)-slow_start+(record_time/2);    %time in slow record at middle of
fast record

%imports data from slow record file
%
[t,T1,T2,T3,T4,T5,T6,T7,T8,T9,T10,T11,T12,T13A,T13B,T13C,T13D,T14,T15,T16,T17,T18,T19,T20,MIC,
MIC2,P1,P2,P3,P4,RH,H1,H2,H3,H4]=textread([directory slow_name],'%f %f %f %f %f %f %f %f %f %f
%f %f %f %f %f %f %f %f %f %f %f %f %f %f %f %f %f %f %f %f %f %f %f %f %f','headerlines',22);
%
[t,T1,T2,T6,T7,T8,T9,T10,T11,T12,T13A,T13B,T13C,T16,MIC,P1,P3,T17,T18,P2,H1,H2,H3,H4]=textrea
d([directory slow_name],'%f %f %f %f %f %f %f %f %f %f %f %f %f %f %f %f %f %f %f %f %f %f %f
%f','headerlines',22);
[t,T1,T2,T3,T4,T5,T6,T7,T8,T9,T10,T11,T12,T13A,T13B,T13C,T13D,T14,T15,T16,T17,T18,T19,T20,T21,
MIC,MIC2,P1,P2,P3,P4,RH_out,RH_in,H1,H2,H3,H4]=textread([directory slow_name],'%f %f %f %f %f
%f %f %f %f %f %f %f %f %f %f %f %f %f %f %f %f %f %f %f %f %f %f %f %f %f %f %f %f %f %f %f
%f','headerlines',22); %2-22-12
%get row of fast records by matching times_slow
row_s=zeros(num_f,1);
for i=1:num_f
   t_s=times_slow_mid(i);
   for j=1:(length(t)-1)
      if t_s>t(j)
         if t_s<t(j+1)
            row_s(i)=j;  %gets slow record row at middle of fast record for each fast record
         end
      end
   end
end
%initialize matrices
T_form=zeros(1,num_f);
P_form=zeros(1,num_f);
T_melt=zeros(1,num_f);
P_melt=zeros(1,num_f);

hs1=zeros(1,num_f);
hs2=zeros(1,num_f);
hs3=zeros(1,num_f);
hs4=zeros(1,num_f);
height=zeros(1,num_f);
%vectors of variables at fast record time specified by k
for k=1:num_f
   T_form(k)=T10(row_s(k));
      if flow_cal==1         % either P3 or P4 depending on setup
      P_form(k)=P3(row_s(k));
      elseif flow_cal==2
      P_form(k)=P4(row_s(k));
```

```
    elseif flow_cal==3
    P_form(k)=P4(row_s(k));
    else P_form(k)=0;
    end

%%%%%%%%%%%%%%%%%%%%%%%%%%%%%%%%%%%%%%%%%%%%%%%%%%%%%%%%%%%%%%
%%%%%%%%%%%%
  T_melt(k)=T11(row_s(k));
  P_melt(k)=P1(row_s(k));


  hs1(k)=H1(row_s(k));
  hs2(k)=H2(row_s(k));
  hs3(k)=H3(row_s(k));
  hs4(k)=H4(row_s(k));

  %--------------height sensor logic------------------
  if hs1(k)==1
    if hs2(k)==0
      hl(k)=1;
    elseif hs2(k)==1
      if hs3(k)==0
        hl(k)=2;
      elseif hs3(k)==1
        if hs4(k)==0
          hl(k)=3;
        elseif hs4(k)==1
          hl(k)=4;
        end
      end
    end
    else hl(k)=0;
  end
  %ooooooooooooooooooooooooooooooooo
  if hl(k)>4     % if the logic finds a problem with the HS
    hl     %display the height logic number and all hs values
    hs1
    hs2
    hs3
    hs3
    error('HS reading problem') %and display error and exit program
  end
  if hl(k)==4
    height(k)=l_reactor-injector_offset-hs4o;
  end
  if hl(k)==3
```

```
      height(k)=l_reactor-injector_offset-hs3o;
   end
   if hl(k)==2
      height(k)=l_reactor-injector_offset-hs2o;
   end
   if hl(k)==1
      height(k)=l_reactor-injector_offset-hs1o;
   end
   if hl(k)==0
      height(k)=0;
   end
end
%save directory name and variables for use in other scripts
save('directory.mat','directory','-mat')
save([directory
'inputs.mat'],'fast_name','slow_name','flow','height','D_o','flow_cal','num_f','record_time','T_form','
P_form','T_melt','P_melt','date','dt','directory','-mat');
```

8.2.2 “peaks_new.m”

```
%%%%%%%%%%%%%%%%%%%%%%%%%%%%%%%%%%%%%%%%%%%%%%%%%%%%%%%%%%%%
%   peaks_new.m
%
%   reads microphone and input files, performs
%   microphone peak analysis and outputs measured.mat
%   file which includes bubble transit time and velocity
%   data vectors
%
%   k.bourne
%%%%%%%%%%%%%%%%%%%%%%%%%%%%%%%%%%%%%%%%%%%%%%%%%%%%%%%%%%%%

clear all;

files=[1 4 3 2];  %list of file numbers to use
tt_guess=3.8;              % guess at transit time

%read input file
dir=load('directory.mat');
directory=[dir.directory];
data=load([directory 'inputs.mat']);
fast_name=[data.fast_name];
record_time=[data.record_time];
```

```
dt=[data.dt];
all_flows=[data.flow];
all_height=[data.height];

% flow_cal=[data.flow_cal];              %imports flow calibration number
% T_form_all=[data.T_form];
% P_bottom_all=[data.P_form];
% T_hot_all=[data.T_melt];
% P_top_all=[data.P_melt];
% D_o=[data.D_o];
%
% g=9.81;  %gravitational constant


for i=1:length(files)
   flow(i)=all_flows(files(i));
   height(i)=all_height(files(i));
end

%-------re-order file vector (f) in order by flow setting-------
[oflows,ixx]=sort(flow,'ascend');
for i=1:length(files)
   f(i)=files(ixx(i));
end
%-------------------------------------------------------------

%get mic and time data
[ft,m1,m2]=textread([directory fast_name],'%f %f %f','headerlines',23);

lf=length(f);              %number of files being looked at
tt_avg=tt_guess;          %pre-set guess at average transit time
end_row=0;  %initialize end row for storage matrix

L=record_time/dt;   %number of points in each fast record
ts=linspace(0,record_time,L);    %sets up a vector of times that go from 0 to record time

for k=1:lf
   clear r h re rer dre delta diff dr h_guess vel
   n=f(k);            %file number looked at this loop
   N=(n-1)*L+1;       %starting number of this fast record
   V1=m1(N:(N+L-1));   %voltage of mic 1 for this file
   V2=m2(N:(N+L-1));   %voltage of mic 2 for this file
   name=int2str(f(k));       %uses name=file number

   %%%%%%%%%%%%%%%%%%%%%%%%%%
   %Normalize and shift microphone signals for plotting and comparison
```

```
   %%%%%%%%%%%%%%%%%%%%%%%%%%
   v1_max=max(V1);
   v1_min=min(V1);
   v1_mean=mean(V1);

   v1_diff=max(abs(v1_max-v1_mean),abs(v1_min-v1_mean));   %gets biggest difference from mean
   v1_sf=1/(v1_diff);
   v1_norm=(V1-v1_mean)*v1_sf;

   v2_max=max(V2);
   v2_min=min(V2);
   v2_mean=mean(V2);

   v2_diff=max(abs(v2_max-v2_mean),abs(v2_min-v2_mean));   %gets biggest difference from mean
   v2_sf=1/(v2_diff);
   v2_norm=((V2-v2_mean)*v2_sf)-2;                %shift v2 normalized below v1 for plotting

   %%%%%%%%%%%%%%%%%%%%%%%%%%

   %%%%%%%%%%%%%%%%%%%%%%%%%%

   plot(ts,v1_norm,ts, v2_norm)      %plots voltages
   title(['v1_norm' name])

   [rer,~]=ginput;        %select releases from V2 signal

   clicktol=.1*(1/dt);    %steps within which to look for a minimum
   re_l=length(rer);      %number of release for this file

%---------get exact values from picked values------------
   for j=1:re_l     %releases
      ci=round(rer(j)*(1/dt));    %indice of center
      si=ci-clicktol/2;          %begining index
      ei=ci+clicktol/2;          %end index
      var=v1_norm(si:ei);        %window of Vb signal to look for min
      [~,I]=min(var);            %gets index of min in var
      re(j)=ts(I+si);            %exact release on 0-20 sec scale
   end
%-----------------------------------------------------

   dre(1)=0;
   for i=2:length(re)          %get release period for all releases
     dre(i)=re(i)-re(i-1);
   end

   dre_avg(k)=sum(dre)/length(dre);   %average release period for this record
```

```
for i=1:length(re)
   h_guess(i)=re(i)+tt_avg(1);     %guess of hit position
end

plot(ts,v1_norm,ts, v2_norm)    %plots voltages
title(['v1_norm' name])


for i=2:length(h_guess)
   line([re(i),h_guess(i)],[-.2*i+0.75,-.2*i+0.75],'color','r')
end

%------pick hit and release pairs, if not a pair, restart pick-------

xx=0;
while xx==0
   [pp,~]=ginput;                      %pick hit and release pairs
   if floor(length(pp)/2)==length(pp)/2    %if picked in pairs
      xx=1;                            %exit while loop
   else
      xx=0;                            %if not, restart point picking loop
   end
end

%------divide pick points into hits and releases
for i=1:length(pp)
   if floor(i/2)==i/2      %if i is even
      hh(i/2)=pp(i);      %then it is a hit
   else
      rr(((i-1)/2)+1)=pp(i);        %then it is a release
   end
end

%--------get exact values of pick points from mic signals----------
for j=1:length(rr)      %releases
   ci=round(rr(j)*(1/dt));    %indice of center
   si=ci-clicktol/2;       %begining index
   ei=ci+clicktol/2;        %end index
   var=v1_norm(si:ei);        %window of Vb signal to look for min
   [~,I]=min(var);       %gets index of min in var
   r(j)=ts(I+si);          %gets time of minimum from ts =>(0-20 sec scale)
end

for j=1:length(hh)      %hits
   ci=round(hh(j)*(1/dt));    %indice of center
```

```
    si=ci-clicktol/2;        %begining index
    ei=ci+clicktol/2;        %end index
    var=V1(si:ei);        %window of Vb signal to look for min
    [~,I]=min(var);       %gets index of min in var
    h(j)=ts(I+si);        %gets time of minimum from ts =>(0-10 sec scale)
  end

  %-------calculate parameters--------------------
  for i=1:length(rr)
    tt(i)=hh(i)-rr(i);     %calculates each transit time
  end

  tt_avg(k)=sum(tt)/length(tt);     %average transit time for this record
  vel=height(k)./tt;                %vector of each bubble velocity for this record
  vel_avg=sum(vel)/length(vel);   %average velocity for this record
  vel_std=std(vel);              %std deviation of vel

  for i=1:length(r)              %gets the bubble formation time for each bubble
    diff=re-r(i);              %with a release and hit by finding the next release
    [~,ix]=min(abs(diff));     %in the list of all releases
    dr(i)=dre(ix);
  end

  for i=1:length(vel)            %stores data for each bubble in a row of a matrix
    sv(end_row+i,:)=[f(k),tt(i),vel(i),dr(i),dre_avg(k)];
  end
  end_row=end_row+length(vel);    %re-calculate what the last row of this file is in matrix

end

save([directory 'measured.mat'],'sv', '-mat');
```

8.2.3 “calculated.m”

```
%%%%%%%%%%%%%%%%%%%%%%%%%%%%%%%%%%%%%%%%%%%%%%%%%%%%%%%%%%%%
%   calculated.m
%
%   calculates values of all experimental variables from bubble
%   velocity experiments, outputs in measured.xls excel file
%
%   k.bourne
%%%%%%%%%%%%%%%%%%%%%%%%%%%%%%%%%%%%%%%%%%%%%%%%%%%%%%%%%%%%
clear all
```

```
dir=load('directory.mat');
directory=[dir.directory];

meas_file=load([directory 'measured.mat']);
sv=[meas_file.sv];
files=sv(:,1);
tt=sv(:,2);
vel=sv(:,3);

data=load([directory 'inputs.mat']);
all_flows=[data.flow];
fc=[data.flow_cal];              %imports flow calibration number
T_form_all=[data.T_form];
P_bottom_all=[data.P_form];
T_hot_all=[data.T_melt];
P_top_all=[data.P_melt];
D_o=[data.D_o];

g=9.81;  %gravitational constant

[rows,~]=size(sv);     %find size of bubble storage matrix

P_bottom=zeros(1,rows);     %initialize matricies of properties
T_form=zeros(1,rows);
T_hot=zeros(1,rows);
P_top=zeros(1,rows);
rho_form=zeros(1,rows);
mu=zeros(1,rows);
sigma_snbi_form=zeros(1,rows);
rho_snbi_form=zeros(1,rows);
rho_b=zeros(1,rows);
rho_t=zeros(1,rows);
sigma_snbi_hot=zeros(1,rows);
rho_snbi_hot=zeros(1,rows);

for j=1:rows          %for each bubble (row in sv matrix) calculate each parameter

   %get data out of sv
   fn=files(j);           %get file number of each bubble
   delta_r(j)=sv(j,4);     %get formation time of each bubble

   %get data out of input file (imported earlier)
   flow(j)=all_flows(fn);  %get flow setting of each bubble

   %measured values from slow record
```

```
P_bottom(j)=P_bottom_all(fn)*6895;    %bubble formation Pressure converted to Pa from psi
T_form(j)=T_form_all(fn)+273.15; %bubble formation Temeperature converted to Kelvin from C
T_hot(j)=T_hot_all(fn)+273.15;   %temperature of hot part of reactor
P_top(j)=P_top_all(fn)*6895;      %pressure at top of reactor

%properties calculated from measurements
rho_form(j)=density('AR',T_form(j),P_bottom(j));    %density of gas at bubble formation
mu(j)=viscosity('AR',T_form(j));                  %viscosity of gas at bubble formation
sigma_snbi_form(j)=0.450-0.0000647*(T_form(j));     %surface tenstion of metal at formation
(Moser)
rho_snbi_form(j)=(10.024-0.00133*T_form(j))*1000;   %density of metal at formation (Moser)
rho_b(j)=density('AR',T_hot(j),P_bottom(j));       %density of gas at bottom of reactor
rho_t(j)=density('AR',T_hot(j),P_top(j));          %density of gas at top of reactor
sigma_snbi_hot(j)=0.450-0.0000647*(T_hot(j));      %surface tension of metal in reactor (Moser)
rho_snbi_hot(j)=(10.024-0.00133*T_hot(j))*1000;     %density of metal in reactor (Moser)

  %--------------m_dot-----------------------analysis 4.3---------
  %determine flow rate based on setting and flow calibration used
if fc==1            %equation from "12-22-10calibrationEquation.EES"
  if P_bottom(j)<206850   %if P_bottom is less than 30 psi use cal at 25 psi
  m_dot(j)=2.91e-8+3.57e-9*flow(j)+1.54e-11*flow(j)^2;
  end
  if P_bottom(j)>275800   %if P_bottom is greater than 40 psi use cal at 50 psi
  m_dot(j)=1.87e-7+9.59e-9*flow(j)+1.20e-10*flow(j)^2;
  end

elseif fc==2         %equations from "06-02-11calibrationEquation.EES"
  if P_bottom(j)<206850   %if P_bottom is less than 30 psi use cal at 25 psi
  m_dot(j)=5.16e-8+2.5e-9*flow(j)+3.37e-11*flow(j)^2;
  end
  if P_bottom(j)>275800   %if P_bottom is greater than 40 psi use cal at 50 psi
  m_dot(j)=1.49e-7+1.87e-8*flow(j)-1.47e-11*flow(j)^2;
  end
end
%xxxxxxxxxxxxxxxxxxxxxxxxxxxxxxxxxxxxxxxxxxxxxxxxxxxxxxxxxxxxxxxxxxxxxx


%----------------------bubble mass-------------------------------
bm(j)=m_dot(j)*delta_r(j);
%xxxxxxxxxxxxxxxxxxxxxxxxxxxxxxxxxxxxxxxxxxxxxxxxxxxxxxxxxxxxxxxxxxxxxx

%---------------------formation diameter-------------------------
V_form(j)=bm(j)/rho_form(j);
Dia_form_meas(j)=2*(3*V_form(j)/(4*pi))^(1/3);
%xxxxxxxxxxxxxxxxxxxxxxxxxxxxxxxxxxxxxxxxxxxxxxxxxxxxxxxxxxxxxxxxxxxxxx
```

```
   %-------------------------avg dia and predicted velocity------------
   dia_b(j)=2*(3*(bm(j)/rho_b(j))/(4*pi))^(1/3);
   dia_t(j)=2*(3*(bm(j)/rho_t(j))/(4*pi))^(1/3);
   dia_avg(j)=(dia_b(j)+dia_t(j))/2;
   U_t(j)=sqrt((2*sigma_snbi_hot(j))/(rho_snbi_hot(j)*dia_avg(j))+(g*dia_avg(j)/2));
   %xxxxxxxxxxxxxxxxxxxxxxxxxxxxxxxxxxxxxxxxxxxxxxxxxxxxxxxxxxxxxxxxxxxxx

   %------------------------non-dimensional parameters-----------------
   Re_o(j)=(m_dot(j)*4)/(mu(j)*pi*D_o); %orifice Reynolds number-inertial/viscous forces
   V_o(j)=m_dot(j)*4/(rho_form(j)*pi*D_o^2);   %orifice gas velocity
   Fr_o(j)=V_o(j)^2/(g*D_o);                %orifice Froude number- inertial/gravity forces
   We_o(j)=D_o*V_o(j)^2*rho_form(j)/sigma_snbi_form(j); %orifice Weber number- inertial/surf
tension forces
   %xxxxxxxxxxxxxxxxxxxxxxxxxxxxxxxxxxxxxxxxxxxxxxxxxxxxxxxxxxxxxxxxxxxxx

end
fcs=fc*ones(length(files),1);

soln=[files,Dia_form_meas',dia_avg',U_t',Re_o',Fr_o',We_o',flow',fcs,m_dot',delta_r',T_form',T_hot'
,P_top',P_bottom',V_o',sigma_snbi_form',sigma_snbi_hot',rho_snbi_form',rho_snbi_hot',tt,vel];
xlswrite([directory 'measured.xls'],soln)
```

8.2.4 "force_balance.m"

```
%%%%%%%%%%%%%%%%%%%%%%%%%%%%%%%%%%%%%%%%%%%%%%%
%   forceBalance.m
%
%   calculates values of bubble formation predicted by force balance
%   and literature data, saves in fb.xls excel file
%
%   k.bourne
%%%%%%%%%%%%%%%%%%%%%%%%%%%%%%%%%%%%%%%%%%%%%%%
clear all

dir=load('directory.mat');
directory=[dir.directory];
data=load([directory 'inputs.mat']);

T_form_all=[data.T_form];
P_form_all=[data.P_form];
T_melt_all=[data.T_melt];
P_top_all=[data.P_melt];
```

```
D_o=[data.D_o];

meas_f=load([directory 'measured.mat']);
sv=[meas_f.sv];
f=sv(:,1);
f_count=length(f);

for i=1:f_count
   T_form(i)=T_form_all(f(i))+273.15;
   P_form(i)=P_form_all(f(i))*6895;
   T_melt(i)=T_melt_all(f(i))+273.15;
   P_top(i)=P_top_all(f(i))*6895;
end

g=9.81;              %gravitational constant [m^2/s]
theta=pi/2;          %bubble contact angle [rad]

D_b_f=zeros(f_count,1);
D_bb=zeros(f_count,1);
D_bt=zeros(f_count,1);
D_b_avg=zeros(f_count,1);
U_fb=zeros(f_count,1);

for i=1:f_count
sigma_snbi_f=0.450-0.0000647*(T_form(i));     %surface tension of snbi at bottom
rho_snbi_f=(10.024-0.00133*T_form(i))*1000;    %density of snbi at bottom

%force balance gets bubble diameter
D_b_f(i)=2*(D_o*sigma_snbi_f*sin(theta)*3/(4*rho_snbi_f*g))^(1/3);

V_bf=4/3*pi*(D_b_f(i)/2)^3;
rho_bf=density('AR',T_form(i),P_form(i));
m_b=V_bf*rho_bf;

rho_bh=density('AR',T_melt(i),P_form(i));       %density of bubble at bottom, hot
rho_th=density('AR',T_melt(i),P_top(i));        %density of bubble at top, hot
D_bb(i)=2*(3*m_b/(rho_bh*4*pi))^(1/3);       %diameter of bubble at bottom
D_bt(i)=2*(3*m_b/(rho_th*4*pi))^(1/3);       %diameter of bubble at top
D_b_avg(i)=(D_bb(i)+D_bt(i))/2;              %average diameter of traveling bubble

sigma_snbi_m=0.450-0.0000647*(T_melt(i));     %surface tension of snbi in main part of melt
rho_snbi_m=(10.024-0.00133*T_melt(i))*1000;    %density of snbi in main part of melt

U_fb(i)=sqrt((2*sigma_snbi_m)/(rho_snbi_m*D_b_avg(i))+(g*D_b_avg(i)/2));
end
```

```
format short g
sln=[D_b_f D_bb D_bt D_b_avg U_fb];
xlswrite([directory 'fb.xls'],sln)
```

8.2.5 "reaction_analysis.m"

```
%%%%%%%%%%%%%%%%%%%%%%%%%%%%%%%%%%%%%%%%%%%%%%%%%%%%%%%%%%%%%%%%%%%%%%%%%%%%%%%%
%%%%%%%%%%%%%%%%
% reaction_analysis.m
%
% performs analysis of chemical reactions, writes to file rxn_results.xls
% excel file
%
% updated 4-25-2012  k.bourne
%%%%%%%%%%%%%%%%%%%%%%%%%%%%%%%%%%%%%%%%%%%%%%%%%%%%%%%%%%%%%%%%%%%%%%%%%%%%%%%%
%%%%%%%%%%%%%%%%

clear all
directory='C:\Documents and Settings\kjbourne\Desktop\MS Analysis\3-6-12_2\';
write_results=1;      % 1 for write results file, 0 for do not write file

filename_data=[directory 'fdata.txt'];
flow_data_file=[directory 'flowdata.txt'];
input_data_file=[directory 'inputs.txt'];

[input_data]=textread(input_data_file,'%s','commentstyle','matlab','headerlines',1);

slow_rec_file=[directory char(input_data(1))];
day=char(input_data(2)); %date format of log files

[sn folder start_time num_logs bks bke T_nom]=textread(filename_data, '%u %s %s %u %u %u
%u','headerlines',2, 'delimiter',' ');

% input gas scan numbers
input_sn=[str2num(char(input_data(3)));str2num(char(input_data(4)))];

% Sensitivity factors
SF=zeros(10,1);
for i=5:15
  SF(i-4)=str2num(char(input_data(i)));
end

% logic for variables
```

```
use_T11=str2num(char(input_data(16)));
use_RH_out=str2num(char(input_data(17)));
use_RH_in=str2num(char(input_data(18)));
use_cond=str2num(char(input_data(20)));
use_snbi=str2num(char(input_data(21)));
input_water=str2num(char(input_data(22)));
input_gas=input_data(19);
hs_number=str2num(char(input_data(23)));

is_he=strcmp(input_gas,'CO');
if is_he==1
   carrier_gas='He';
else
   carrier_gas='AR';
end

if input_water==1
   if use_snbi==1
      reactants=strcat(input_gas,'+',carrier_gas,'+H2O+SnBi')
   else
      reactants=strcat(input_gas,'+',carrier_gas,'+H2O')
   end
else
   if use_snbi==1
      reactants=strcat(input_gas,'+',carrier_gas,'+SnBi')
   else
      reactants=strcat(input_gas,'+',carrier_gas)
   end
end
%inputs
%xxxxxxxxxxxxxxxxxxxxxxxxxxxxxxxxxxxxxxxxxxxxxxxxxxxxxxxxxxxxxxxxxxxxxxxxxxxxxxxxxxxxxxx
%xxxxxxxxxxxxxxxxxxxxxxxxxxxxxxxxxxxxxxxxxxxxxxxxxxxxxxxxxxxxxxxxxxxxxxxxxxxxxxxxxxxxxxx

id=0.0625*.0254; %id of reactor in m
Ax_reactor=2*pi*(id/2)^2;   %x-section area of double bore tube
l_reactor=36*.0254;  %length of reactor in m

vel_bubble=0.209;          %[m/s] average velocity of bubble from 3-15-12
injector_offset=0.874;  %[m] (.889-.015) distance from injector to top of reactor

if hs_number==1        %height sensor offsets for 2-17-12 to 3-26-12
   hs1o=0.0222;
   hs2o=0.0095;
   hs3o=0.0079;
   hs4o=0.0048;
elseif hs_number==2     %height sensor offsets for 3-27-12 on
```

```
   hs1o=0.0980;
   hs2o=0.0858;
   hs3o=0.0842;
   hs4o=0.081;
end

R_bar=8.314;    %[J/mol-K] universal gas constant
prf=1;
   gases=['AR  ' ;'CO2 ' ;'CO  ' ;'H2  ' ;'CH4 ' ;'O2  ';'H2O ';'He  ' ;'C2H2';'C2H4';'C2H6'];
mw=[39.948;44.009;28.01;2.0158;16.0426;32.998;18.0148;4.0026;26.0378;28.0536;30.0694];
%from periodic table
mw=mw/1000; %convert from g/mol to kg/mol
n_gas=length(mw);

%xxxxxxxxxxxxxxxxxxxxxxxxxxxxxxxxxxxxxxxxxxxxxxxxxxxxxxxxxxxxxxxxxxxxxxxxxxxxxxxxxx
%xxxxxxxxxxxxxxxxxxxxxxxxxxxxxxxxxxxxxxxxxxxxxxxxxxxxxxxxxxxxxxxxxxxxxxxxxxxxxxxxxx
% get input gas composition
%=========================================================================
%=========================================================================
      %INPUT 1 BACKGROUND
      %file name for background before input scan 1
fn_i1bk1=[directory char(folder(bks(input_sn(1)))) day char(start_time(bks(input_sn(1)))) '.txt'];
      %file name for background after input scan 1
fn_i1bk2=[directory char(folder(bke(input_sn(1)))) day char(start_time(bke(input_sn(1)))) '.txt'];
      %get ion currents for background files
[mz ig1_bk1]=textread(fn_i1bk1,'%f %f','headerlines',22, 'delimiter',',');
[mz ig1_bk2]=textread(fn_i1bk2,'%f %f','headerlines',22, 'delimiter',',');
      %average background ion current for input gas 1
ig_bk(1,:)=(ig1_bk1+ig1_bk2)/2;

      %INPUT 2 BACKGROUND
      %file name for background before input scan 2
fn_i2bk1=[directory char(folder(bks(input_sn(2)))) day char(start_time(bks(input_sn(2)))) '.txt'];
      %file name for background after input scan 2
fn_i2bk2=[directory char(folder(bke(input_sn(2)))) day char(start_time(bke(input_sn(2)))) '.txt'];
      %get ion currents for background files
[mz ig2_bk1]=textread(fn_i2bk1,'%f %f','headerlines',22, 'delimiter',',');
[mz ig2_bk2]=textread(fn_i2bk2,'%f %f','headerlines',22, 'delimiter',',');
      %average background ion current for input gas 2
ig_bk(2,:)=(ig2_bk1+ig2_bk2)/2;

      %make file names for input gases, import files, plot, find avg comp

incr=30;          %seconds between scans
% if using CH4 as input gas, update CH4 sensitivity factor
if strcmp(input_gas,'CH4')==1
```

```
  new_SF='re-calculate SF for CH4'
  for f=1:2   %for each input file
    clear ts Pp
    n_file=num_logs(input_sn(f));     %gets number of files in log
    sec_tot=zeros(n_file,1);       %initialize vector
    time_start_all=char(start_time(input_sn(f)));

    [sec_tot,ts]=LogNames(time_start_all,incr,n_file,day);
    for i=1:n_file
      fni=[char(directory) char(folder(input_sn(f))) char(ts(i,:))];
      [mz ics(i,:)]=textread(fni,'%f %f','headerlines',22, 'delimiter',',');
      ics(i,:)=ics(i,:)-ig_bk(f); %subtract averaged background ion currents
      H=ms_peaks(ics(i,:));
      [Pp(i,:) pp sigma_in_cal(i,:) sigma_in_fit_cal(i)]=SVD_LSF(H,prf,SF,n_gas);
    end

    figure(f)
    semilogy(sec_tot,Pp,'.-')

    [xx,~]=ginput(2);         %click on ends of steady state period
    diff1=abs(sec_tot-xx(1));   %find indicies of steady state period
    [~,i1]=min(diff1);
    diff2=abs(sec_tot-xx(2));
    [~,i2]=min(diff2);
    Pp_1(f,:)=mean(Pp(i1:i2,:));   %average partial pressures over ss period
  end
  Pp_1_avg=mean(Pp_1);
  Pp_ch4_ideal=38;              %gas cert sheet says 5% CH4, sample at 760 torr
  SF_ch4=SF(5)*Pp_ch4_ideal/Pp_1_avg(5);
  SF(5)=SF_ch4;
end

% Get composition of input gas

for f=1:2   %for each input file
  clear ts Pp
  n_file=num_logs(input_sn(f));     %gets number of files in log
  sec_tot=zeros(n_file,1);       %initialize vector
  time_start_all=char(start_time(input_sn(f)));

  [sec_tot,ts]=LogNames(time_start_all,incr,n_file,day);
  sigma_in_fit=zeros(n_file,1);
  sigma_in=zeros(n_file,n_gas);
  for i=1:n_file
    fni=[char(directory) char(folder(input_sn(f))) char(ts(i,:))];
    [mz ics(i,:)]=textread(fni,'%f %f','headerlines',22, 'delimiter',',');
```

```
    ics(i,:)=ics(i,:)-ig_bk(f); %subtract averaged background ion currents
    H=ms_peaks(ics(i,:));
    [Pp(i,:) pp sigma_in(i,:) sigma_in_fit(i)]=SVD_LSF(H,prf,SF,n_gas);
  end

  figure(f)
  semilogy(sec_tot,Pp,'.-')

  [xx,~]=ginput(2);          %click on ends of steady state period
  diff1=abs(sec_tot-xx(1));   %find indicies of steady state period
  [~,i1]=min(diff1);
  diff2=abs(sec_tot-xx(2));
  [~,i2]=min(diff2);
  Pp_ins(f,:)=mean(Pp(i1:i2,:));   %average partial pressures over ss period
  sigma_fit_avg_ins(f)=mean(sigma_in_fit(i1:i2,:));
  sigma_avg_ins(f,:)=mean(sigma_in(i1:i2,:));

  [pk_x,peak,icp]=extra_peaks(n_gas,Pp(i2,:),ics(i2,:));
  figure(4)
  semilogy(mz,ics(i2,:),pk_x,peak,'x',pk_x,icp,'o')
  title(strcat(reactants,'input number',num2str(f)))
  legend('ion current','measured peaks','predicted peaks','Location','NorthEast')
  saveas(gcf,[directory 'input_extra' num2str(f)],'fig')
end

Pp_avg_in=mean(Pp_ins);
sigma_avg_in=mean(sigma_avg_ins);
sigma_fit_avg_in=mean(sigma_fit_avg_ins);

Pp_in_dry=Pp_avg_in;
Pp_in_dry(:,7)=0;                %set water pp to zero
mol_f_in_dry=Pp_in_dry/sum(Pp_in_dry);  %mol fraction of dry gas components
%=========================================================================
%=========================================================================

% get data at each temperature
%xxxxxxxxxxxxxxxxxxxxxxxxxxxxxxxxxxxxxxxxxxxxxxxxxxxxxxxxxxxxxxxxxxxxxxxxxxxxxx
%xxxxxxxxxxxxxxxxxxxxxxxxxxxxxxxxxxxxxxxxxxxxxxxxxxxxxxxxxxxxxxxxxxxxxxxxxxxxxx

%import flow data: hr,min,flow meter,flow setting
[flow_data(:,1) flow_data(:,2) flow_data(:,3) flow_data(:,4)]=textread(flow_data_file, '%u %u %u
%f','headerlines',2, 'delimiter','   ');

%import slow record data
[t_sl,T1,T2,T3,T4,T5,T6,T7,T8,T9,T10,T11,T12,T13A,T13B,T13C,T13D,T14,T15,T16,T17,T18,T19,T20,T
21,MIC,MIC2,P1,P2,P3,P4,RH_out,RH_in,H1,H2,H3,H4]=textread(slow_rec_file,'%f %f %f %f %f %f %f
```

```
%f %f %f %f %f %f %f %f %f %f %f %f %f %f %f %f %f %f %f %f %f %f %f %f %f %f %f %f %f %f %f
%f','headerlines',22);
for i=1:length(T13A)
   T13(i)=mean([T13A(i) T13B(i) T13C(i) T13D(i)]);

   if use_T11==1              %reactor temperature logic, set in inputs.txt
      T_reactor=T11;
   elseif use_T11==0
      if use_snbi==1
         T_reactor(i)=T13(i)*.958+3.76;  %average reactor temperature from heater offset.xls
      else
         T_reactor=T13;
      end
   end
   mf_in_rh(i)=exp((T21(i)*17.3/(T21(i)+238))+6.416)*(RH_in(i)/100)/(P4(i)*6894.8);
   mf_out_rh(i)=exp((T20(i)*17.3/(T20(i)+238))+6.416)*(RH_out(i)/100)/(P1(i)*6894.8);

   if H4(i)>0        %logic to determine height of melt, use highest HS reading
      hs_o(i)=hs4o;
   elseif H3(i)>0
      hs_o(i)=hs3o;
   elseif H2(i)>0
      hs_o(i)=hs2o;
   elseif H1(i)>0
      hs_o(i)=hs1o;
   else
      hs_o(i)=999;
   end
   if hs_o(i)==999
      rho_snbi_hot(i)=(10.024-0.00133*T_reactor(i))*1000;     %density of metal in reactor (Moser)
      height(i)=((P4(i)-P1(i))*6894.8)/(rho_snbi_hot(i)*9.81);
      hsm(i)=1;
   else
      height(i)=injector_offset-hs_o(i);     %distance traveled by bubble through melt
height(i)=((P4(i)-P1(i))*6894.8)/(rho_snbi_hot*9.81);
      hsm(i)=0;
   end
end
P_reactor=((P1+P4)/2)*6894.8;    %pressure in Pascals

% synchronize times
   %slow record time
s_s=textread(slow_rec_file,'%s',2,'headerlines',10);
slow_v= datevec(s_s(2), 13); %time and date vector
hr_slow=slow_v(4);
min_slow=slow_v(5);
```

```
sec_slow=slow_v(6);
s_s_midnight=hr_slow*3600+min_slow*60+round(sec_slow);     %slow start in sec after midnight
t_slow=t_sl+s_s_midnight;       %slow time in sec since midnight
   %hand record time
t_hand=flow_data(:,1)*3600+flow_data(:,2)*60;   %hand record times in sec since midnight
   %rga file times
t_rga_starts=sec_tot';     %rga record start times in sec since midnight

%Process Temperature Data Sets
n_temp=0;
for i=1:length(T_nom)   %count number of temperatures tested
   if T_nom(i)>0
      n_temp=n_temp+1;
      sn_t(n_temp)=sn(i); %get indcies of temperature files
   end
end
   si_s=1;  %storage matrix start index
for i=1:n_temp
   clear t_rga_i temp_names Pp Pp_i Pp_h2o_rh diff1 diff2 diff3 diff4 diff5 diff6
   j=sn_t(i);     %index of logs in filename_data.txt
   [t_rga_i temp_names]=LogNames(char(start_time(j)),incr,num_logs(j),day);

   %get average background ic for log set

   bks_i=bks(j);    %index of background at start of log
   fname_bks=[char(directory) char(folder(bks_i)) char(day) char(start_time(bks(j))) '.txt'];
   [mz ic_bks]=textread(fname_bks,'%f %f','headerlines',22, 'delimiter',',');

   bke_i=bke(j);    %index of background at end of log
   fname_bke=[char(directory) char(folder(bke_i)) char(day) char(start_time(bke(j))) '.txt'];
   [mz ic_bke]=textread(fname_bke,'%f %f','headerlines',22, 'delimiter',',');

   ic_bk=(ic_bke+ic_bks)/2;    %average background for this log set

   %import log files and calculate partial pressures
   sigma_out_fit=zeros(num_logs(j),1);
   sigma_out=zeros(num_logs(j),n_gas);
   for k=1:num_logs(j)
      clear diff_t
      fni=[char(directory) char(folder(j)) char(temp_names(k,:))];
      [mz ics(k,:)]=textread(fni,'%f %f','headerlines',22, 'delimiter',',');
      ics(k,:)=ics(k,:)-ic_bk';      %subtract background
      H=ms_peaks(ics(k,:));          %get peaks
      [Pp(k,:) pp sigma_out(k,:) sigma_out_fit(k)]=SVD_LSF(H,prf,SF,n_gas);   %calculate partial
pressure
      Pp_raw(k,:)=Pp(k,:);          %saves Pp before modified for h2o etc.
```

```
    diff_t=abs(t_slow-t_rga_i(k));
    [cc i_slow]=min(diff_t);   %get index of nearest slow time to each rga time
    Pp_h2o_out(k)=mf_out_rh(i_slow)*760;
    if use_RH_out==1       %if using RH out for water output
      Pp(k,7)=Pp_h2o_out(k);  %set Pp7 to RH pp value
    end                 %if not, do not change Pp
  end



  %if using RH_in, replace rga h2o data with RH data,if not, do not
  if use_RH_in==1
    for k=1:num_logs(j)
      clear diff_t
      diff_t=abs(t_slow-t_rga_i(k));
      [cc i_slow]=min(diff_t);   %get index of nearest slow time to each rga time
      Pp_h2o_in(k)=mf_in_rh(i_slow)*760;    %Pp of h2o in over rga time range
      for j=1:length(mol_f_in_dry)
        mol_f_in(k,j)=(1-mf_in_rh(i_slow))*mol_f_in_dry(j);
      end
      mol_f_in(k,7)=mf_in_rh(i_slow);
    end
  elseif use_RH_in==0
    for k=1:num_logs(j)
      mol_f_in(k,:)=Pp_avg_in./sum(Pp_avg_in);
    end
  end

  si_e=si_s+num_logs(j)-1;
  figure(3)
  [ax h1 h2]=plotyy(t_rga_i,Pp,t_slow,T_reactor,'semilogy','plot');
  set(h2,'LineStyle','--')
  linkaxes(ax,'x')
  zoom on

legend('AR','CO2','CO','H2','CH4','O2','H2O','He','C2H2','C2H4','C2H6','Temp','Location','EastOutside')

  si_s=si_e+1;  %set next start index to end index + 1
  [~]=input(['zoom then push enter-' num2str(i)]);
  [xx,~]=ginput(2);          %click on ends of steady state period
  diff1=abs(t_rga_i-xx(1));   %find indicies of steady state period
  [~,i1]=min(diff1);
  diff2=abs(t_rga_i-xx(2));
  [~,i2]=min(diff2);
  Pp_avg(i,:)=mean(Pp(i1:i2,:));   %average partial pressures over ss period
  sigma_avg_out(i,:)=mean(sigma_out(i1:i2,:));
```

```
    sigma_fit_avg_out(i)=mean(sigma_out_fit(i1:i2));
    diff3=abs(t_slow-xx(1));
    diff4=abs(t_slow-xx(2));
    [~,i3]=min(diff3);
    [~,i4]=min(diff4);
    T_avg(i)=mean(T_reactor(i3:i4));
    P_avg(i)=mean(P_reactor(i3:i4));
    height_avg(i)=mean(height(i3:i4));
    hsm_avg(i)=min(hsm(i3:i4));
    mf_h2o_in_avg(i)=mean(mf_in_rh(i3:i4));
    T21_avg(i)=mean(T21(i3:i4));
    P4_avg(i)=mean(P4(i3:i4));
    RH_in_avg(i)=mean(RH_in(i3:i4));
    mol_f_in_avg(i,:)=mean(mol_f_in(i1:i2,:));
    mf_h2o_out_avg(i)=mean(mf_out_rh(i3:i4));
    T20_avg(i)=mean(T20(i3:i4));
    P1_avg(i)=mean(P1(i3:i4));
    RH_out_avg(i)=mean(RH_out(i3:i4));
    rho_snbi_hot_avg(i)=mean(rho_snbi_hot(i3:i4));

    diff5=abs(t_hand-xx(1));
    diff6=abs(t_hand-xx(2));
    [~,i5]=min(diff5);
    [~,i6]=min(diff6);
    flow_avg(i)=mean(flow_data(i5:i6,4));   %average flow setting over ss period
    ic_save(i,:)=ics(i2,:);              %save last ic from SS period

    %make plot of extra peaks for last log file used in analysis

    [pk_x,peak,icp]=extra_peaks(n_gas,Pp_raw(i2,:),ics(i2,:));
    figure(4)
    semilogy(mz,ics(i2,:),pk_x,peak,'x',pk_x,icp,'o')
    title(strcat(reactants,' at ',num2str(round(T_avg(i))),' °C'))
    legend('ion current','measured peaks','predicted peaks','Location','NorthEast')
    saveas(gcf,[directory 'extra' num2str(i)],'fig')

end
figure(4)
semilogy(T_avg,Pp_avg)
legend('AR','CO2','CO','H2','CH4','O2','H2O','He','C2H2','C2H4','C2H6','Location','EastOutside')

%xxxxxxxxxxxxxxxxxxxxxxxxxxxxxxxxxxxxxxxxxxxxxxxxxxxxxxxxxxxxxxxxxxxxxxxxxxxxxxxxxxxxxxx
%xxxxxxxxxxxxxxxxxxxxxxxxxxxxxxxxxxxxxxxxxxxxxxxxxxxxxxxxxxxxxxxxxxxxxxxxxxxxxxxxxxxxxxx


% compare steady state gas composition to input gas composition
```

```
%-------------------------------------------------------------------------
%-------------------------------------------------------------------------

for i=1:n_temp
   mol_f_out(i,:)=Pp_avg(i,:)./sum(Pp_avg(i,:));
end

is_co=strcmp(input_gas,'CO');
is_ch4=strcmp(input_gas,'CH4');
is_h2=strcmp(input_gas,'H2');
is_cal=strcmp(input_gas,'CAL');
is_ar=strcmp(input_gas,'AR');

%get molar flow rate at each temperature
for i=1:n_temp
   if is_co==1
      m_dot(i)=8.2e-10*flow_avg(i)+3.72e-9;
   elseif is_ch4==1
      m_dot(i)=2.81e-11*flow_avg(i)^2+3.25e-9*flow_avg(i)+7.73e-8;
   elseif is_h2==1
      m_dot(i)=3.86e-9*flow_avg(i)+1.23e-7;
   elseif is_cal==1
      m_dot(i)=4.41e-9*flow_avg(i)+9.85e-8;
   elseif is_ar==1
      m_dot(i)=3.37e-11*flow_avg(i)^2+2.50e-9*flow_avg(i)+5.16e-8;
   end

   mw_avg(i)=sum(mol_f_in_avg(i,:).*mw');
   mol_dot_in_t(i)=m_dot(i)/mw_avg(i);
   for j=1:n_gas
      mol_dot_in(i,j)=mol_f_in_avg(i,j)*mol_dot_in_t(i);
   end

   if is_he==1     %if carrier gas is helium
      mol_dot_out_t(i)=mol_dot_in(i,8)/mol_f_out(i,8);   %assume constant helium flow rate
   else          %if not helium, then it is Argon
      mol_dot_out_t(i)=mol_dot_in(i,1)/mol_f_out(i,1);   %assume constant argon flow rate
   end

   for j=1:n_gas
      mol_dot_out(i,j)=mol_dot_out_t(i)*mol_f_out(i,j);  %mol fraction of each gas out
   end
end

%%% Element Balance  %%%%%%
%%%%%%%%%%%%%%%%%%%%%%%%%%%%
```

```
mol_dot_in(:,12)=zeros(n_temp,1);   %add column for solid sno2
mol_dot_in(:,13)=zeros(n_temp,1);   %add column for solid c
mol_dot_out(:,12)=zeros(n_temp,1);   %add column for solid sno2
mol_dot_out(:,13)=zeros(n_temp,1);   %add column for solid c

%elemental compostion of gas components
ec=[1 0 0 0 0 0 0 0 0 0 0 0;    %AR
   0 1 1 0 1 0 0 0 2 2 2 0 1;    %C
   0 2 1 0 0 2 1 0 0 0 0 2 0;    %O
   0 0 0 2 4 0 2 0 2 4 6 0 0;    %H
   0 0 0 0 0 0 0 1 0 0 0 0 0];   %He

for i=1:n_temp
   mol_dot_xAR(i)=(mol_dot_in(i,:)-mol_dot_out(i,:))*ec(1,:)';
   mol_dot_xC(i)=(mol_dot_in(i,:)-mol_dot_out(i,:))*ec(2,:)';
   mol_dot_xO(i)=(mol_dot_in(i,:)-mol_dot_out(i,:))*ec(3,:)';
   mol_dot_xH(i)=(mol_dot_in(i,:)-mol_dot_out(i,:))*ec(4,:)';
   mol_dot_xHe(i)=(mol_dot_in(i,:)-mol_dot_out(i,:))*ec(5,:)';
end
mol_dot_x=[mol_dot_xAR;mol_dot_xC;mol_dot_xO;mol_dot_xH;mol_dot_xHe];

if use_RH_out==0       %if not using RH out and using the condenser
   if use_cond==1
      mol_dot_h2o_c=mol_dot_xH/2;   %mol flow rate of water out at condenser
      mol_dot_out(:,7)=mol_dot_out(:,7)+mol_dot_h2o_c';    %combine h2o out meas and
condensed
   end
else
   mol_dot_h2o_c=0;    %otherwise ignore water out at condenser
end

mol_dot_sno2=(mol_dot_xO-mol_dot_h2o_c)/2;   %unnaccounted for O flow rate to SnO2
mol_dot_xtraC=mol_dot_xC;    %unnaccounted for C flow rate
mol_dot_out(:,12)=mol_dot_sno2;     %molar formation rate of SnO2
mol_dot_out(:,13)=mol_dot_xtraC;    %add molar flow rate out of solid carbon

%%%%%%%%%%%%%%%%%%%%%%%%%%%%
%%%%%%%%%%%%%%%%%%%%%%%%%%%%


%get residence time in reactor
for i=1:n_temp
   V_dot_in(i)=sum(mol_dot_in(i,:))*R_bar*(T_avg(i)+273.15)/P_avg(i);
   V_dot_out(i)=sum(mol_dot_out(i,:))*R_bar*(T_avg(i)+273.15)/P_avg(i);
```

```
   if use_snbi==1                %if using SnBi in reactor
      vel(i)=vel_bubble;         %gas velocity is bubble velocity
      LR(i)=height_avg(i);    %length of travel is metal height
   elseif use_snbi==0            %if not using SnBi in reactor
      vel(i)=((V_dot_in(i)+V_dot_out(i)))/2/Ax_reactor; %gas velocity calculated from geom.
      LR(i)=l_reactor;       %lenght of travel is heated reactor L
   end
   t_res(i)=LR(i)/vel(i);  %residence time of gas in reactor
end

rxn_gas=zeros(1,(n_gas+2));
if input_water==1
   rxn_gas(7)=1;
end

if is_co==1
   rxn_gas(3)=1;
elseif is_ch4==1
   rxn_gas(5)=1;
elseif is_h2==1
   rxn_gas(4)=1;
elseif is_cal==1
   rxn_gas(2)=1;
   rxn_gas(3)=1;
   rxn_gas(4)=1;
   rxn_gas(5)=1;
   rxn_gas(6)=1;
end

scaling=mol_dot_in(1,:).*rxn_gas;

for i=1:n_temp
   for j=1:n_gas+2
      rate(i,j)=(mol_dot_out(i,j)-mol_dot_in(i,j))/t_res(i);
      pc_cv(i,j)=100*(mol_dot_in(i,j)-mol_dot_out(i,j))/mol_dot_in(i,j);
      conc_in(i,j)=mol_dot_in(i,j)/V_dot_in(i);
      conc_out(i,j)=mol_dot_out(i,j)/V_dot_out(i);
      rate_c(i,j)=(conc_out(i,j)-conc_in(i,j))/t_res(i);  %rate of increase in conc of each component
   end
end

rate_errors

%-------------------------------------------------------------------------
%-------------------------------------------------------------------------
if write_results==1
```

```
  xlswrite([directory 'rxn_results.xls'],input_data(2),'Sheet1','A1')
  xlswrite([directory 'rxn_results.xls'],reactants,'Sheet1','B1')
  xlswrite([directory 'rxn_results.xls'],T_avg','Sheet1','B4')
  xlswrite([directory 'rxn_results.xls'],P_avg','Sheet1','C4')
  xlswrite([directory 'rxn_results.xls'],vel','Sheet1','D4')
  xlswrite([directory 'rxn_results.xls'],LR','Sheet1','E4')
  xlswrite([directory 'rxn_results.xls'],t_res','Sheet1','F4')
  xlswrite([directory 'rxn_results.xls'],flow_avg','Sheet1','G4')
  xlswrite([directory 'rxn_results.xls'],m_dot','Sheet1','H4')
  xlswrite([directory 'rxn_results.xls'],SF','Sheet1','C16')
  xlswrite([directory 'rxn_results.xls'],Pp_avg_in,'Sheet1','C18')
  xlswrite([directory 'rxn_results.xls'],sigma_fit_avg_in,'Sheet1','P18')
  xlswrite([directory 'rxn_results.xls'],Pp_avg,'Sheet1','C19')
  xlswrite([directory 'rxn_results.xls'],sigma_fit_avg_out','Sheet1','P19')
  xlswrite([directory 'rxn_results.xls'],mol_dot_in,'Sheet1','C32')
  xlswrite([directory 'rxn_results.xls'],mol_dot_out,'Sheet1','C46')
  xlswrite([directory 'rxn_results.xls'],mol_f_out,'Sheet1','C60')
  xlswrite([directory 'rxn_results.xls'],rate,'Sheet1','C74')
  xlswrite([directory 'rxn_results.xls'],rate_c,'Sheet1','C88')
  xlswrite([directory 'rxn_results.xls'],pc_cv,'Sheet1','C102')
  xlswrite([directory 'rxn_results.xls'],mol_dot_x','Sheet1','C116')
  xlswrite([directory 'rxn_results.xls'],T_avg,'Sheet1','B129')
  xlswrite([directory 'rxn_results.xls'],mz,'Sheet1','A132')
  xlswrite([directory 'rxn_results.xls'],ic_save','Sheet1','B132')
  xlswrite([directory 'rxn_results.xls'],D_height','Sheet1','U4')
  xlswrite([directory 'rxn_results.xls'],D_t_res','Sheet1','V4')
  xlswrite([directory 'rxn_results.xls'],sigma_avg_in,'Sheet1','R18')
  xlswrite([directory 'rxn_results.xls'],sigma_avg_out,'Sheet1','R19')
  xlswrite([directory 'rxn_results.xls'],D_mf_out,'Sheet1','R60')
  xlswrite([directory 'rxn_results.xls'],D_modin,'Sheet1','R32')
  xlswrite([directory 'rxn_results.xls'],D_modout,'Sheet1','R46')
  xlswrite([directory 'rxn_results.xls'],D_rate,'Sheet1','R74')
  xlswrite([directory 'rxn_results.xls'],D_rate_c,'Sheet1','R88')
  xlswrite([directory 'rxn_results.xls'],D_pc_cv,'Sheet1','R102')
end
```

8.2.7 “ms_peaks.m”

```
function[peak]=ms_peaks(ic)
%%%%%%%%%%%%%%%%%%%%%%%%%%%%%%%%%%%%%%%%%%%%%%%%%%%%%%%%%%%%%%%%%%%%%%%%
%   ms_peaks.m
%   finds peaks in ion current vector and outputs
```

```
%   as list in peak vector
%
%   ic= vector of ion currents from 1 to 65 amu
%   peak= max value for each amu division
%   k.bourne
%%%%%%%%%%%%%%%%%%%%%%%%%%%%%%%%%%%%%%%%%%%%%%%%%%%%%%%%%%%%%%%%

% find peaks
   pk=(1e-04)*ones(length(ic),1);% set to small number to avoid zeros
   for i=2:length(ic)-1
      if ic(i-1)<ic(i)    % peak if bigger than previous point
         if ic(i+1)<=ic(i)   % AND bigger or equal to next point
            pk(i)=ic(i);    %otherwise not a peak
         end
      end
   end

   peak=zeros(65,1);
   a=1;
   b=5;
   for i=1:64              % get biggest peak for each AMU 0.5 to 1.4
      peak(i)=max(pk(a:b));
      a=b+1;
      b=a+9;
   end
   peak(65)=max(pk(636:641));
```

8.2.8 "SVD_LSF.m"

```
function[P_svd P_lsf sigma sigma_fit]=SVD_LSF(H,prf,S,g)
%%%%%%%%%%%%%%%%%%%%%%%%%%%%%%%%%%%%%%%%%%%%%%%%%%%%%%%%%%%%%%%%
%   SVD_LSF.m
%   performs matrix inversion Least Squares Fit and Singular Value
%   Decomposition least squares fit on mass spectrometer data, outputs
%   partial pressure vectors as well as fit statistics
%
%   k.bourne
%%%%%%%%%%%%%%%%%%%%%%%%%%%%%%%%%%%%%%%%%%%%%%%%%%%%%%%%%%%%%%%%
% H= vector of peaks
% prf= pressure reduction factor used
% S= g x 1 vector of sensitivity factors for each gas
% g= number of gases analyzed
```

```
%
% P_svd= partial pressures found from SVD analysis
% P_lsf= partial pressures found from least squares fit analysis
% -- P_svd and P_lsf should be the same --
% sigma is standard deviation estimate of each Pp
% sigma_fit is measure of quality of overall fit

%%%%%%%%%%%%%% Least Squares Fit %%%%%%%%%%%%%%%%%%%%%%%%%%%%%%%%

   m=length(H);
   alpha=zeros(m,g);   %fragmentation factors (peaks x gases)
   gases=['AR  ';'CO2 ';'CO  ';'H2  ';'CH4 ';'O2  ';'H2O ';'He  ';'C2H2';'C2H4';'C2H6'];
     %Argon
   alpha(40,1)=.904977;
   alpha(20,1)=.0904977;
   alpha(36,1)=.00271493;
   alpha(38,1)=.00090498;
   alpha(18,1)=.00090498;

   %CO2
   alpha(44,2)=0.784314;
   alpha(28,2)=0.0862745;
   alpha(16,2)=0.075882;
   alpha(12,2)=0.0470588;
   alpha(45,2)=0.00784314;
   alpha(46,2)=0.00392157;

   %CO
   alpha(28,3)=0.915751;
   alpha(12,3)=0.0457875;
   alpha(16,3)=0.018315;
   alpha(14,3)=0.00915751;
   alpha(29,3)=0.00915751;
   alpha(30,3)=0.0018315;

   %H2
   alpha(2,4)=0.952381;
   alpha(1,4)=0.0476191;

   %CH4
   alpha(16,5)=0.459348;
   alpha(15,5)=0.395039;
   alpha(14,5)=0.0734956;
   alpha(13,5)=0.0367478;
   alpha(1,5)=0.0183739;
   alpha(12,5)=0.0114837;
```

```
alpha(17,5)=0.00551217;

%O2
alpha(32,6)=0.8936655;
alpha(16,6)=0.101877;
alpha(34,6)=0.00357462;
alpha(33,6)=0.00089366;

%H2O
alpha(18,7)=0.744048;
alpha(17,7)=0.171131;
alpha(16,7)=0.0818452;
alpha(20,7)=0.00223214;
alpha(19,7)=0.00074405;

%He
alpha(4,8)=1;

%Acetylene C2H2

alpha(14,9)=0.0014556;
alpha(28,9)=0.0014556;
alpha(12,9)=0.0218341;
alpha(27,9)=0.0218341;
alpha(24,9)=0.0400291;
alpha(13,9)=0.0400291;
alpha(25,9)=0.14556;
alpha(26,9)=0.727802;

%Ethene C2H4
alpha(29,10)=0.0085106;
alpha(12,10)=0.0081238;
alpha(13,10)=0.0135397;
alpha(24,10)=0.0143133;
alpha(14,10)=0.0309478;
alpha(25,10)=0.0464217;
alpha(26,10)=0.239845;
alpha(27,10)=0.251451;
alpha(28,10)=0.386847;

%Ethane C2H6
alpha(14,11)=0.01182;
alpha(15,11)=0.014184;
alpha(25,11)=0.014184;
alpha(26,11)=0.108747;
alpha(27,11)=0.156028;
```

```
alpha(28,11)=0.472813;
alpha(29,11)=0.099291;
alpha(30,11)=0.122931;

for i=1:g
   alpha_sum(i)=sum(alpha(:,i));
end

obs=0;
for i=1:m
   row_sum=0;
   row_sum=sum(alpha(i,:));
   if row_sum>0
      obs=obs+1;  %number of peaks used in analysis
   end
end

s=prf*ones(g,1);          %combine sensitiviy and pressure reduction factors

% Least Squares Matricies

A=zeros(g,g);   %initialize matricies
P=zeros(g,1);
y=zeros(g,1);
am=zeros(m,1);
hm=zeros(m,1);

for i=1:g
   for j=1:g
      for M=1:m
         am(M)=alpha(M,i)*s(i)*alpha(M,j)*s(j);
      end
      A(i,j)=sum(am);
   end
end

for i=1:g
   for M=1:m
      hm(M)=H(M)*alpha(M,i)*s(i);
   end
   y(i)=sum(hm);
end

P=A\y;
P_lsf=transpose(P.*S);
```

```
   %%%%%%%%%%%%%%%%%%%%%%%%%%%% SVD Analysis
%%%%%%%%%%%%%%%%%%%%%%%%%%

   for i=1:m
      for j=1:g
         Av(i,j)=alpha(i,j)*s(j);
      end
   end

   [U,w,V]=svd(Av,0);
   wr=zeros(g,g);
   for i=1:g
      for j=1:g
         if w(i,j)>0.001
            wr(i,j)=1/w(i,j);
         end
      end
   end
   Pv=V*wr*transpose(U)*H;
   P_svd=transpose(Pv.*S);

   %%%%%%%%%%%%%%%%%%%%%% estimation of standard deviation %%%%%%%%%%%%%
   sigma=zeros(1,g);
   for j=1:g
      clear ss
      for i=1:g
         ss(i)=(V(j,i)/wr(i,i))^2;
      end
      sigma(j)=sqrt(sum(ss));     % eq 15.4.19 p 677 in Recipes
   end

   for j=1:g
      for k=1:g
         for i=1:g
            cvs(i)=V(j,i)*V(k,i)/w(i,i)^2;
         end
         cov(j,k)=sum(cvs);
      end
   end

   %%%%%%%%%%%%%%%%%%%%%% estimation of quality of fit %%%%%%%%%%%%%
   for i=1:g
      P_sf(i)=P_svd(i)/S(i);         %Partial pressure un-scaled by SF
      h_p(1:m,i)=alpha(:,i)*P_sf(i);  %prediced peak heights for each gas
   end
   for j=1:m
```

```
    H_P(j)=sum(h_p(j,:));      %total predicted peak height
    Qs(j)=(H_P(j)-H(j))^2;     %square of predicted-observed height
  end
  Q=sum(Qs);                  %sum of squares
  sigma_fit=sqrt(Q/(obs-g));       %estimate of Std Dev from NIST 4.4.3.1
```

8.2.9 "rate_errors.m"

```
%%%%%%%%%%%%%%%%%%%%%%%%%%%%%%%%%%%%%%%%%%%%%%
%   rate_errors.m
%
%   performs error propagation analysis on data from reaction_analysis.m
%   runs in and shares variables with reaction_analysis.m
%
%   k.bourne
%%%%%%%%%%%%%%%%%%%%%%%%%%%%%%%%%%%%%%%%%%%%%%

%constants
R=8.314;          %universal gas constant

%fixed errors
D_T=5;            %heater controler tolerance
D_rho_snbi=711;    %from Moser
D_vel_snbi=0.029;   %velocity in SnBi exp. from bubble velocity 3-15-12.xlsx
D_H_hs=0.0046;     %height if using HS, from HS geometry
D_H_er=0.03;       %height if using baseline reactor, estimate from geom.
D_id=0.0002;       %empty reactor id tolerance

%percent (fraction form) errors
fD_Pp=0.15;        %estimate from analysis
fD_RH=0.03;        %from RH data sheet
fD_P=0.02;         %from PX309 data sheet
fD_T=0.0075;       %from TC data sheet
fD_m_dot=0.20;     %conservative from calibration summary.xlxs

%%%%%%%%%%%%%%%
%mol_f_in
%%%%%%%%%%%%%%%

for j=1:n_gas
  D_Pp_in(j)=Pp_in_dry(j)*fD_Pp;
  D_Pp_in_sq(j)=D_Pp_in(j)^2;
end
```

```
for i=1:n_temp
   D_sumPpind(i)=(sum(D_Pp_in_sq))^0.5;
   for j=1:n_gas
      dmfindPpind(i,j)=1/sum(Pp_in_dry);
      dmfindsumPpind(i,j)=-Pp_in_dry(j)/(sum(Pp_in_dry)^2);

D_mf_in_dry(i,j)=(dmfindPpind(i,j)^2*D_Pp_in(j)^2+(dmfindsumPpind(i,j))^2*D_sumPpind(i)^2)^0.5
;
   end
end

D_mf_in=D_mf_in_dry;

if use_RH_in==1
  for i=1:n_temp
     dmfinRHdt21(i)=mf_h2o_in_avg(i)*(4117.4/(T21_avg(i)^2+476*T21_avg(i)+238^2));
     dmfinRHdP4(i)=mf_h2o_in_avg(i)/RH_in_avg(i);
     dmfinRHdRHin(i)=-mf_h2o_in_avg(i)/P4_avg(i);

D_mf_in_rh(i)=(dmfinRHdt21(i)^2*(fD_T*T21_avg(i))^2+dmfinRHdP4(i)^2*(fD_P*P4_avg(i))^2+dmfi
nRHdRHin(i)^2*(fD_RH*RH_in_avg(i))^2)^0.5;
  end
  D_mf_in(:,7)=D_mf_in_rh';
end

mf_in_percent=D_mf_in./mol_f_in_avg(:,1:n_gas)

%%%%%%%%%%
%mol_f_out
%%%%%%%%%%

for i=1:n_temp
   for j=1:n_gas
   D_Pp_out(i,j)=Pp_avg(i,j)*fD_Pp;
   D_Pp_out_sq(i,j)=D_Pp_out(i,j)^2;
   end
end
for i=1:n_temp
   D_sumPpod(i)=(sum(D_Pp_out_sq(i,:)))^0.5;
   for j=1:n_gas
      dmfodPpod(i,j)=1/sum(Pp_avg(i,:));
      dmfodsumPpod(i,j)=-Pp_avg(i,j)/(sum(Pp_avg(i,:))^2);

D_mf_out_dry(i,j)=(dmfodPpod(i,j)^2*D_Pp_out(i,j)^2+(dmfodsumPpod(i,j))^2*D_sumPpod(i)^2)^0.
5;
   end
```

```
end

D_mf_out=D_mf_out_dry;

if use_RH_out==1
  for i=1:n_temp
     dmfoRHdt20(i)=mf_h2o_out_avg(i)*(4117.4/(T20_avg(i)^2+476*T20_avg(i)+238^2));
     dmfoRHdP1(i)=mf_h2o_out_avg(i)/RH_out_avg(i);
     dmfoRHdRHo(i)=-mf_h2o_out_avg(i)/P1_avg(i);

D_mf_out_rh(i)=(dmfoRHdt20(i)^2*(fD_T*T20_avg(i))^2+dmfoRHdP1(i)^2*(fD_P*P1_avg(i))^2+dmf
oRHdRHo(i)^2*(fD_RH*RH_out_avg(i))^2)^0.5;
  end
  D_mf_out(:,7)=D_mf_out_rh';
end

mf_out_percent=D_mf_out./mol_f_out(:,1:n_gas)

%%%%%%%%%%%%
%mol_dot_in
%%%%%%%%%%%%

for i=1:n_temp
   for j=1:n_gas
      mwDmfsq(i,j)=mw(j)^2*D_mf_in(i,j)^2;
   end
end
for i=1:n_temp
   summwDmfsq(i)=(sum(mwDmfsq(i,:)))^0.5;
   dmoldidmfi(i)=mol_dot_in_t(i);
   for j=1:n_gas
      dmoldidmwa(i,j)=-mol_f_in_avg(i,j)*m_dot(i)/mw_avg(i)^2;
      dmoldidmd(i,j)=mol_f_in_avg(i,j)/mw_avg(i);

D_modin(i,j)=(dmoldidmfi(i)^2*D_mf_in(i,j)^2+dmoldidmwa(i,j)^2*summwDmfsq(i)^2+dmoldidmd(i
,j)^2*(fD_m_dot*m_dot(i))^2)^0.5;
   end
end

md_in_percent=D_modin./mol_dot_in(:,1:n_gas)


%%%%%%%%%%%%
%mol_dot_out
%%%%%%%%%%%%
```

```
if is_he==1        %if the carrier gas is Helium
   cg=8;          %carrier gas is gas #8
elseif is_he==0    %if it isn't Helium, it is Argon
   cg=1;          %carrier gas is gas #1
end

for i=1:n_temp
   for j=1:n_gas
      dmdodmdc(i,j)=mol_f_out(i,j)/mol_f_out(i,cg);
      dmdodmfo(i,j)=mol_dot_in(i,cg)/mol_f_out(i,cg);
      dmdodmfoc(i,j)=-mol_dot_in(i,cg)*mol_f_out(i,j)/mol_f_out(cg)^2;

D_modout(i,j)=(dmdodmdc(i,j)^2*D_modin(i,cg)^2+dmdodmfo(i,j)^2*D_mf_out(i,j)^2+dmdodmfoc(
i,j)^2*D_mf_out(i,cg)^2)^0.5;
   end
end

md_out_percent=D_modout./mol_dot_out(:,1:n_gas)


%%%%%%%%%%%%
%t_res
%%%%%%%%%%%%

if use_snbi==1
   D_vel=0.029;    %from velocity data 3-15-12.xlsx
   if hsm_avg==0
      D_height=ones(1,n_temp)*D_H_hs;    %if using height sensor
   else
      for i=1:n_temp
         dHdP1(i)=-6894/(rho_snbi_hot_avg(i)*9.81);
         dHdP4(i)=6894/(rho_snbi_hot_avg(i)*9.81);
         dHdrho(i)=-(P4_avg(i)-P1_avg(i))*6894/(rho_snbi_hot(i)^2*9.81);

D_height(i)=(dHdP1(i)^2*(fD_P*P1_avg(i))^2+dHdP4(i)^2*(fD_P*P4_avg(i))^2+dHdrho(i)^2*D_rho_s
nbi^2)^0.5;
      end
   end
   for i=1:n_temp
      D_moldin_t(i)=(sum(D_modin(i,:).^2))^0.5;
      D_moldout_t(i)=(sum(D_modout(i,:).^2))^0.5;
      dtdH(i)=1/vel(i);
      dtdvel(i)=-height_avg(i)/vel(i)^2;
      D_t_res(i)=(dtdH(i)^2*D_height(i)^2+dtdvel(i)^2*D_vel^2)^0.5;
   end
else
```

```
   D_height=ones(1,n_temp)*D_H_er;
   dAxdid=pi*id;
   D_Ax=((dAxdid)^2*D_id^2)^0.5;

   for i=1:n_temp
      D_moldin_t(i)=(sum(D_modin(i,:).^2))^0.5;
      D_moldout_t(i)=(sum(D_modout(i,:).^2))^0.5;
      dtdl(i)=Ax_reactor/((mol_dot_in_t(i)+mol_dot_out_t(i))/2*R*(T_avg(i)+273.15)/P_avg(i));
      dtdAx(i)=LR(i)/((mol_dot_in_t(i)+mol_dot_out_t(i))/2*R*(T_avg(i)+273.15)/P_avg(i));
      dtdP(i)=LR(i)*Ax_reactor/((mol_dot_in_t(i)+mol_dot_out_t(i))/2*R*(T_avg(i)+273.15));
      dtdmoldin(i)=-
LR(i)*Ax_reactor/(R*(T_avg(i)+273.15)/P_avg(i)*(2*mol_dot_in_t(i)^2+4*mol_dot_in_t(i)*mol_dot_
out_t(i)+2*mol_dot_out(i)^2));
      dtdmoldout(i)=dtdmoldin(i);
      dtdTavg(i)=-
LR(i)*Ax_reactor/((mol_dot_in_t(i)+mol_dot_out_t(i))/2*R/P_avg(i)*(T_avg(i)+2*(273+T_avg(i))+273
^2));

D_t_res(i)=(dtdl(i)^2*D_height(i)^2+dtdAx(i)^2*D_Ax^2+dtdmoldin(i)^2*D_moldin_t(i)^2+dtdmoldo
ut(i)^2*D_moldout_t(i)^2+dtdTavg(i)^2*(fD_T*T_avg(i)+D_T)^2+dtdP(i)^2*(fD_P*P_avg(i))^2)^0.5;
   end
end

t_res_percent=D_t_res./t_res


%%%%%%%%%%%%
%rate
%%%%%%%%%%%%
for i=1:n_temp
   for j=1:n_gas
      D_modin(i,j)=mol_dot_in(i,j)*0.005;
      D_modout(i,j)=mol_dot_out(i,j)*0.005;
   end
end

for i=1:n_temp
   dratedmodin(i)=-1/t_res(i);
   dratedmodout(i)=1/t_res(i);
   for j=1:n_gas
      dratedt_res(i,j)=-(mol_dot_out(i,j)-mol_dot_in(i,j))/t_res(i)^2;

D_rate(i,j)=(dratedmodin(i)^2*D_modin(i,j)^2+dratedmodout(i)^2*D_modout(i,j)^2+dratedt_res(i,j)
^2*D_t_res(i)^2)^0.5;
   end
end
```

```
rate_percent=D_rate./abs(rate(:,1:n_gas))


%%%%%%%%%%%%
%concentration in
%%%%%%%%%%%%

for i=1:n_temp
   dcindmdin(i)=1/V_dot_in(i);
   for j=1:n_gas
      dcindP(i,j)=mol_dot_in(i,j)/(mol_dot_in_t(i)*R*(T_avg(i)+273.15));
      dcindmdt(i,j)=-mol_dot_in(i,j)*P_avg(i)/(mol_dot_in_t(i)^2*R*(T_avg(i)+273.15));
      dcindT(i,j)=-
mol_dot_in(i,j)*P_avg(i)/(mol_dot_in_t(i)^2*R*(T_avg(i)^2+2*T_avg(i)*273.15+273.15^2));

D_conc_in(i,j)=(dcindmdin(i)^2*D_modin(i,j)^2+dcindP(i,j)^2*(fD_P*P_avg(i))^2+dcindmdt(i,j)^2*D_
moldin_t(i)^2+dcindT(i,j)^2*(fD_T*T_avg(i))^2)^0.5;
   end
end

conc_in_percent=D_conc_in./conc_in(:,1:n_gas)


%%%%%%%%%%%%
%concentration out
%%%%%%%%%%%%

for i=1:n_temp
   dcindmdo(i)=1/V_dot_out(i);
   for j=1:n_gas
      dcodP(i,j)=mol_dot_out(i,j)/(mol_dot_out_t(i)*R*(T_avg(i)+273.15));
      dcodmdt(i,j)=-mol_dot_out(i,j)*P_avg(i)/(mol_dot_out_t(i)^2*R*(T_avg(i)+273.15));
      dcodT(i,j)=-
mol_dot_out(i,j)*P_avg(i)/(mol_dot_out_t(i)^2*R*(T_avg(i)^2+2*T_avg(i)*273.15+273.15^2));

D_conc_out(i,j)=(dcindmdo(i)^2*D_modout(i,j)^2+dcodP(i,j)^2*(fD_P*P_avg(i))^2+dcodmdt(i,j)^2*D
_moldout_t(i)^2+dcodT(i,j)^2*(fD_T*T_avg(i)+D_T)^2)^0.5;
   end
end

conc_out_percent=D_conc_out./conc_out(:,1:n_gas)


%%%%%%%%%%%%
%rate_c
```

```
%%%%%%%%%%%%

for i=1:n_temp
   dratecdco(i)=1/t_res(i);
   dratecdci(i)=-1/t_res(i);
   for j=1:n_gas
      dratecdt(i,j)=-(conc_out(i,j)-conc_in(i,j))/t_res(i)^2;

D_rate_c(i,j)=(dratecdco(i)^2*D_conc_out(i,j)^2+dratecdci(i)^2*D_conc_in(i,j)^2+dratecdt(i,j)^2*D_
t_res(i)^2)^0.5;
   end
end

rate_c_percent=D_rate_c./rate_c(:,1:n_gas)


%%%%%%%%%%%%
%percent conversion
%%%%%%%%%%%%

for i=1:n_temp
   for j=1:n_gas
      dpcdmdi(i,j)=100*mol_dot_out(i,j)/mol_dot_in(i,j)^2;
      dpcdmdo(i,j)=-100/mol_dot_in(i,j);
      D_pc_cv(i,j)=(dpcdmdi(i,j)^2*D_modin(i,j)^2+dpcdmdo(i,j)^2*D_modout(i,j)^2)^0.5;
   end
end

pc_cv_percent=D_pc_cv./pc_cv(:,1:n_gas)
```

8.2.10 "LogNames.m"

```
function[sec_tot ts]=LogNames(time_start_all,incr,n_file,day)
%%%%%%%%%%%%%%%%%%%%%%%%%%%%%%%%%%%%%%%%%%%%%%%%%%%%%%%%%%%%
%   LogNames.m
%
%   creates list of file names for mass spectrometer log files
%
%   k.bourne
%%%%%%%%%%%%%%%%%%%%%%%%%%%%%%%%%%%%%%%%%%%%%%%%%%%%%%%%%%%%
sec_tot=zeros(n_file,1);    %initialize vectors
```

```
if time_start_all(10)=='P'
   if str2num(time_start_all(1:2))<12
   ampm=12;       %adds 12 to hr in afternoon
   else ampm=0;
   end
else ampm=0;       %0 if in morning
end
hr_start=str2num(time_start_all(1:2))+ampm;
min_start=str2num(time_start_all(4:5));
sec_start=str2num(time_start_all(7:8));

sec_tot(1)=3600*hr_start+60*min_start+sec_start;    %sec since midnight

for i=2:n_file
   sec_tot(i)=sec_tot(i-1)+incr;      % gets sec since midnight
end                                   % for each scan

for i=1:n_file                %converts sec to hr min sec am/pm matrix
   hr=floor(sec_tot(i)/3600);
   mi=floor((sec_tot(i)-3600*hr)/60);
   sec=floor(sec_tot(i)-3600*hr-60*mi);
   if hr>11
      mm=2;   %decides if am or pm
   else mm=1;
   end
   if hr>12
      hr=hr-12;   % converts to 12/12 day for file format
   end
   time(i,1)=hr;   %saves in matrix
   time(i,2)=mi;
   time(i,3)=sec;
   time(i,4)=mm;
end

   for i=1:n_file      %gets time matrix into file name format
      ts(i,:)=[day '0' '0' '-' '0' '0' '-' '0' '0' '_' 'aa' '.txt'];
      if time(i,4)==1
         am='AM';
      else am='PM';
      end
      ts(i,24:25)=am;
      if time(i,1)>9
         ts(i,15:16)=num2str(time(i,1));
      else
         ts(i,16)=num2str(time(i,1));
      end
```

```
    if time(i,2)>9
       ts(i,18:19)=num2str(time(i,2));
    else
       ts(i,19)=num2str(time(i,2));
    end
    if time(i,3)>9
       ts(i,21:22)=num2str(time(i,3));
    else
       ts(i,22)=num2str(time(i,3));
    end
  end
```

8.2.11 "extra_peaks.m"

```
function[pk_x,peak,icp]=extra_peaks(g,P_svd,ic)
%%%%%%%%%%%%%%%%%%%%%%%%%%%%%%%%%%%%%%%%%%%%%%%%%%%%%%%%%%%%%%%%%%%%%%%%
%   extra_peaks.m
%
%   determines which mass spectrum peaks are used in each analysis
%   and determines what mass spectrum peak values from calculated
%   partial pressures, for comparison with original mass spectrum
%
%   k.bourne
%%%%%%%%%%%%%%%%%%%%%%%%%%%%%%%%%%%%%%%%%%%%%%%%%%%%%%%%%%%%%%%%%%%%%%%%
% g = number of gases in analysis
% P_svd = partial pressure predicted by SVD analysis
% ic = ion current used in SVD analysis (with bk subrtacted)

% pk_x = m/z ratio for each peak and icp
% peak = peaks used in SVD analysis
% icp = peaks heights predicted from fit partial pressures

peak=ms_peaks(ic);

for i=1:65
   pk_x(i)=i;
end

alpha=zeros(65,g);

     %Argon
   alpha(40,1)=.904977;
   alpha(20,1)=.0904977;
```

```
alpha(36,1)=.00271493;
alpha(38,1)=.00090498;
alpha(18,1)=.00090498;

%CO2
alpha(44,2)=0.784314;
alpha(28,2)=0.0862745;
alpha(16,2)=0.075882;
alpha(12,2)=0.0470588;
alpha(45,2)=0.00784314;
alpha(46,2)=0.00392157;

%CO
alpha(28,3)=0.915751;
alpha(12,3)=0.0457875;
alpha(16,3)=0.018315;
alpha(14,3)=0.00915751;
alpha(29,3)=0.00915751;
alpha(30,3)=0.0018315;

%H2
alpha(2,4)=0.952381;
alpha(1,4)=0.0476191;

%CH4
alpha(16,5)=0.459348;
alpha(15,5)=0.395039;
alpha(14,5)=0.0734956;
alpha(13,5)=0.0367478;
alpha(1,5)=0.0183739;
alpha(12,5)=0.0114837;
alpha(17,5)=0.00551217;

%O2
alpha(32,6)=0.8936655;
alpha(16,6)=0.101877;
alpha(34,6)=0.00357462;
alpha(33,6)=0.00089366;

%H2O
alpha(18,7)=0.744048;
alpha(17,7)=0.171131;
alpha(16,7)=0.0818452;
alpha(20,7)=0.00223214;
alpha(19,7)=0.00074405;
```

```
%He
alpha(4,8)=1;

%Acetylene C2H2

alpha(14,9)=0.0014556;
alpha(28,9)=0.0014556;
alpha(12,9)=0.0218341;
alpha(27,9)=0.0218341;
alpha(24,9)=0.0400291;
alpha(13,9)=0.0400291;
alpha(25,9)=0.14556;
alpha(26,9)=0.727802;

%Ethene C2H4
alpha(29,10)=0.0085106;
alpha(12,10)=0.0081238;
alpha(13,10)=0.0135397;
alpha(24,10)=0.0143133;
alpha(14,10)=0.0309478;
alpha(25,10)=0.0464217;
alpha(26,10)=0.239845;
alpha(27,10)=0.251451;
alpha(28,10)=0.386847;

%Ethane C2H6
alpha(14,11)=0.01182;
alpha(15,11)=0.014184;
alpha(25,11)=0.014184;
alpha(26,11)=0.108747;
alpha(27,11)=0.156028;
alpha(28,11)=0.472813;
alpha(29,11)=0.099291;
alpha(30,11)=0.122931;

icp=zeros(65);
for i=1:g
   for j=1:65
      icp(j)=icp(j)+alpha(j,i)*P_svd(i);
   end
end
```

8.2.12 "sensitivity_factors.m"

```
%%%%%%%%%%%%%%%%%%%%%%%%%%%%%%%%%%%%%%%%%%%%%%%
%   sensitivity_factors.m
%
%   performs analysis of data set specified in script, and determines
%   mass spectrometer sensitivity factors for each gas specified from
%   data set and specified calibration gas
%
%   k.bourne
%%%%%%%%%%%%%%%%%%%%%%%%%%%%%%%%%%%%%%%%%%%%%%%

clear all
directory='C:\Documents and Settings\kjbourne\Desktop\MS Analysis\3-29-12\';

filename_data=[directory 'fdata.txt'];
flow_data_file=[directory 'flowdata.txt'];
day='\Mar_29_2012__'; %date format of log files

[sn folder start_time num_logs bks bke T_nom]=textread(filename_data, '%u %s %s %u %u %u
%u','headerlines',2, 'delimiter',' ');

%inputs
%xxxxxxxxxxxxxxxxxxxxxxxxxxxxxxxxxxxxxxxxxxxxxxxxxxxxxxxxxxxxxxxxxxxxxxxxx
%xxxxxxxxxxxxxxxxxxxxxxxxxxxxxxxxxxxxxxxxxxxxxxxxxxxxxxxxxxxxxxxxxxxxxxxxx
prf=1;
gases=['AR ' ;'CO2' ;'CO ' ;'H2 ' ;'CH4' ;'O2 ' ;'H2O'];
% percent_calgas=[0.950086 0.009701 0.01002 0.01009 0.01020 0.009903 0.0];
% percent_calgas=[0.95 0.0 0.0 0.0 0.05 0.0 0.0];         %CH4 mix
% percent_calgas=[0.94913 0.0 0.0 0.05087 0.0 0.0 0.0];    %H2 mix
percent_calgas=[0 0 0.05 0 0 0 0 .95];                  %CO mix

% input gas scan numbers
input_sn=[4;21];
%xxxxxxxxxxxxxxxxxxxxxxxxxxxxxxxxxxxxxxxxxxxxxxxxxxxxxxxxxxxxxxxxxxxxxxxxx
%xxxxxxxxxxxxxxxxxxxxxxxxxxxxxxxxxxxxxxxxxxxxxxxxxxxxxxxxxxxxxxxxxxxxxxxxx

% get input gas composition with SFs=1
%==========================================================================
%==========================================================================

SF=ones(length(percent_calgas),1);
     %INPUT 1 BACKGROUND
     %file name for background before input scan 1
fn_i1bk1=[directory char(folder(bks(input_sn(1)))) day char(start_time(bks(input_sn(1)))) '.txt'];
```

```
      %file name for background after input scan 1
fn_i1bk2=[directory char(folder(bke(input_sn(1)))) day char(start_time(bke(input_sn(1)))) '.txt'];
      %get ion currents for background files
[mz ig1_bk1]=textread(fn_i1bk1,'%f %f','headerlines',22, 'delimiter',',');
[mz ig1_bk2]=textread(fn_i1bk2,'%f %f','headerlines',22, 'delimiter',',');
      %average background ion current for input gas 1
ig_bk(1,:)=(ig1_bk1+ig1_bk2)/2;

      %INPUT 2 BACKGROUND
      %file name for background before input scan 2
fn_i2bk1=[directory char(folder(bks(input_sn(2)))) day char(start_time(bks(input_sn(2)))) '.txt'];
      %file name for background after input scan 2
fn_i2bk2=[directory char(folder(bke(input_sn(2)))) day char(start_time(bke(input_sn(2)))) '.txt'];
      %get ion currents for background files
[mz ig2_bk1]=textread(fn_i2bk1,'%f %f','headerlines',22, 'delimiter',',');
[mz ig2_bk2]=textread(fn_i2bk2,'%f %f','headerlines',22, 'delimiter',',');
      %average background ion current for input gas 2
ig_bk(2,:)=(ig2_bk1+ig2_bk2)/2;

      %make file names for input gases, import files, plot, find avg comp

incr=30;          %seconds between scans

for f=1:2   %for each input file
   clear ts Pp
   n_file=num_logs(input_sn(f));     %gets number of files in log
   sec_tot=zeros(n_file,1);       %initialize vector
   time_start_all=char(start_time(input_sn(f)));

   [sec_tot,ts]=LogNames(time_start_all,incr,n_file,day);

   for i=1:n_file
      fni=[char(directory) char(folder(input_sn(f))) char(ts(i,:))];
      [mz ics(i,:)]=textread(fni,'%f %f','headerlines',22, 'delimiter',',');
      ics(i,:)=ics(i,:)-ig_bk(f); %subtract averaged background ion currents
      H=ms_peaks(ics(i,:));
%       [Pp(i,:) pp]=SVD_LSF(H,prf,SF,7);
            [Pp(i,:) pp]=SVD_LSF_He(H,prf,SF,8);
   end
   figure(f)
   semilogy(sec_tot,Pp,'.-')

   [xx,~]=ginput(2);          %click on ends of steady state period
   diff1=abs(sec_tot-xx(1));   %find indicies of steady state period
   [~,i1]=min(diff1);
   diff2=abs(sec_tot-xx(2));
```

```
   [~,i2]=min(diff2);
   Pp_avg(f,:)=mean(Pp(i1:i2,:));   %average partial pressures over ss period
end
Pp_meas=mean(Pp_avg);               %average gas composition measured with SFs=1

Pp_sum=sum(Pp_meas);   %total of all partial pressures measured
Pp_calgas=percent_calgas*Pp_sum;    %expected partial pressure of cal gas

percent_gas=Pp_meas/Pp_sum

SF=Pp_calgas./Pp_meas    %calculated sensitivity factors
```